A strategy for a general search for new phenomena using data-derived signal regions and its application within the ATLAS experiment

The ATLAS Collaboration

This paper describes a strategy for a general search used by the ATLAS Collaboration to find potential indications of new physics. Events are classified according to their final state into many event classes. For each event class an automated search algorithm tests whether the data are compatible with the Monte Carlo simulated expectation in various distributions sensitive to the effects of new physics. The significance of a deviation is quantified using pseudo-experiments. A data selection with a significant deviation defines a signal region for a dedicated follow-up analysis with an improved background expectation. The analysis of the data-derived signal regions on a new dataset allows a statistical interpretation without the large look-elsewhere effect. The sensitivity of the approach is discussed using Standard Model processes and benchmark signals of new physics. As an example, results are shown for 3.2 fb^{-1} of proton–proton collision data at a centre-of-mass energy of 13 TeV collected with the ATLAS detector at the LHC in 2015, in which more than 700 event classes and more than 10^5 regions have been analysed. No significant deviations are found and consequently no data-derived signal regions for a follow-up analysis have been defined.

arXiv:1807.07447v1 [hep-ex] 19 Jul 2018

1 Introduction

Direct searches for unknown particles and interactions are one of the primary objectives of the physics programme at the Large Hadron Collider (LHC). The ATLAS experiment at the LHC has thoroughly analysed the Run 1 pp collision dataset (recorded in 2010–2012) and roughly a quarter of the expected Run 2 dataset (2015–2018). No evidence of physics beyond the Standard Model (SM) has been found in any of the searches performed so far.

Searches that have been performed to date do not fully cover the enormous parameter space of masses, cross-sections and decay channels of possible new particles. Signals might be hidden in kinematic regimes and final states that have remained unexplored. This motivates a model-independent[1] analysis to search for physics beyond the Standard Model (BSM) in a structured, global and automated way, where many of the final states not yet covered can be probed.

General searches without an explicit BSM signal assumption have been been performed by the DØ Collaboration [1–4] at the Tevatron, by the H1 Collaboration [5, 6] at HERA, and by the CDF Collaboration [7, 8] at the Tevatron. At the LHC, preliminary versions of such searches have been performed by the ATLAS Collaboration at $\sqrt{s}$ = 7, 8 and 13 TeV, and by the CMS Collaboration at $\sqrt{s}$ = 7 TeV.

This paper outlines a strategy employed by the ATLAS Collaboration to search in a systematic and (quasi-)model-independent way for deviations of the data from the SM prediction. This approach assumes only generic features of the potential BSM signals. Signal events are expected to have reconstructed objects with relatively large momentum transverse to the beam axis. In contrast to previous generic searches, the main objective of this strategy is not to finally access the exact level of significance of a deviation with all available data, but rather to identify with a first dataset those phase-space regions where significant deviations of the data from SM prediction are present for a further dedicated analysis. The observation of one or more significant deviations in some phase-space region(s) serves as a trigger to perform dedicated and model-dependent analyses where these 'data-derived' phase-space region(s) can be used as signal regions. Such an analysis can then determine the level of significance using a second dataset. The main advantage of this procedure is that it allows a large number of phase-space regions to be tested with the available resources, thereby minimizing the possibility of missing a signal for new physics, while simultaneously maintaining a low false discovery rate by testing the data-derived signal region(s) on an independent dataset in a dedicated analysis. The dedicated analysis with data-derived signal regions also allows an improved background prediction.

In this approach, events are first classified into different (exclusive) categories, labelled with the multiplicity of final-state objects (e.g. muons, electrons, jets, missing transverse momentum, etc.) in an event. These final-state categories are then automatically analysed for deviations of the data from the SM prediction in several BSM-sensitive distributions using an algorithm that locates the region of largest excess or deficit. Sensitivity tests for specific signal models are performed to demonstrate the effectiveness of this approach. The methodology has been applied to a subset of the $\sqrt{s}$ = 13 TeV proton–proton collision data as reported in this paper. The data were collected with the ATLAS detector in 2015, and correspond to an integrated luminosity of 3.2 fb^{-1}.

---

[1] 'Model-independent' refers to the absence of a beyond the Standard Model signal assumption. The analysis depends on the Standard Model prediction.

The paper is organized as follows: the general analysis strategy is outlined in Section 2, while Section 3 provides specific details about its application to the ATLAS 2015 pp collision dataset. Conclusions are given in Section 4.

2 Strategy

The analysis strategy assumes that a signal of unknown origin can be revealed as a statistically significant deviation of the event counts in the data from the expectation in a specific data selection. A data selection can be any set of requirements on objects or variables needed to define a signal region (e.g. an event class or a specific range in one or multiple observables). In order to search for these signals a large variety of data selections need to be tested. This requires a high degree of automation and a categorization of the data events according to their main features. The main objective of this analysis is to identify selections for which the data deviates significantly from the SM expectation. These selections can then be applied as data-derived signal regions in a dedicated analysis to determine the level of significance using a new dataset. This has the advantage of a more reliable background expectation, which should allow an increase in signal sensitivity compared to a strategy that only relies on Monte Carlo expectations with a typically conservative evaluation of uncertainties. The strategy is divided into the seven steps described below.

2.1 Step 1: Data selection and Monte Carlo simulation

The recorded data are reconstructed via the ATLAS software chain. Events are selected by applying event-quality and trigger criteria, and are classified according to the type and multiplicity of reconstructed objects with high transverse momentum (p_T). Objects that can be considered in the classification are those typically used to characterize hadron collisions such as electrons, muons, τ-leptons, photons, jets, b-tagged jets and missing transverse momentum. More complex objects, which were not implemented in the example described in Section 3, could also be considered. Examples are resonances reconstructed by a specific decay (e.g. Z or Higgs bosons decaying into two or four isolated leptons respectively, or decaying hadronically and giving rise to large radius jets with substructure) and displaced vertices. Event classes (or channels) are then defined as the set of events with a given number of reconstructed objects for each type, e.g. two muons and a jet.

Monte Carlo (MC) simulations are used to estimate the expected event counts from SM processes. To allow the investigation of signal regions with a low number of expected events it is important that the equivalent integrated luminosity of the MC samples significantly exceeds that of the data, and that all relevant background processes are included, in particular rare processes which might dominate certain multi-object event classes.

2.2 Step 2: Systematic uncertainties and validation

The particular nature of this analysis, in which a large number of final states are explored, makes the definition of control and validation regions difficult. In searches for BSM physics at the LHC, control regions are used to constrain MC-based background predictions with auxiliary measurements. Validation regions are used to test the validity of the background model prediction with data.

The simplest way to construct a background model is to obtain the background expectation from the MC prediction including the corresponding theoretical and experimental uncertainties. This approach, which is applied in the example in Section 3, has the advantage that it prevents the absorption of BSM signal contributions into a rescaling of the SM processes. Another possible approach is to automatically define, for each data selection and algorithmic hypothesis test, statistically independent control selections. The data in the control selections can be used to rescale the MC background predictions and to constrain the systematic uncertainties. This comes at the price of reduced sensitivity for the case in which a BSM model predicts a simultaneous effect in the signal region and control region, which would be absorbed in the rescaling.

To verify the proper modelling of the SM background processes, several validation distributions are defined using inclusive selections for which observable signals for new physics are excluded. If these validation distributions show problems in the MC modelling, either corrections to the MC backgrounds are applied or the affected event class is excluded.

Uncertainties in the background estimate arise from experimental effects, and the theoretical accuracy of the prediction of the (differential) cross-section and acceptance of the MC simulation. Their effect is evaluated for all contributing background processes as well as for benchmark signals.

2.3 Step 3: Sensitive variables and search algorithm

Distributions of observables in the form of histograms are investigated for all event classes considered in the analysis. Observables are included if they have a high sensitivity to a wide range of BSM signals. The total number of observables considered is, however, restricted to a few to avoid a large increase in the number of hypothesis tests, as the latter also increases the rate of deviations from background fluctuations. In high-energy physics this effect is commonly known as the 'trial factor' or 'look-elsewhere effect'. Examples of such observables are the effective mass m_{eff} (defined as the sum of the scalar transverse momenta of all objects plus the scalar missing transverse momentum), the total invariant mass m_{inv} (defined as the invariant mass of all visible objects), the invariant mass of any combination of objects (such as the dielectron invariant mass in events with two electrons and two muons), event shape variables such as thrust [9, 10] or even more complicated variables such as the output of a machine-learning algorithm.

A statistical algorithm is used to scan these distributions for each event class and quantify the deviations of the data from the SM expectation. The algorithm identifies the data selection that has the largest deviation in the distribution of the investigated observable by testing many data selections to minimize a test statistic. A possible test statistic is a local p_0-value, which gives the expected probability of observing a fluctuation that is at least as far from the SM expectation as the observed number of data events in a given region, if the experiment were to be repeated. A possible definition of the local p_0-value is:

$$p_0 = 2 \cdot \min\left[P(n \leq N_{\text{obs}}),\ P(n \geq N_{\text{obs}}) \right] \tag{1}$$

$$P(n \leq N_{\text{obs}}) = \int_0^\infty \mathrm{d}x\, G(x; N_{\text{SM}}, \delta N_{\text{SM}}) \cdot \sum_{n=0}^{N_{\text{obs}}} \frac{\mathrm{e}^{-x} x^n}{n!} + \int_{-\infty}^0 \mathrm{d}x\, G(x; N_{\text{SM}}, \delta N_{\text{SM}}) \tag{2}$$

$$P(n \geq N_{\text{obs}}) = \int_0^\infty \mathrm{d}x\, G(x; N_{\text{SM}}, \delta N_{\text{SM}}) \cdot \sum_{n=N_{\text{obs}}}^{\infty} \frac{\mathrm{e}^{-x} x^n}{n!} \tag{3}$$

where n is the independent variable of the Poisson probability mass function (pmf), N_{obs} is the observed number of data events for a given selection, $P(n \leq N_{\text{obs}})$ is the probability of observing no more than the number of events observed in the data and $P(n \geq N_{\text{obs}})$ is the probability of observing at least the number of events observed in the data. The quantity N_{SM} is the expectation for the number of events with its total uncertainty δN_{SM} for a given selection. The convolution of the Poisson pmf (with mean x) with a Gaussian probability density function (pdf), $G(x; N_{\text{SM}}, \delta N_{\text{SM}})$ with mean N_{SM} and width δN_{SM}, takes the effect of both non-negligible systematic uncertainties and statistical uncertainties into account.[2] If the Gaussian pdf G is replaced by a Dirac delta function $\delta(x - N_{\text{SM}})$ the estimator p_0 results in the usual Poisson probability. The selection with the largest deviation identified by the algorithm is defined as the selection giving the smallest p_0-value. The smallest p_0 for a given channel is defined as p_{channel}, which therefore corresponds to the local p_0-value of the largest deviation in that channel.

Data selections are not considered in the scan if large uncertainties in the expectation arise due to a lack of MC events, or from large systematic uncertainties. To avoid overlooking potential excesses in these selections the p_0-values of selections with more than three data events are monitored separately.

The result of scanning the distributions for all event classes is a list of data selections, one per event class containing the largest deviation in that class, and their local statistical significance. Details of the procedure and the statistical algorithm used for the 2015 dataset are explained in Section 3.3.

2.4 Step 4: Generation of pseudo-experiments

The probability that for a given observable one or more deviations of a certain size occur somewhere in the event classes considered is modelled by pseudo-experiments. Each pseudo-experiment consists of exactly the same event classes as those considered when applying the search algorithm to data. However, the data counts are replaced by pseudo-data counts which are generated from the SM expectation using an MC technique. Pseudo-data distributions are produced taking into account both statistical and systematic uncertainties by drawing pseudo-random data counts for each bin from the convolved pmf used in Eqs. (1)–(3) to compute a p_0-value.

Correlations in the uncertainties of the SM expectation affect the chance of observing one or more deviations of a given size. The effect of correlations between bins of the same distribution or between distributions of different event classes are therefore taken into account when generating pseudo-data for pseudo-experiments. Correlations between distributions of different observables are not taken into account, since the results obtained for different observables are not combined in the interpretation.

The search algorithm is then applied to each of the distributions, resulting in a p_{channel}-value for each event class. The p_{channel} distributions of many pseudo-experiments and their statistical properties can be compared with the p_{channel} distribution obtained from data to interpret the test statistics in a frequentist manner. The fraction of pseudo-experiments having one of the p_{channel}-values smaller than a given value

---

[2] The second term in Eq. (2) gives the probability of observing no events given a negative expectation from downward variations of the systematic uncertainties. It can be derived as follows:

$$\int_{-\infty}^{0} dx\, G(x; N_{\text{SM}}, \delta N_{\text{SM}}) \cdot \sum_{n=0}^{N_{\text{obs}}} \lim_{\mu \to 0} \left(\frac{e^{-\mu} \mu^n}{n!} \right) = \int_{-\infty}^{0} dx\, G(x; N_{\text{SM}}, \delta N_{\text{SM}}) \cdot \sum_{n=0}^{N_{\text{obs}}} \delta_{n0} = \int_{-\infty}^{0} dx\, G(x; N_{\text{SM}}, \delta N_{\text{SM}})$$

where μ is the mean of the Poisson pmf and $\delta_{n0} = \{1 \text{ if } n = 0,\ 0 \text{ if } n \neq 0\}$ is the Kronecker delta. In Eq. (3) this term vanishes for $N_{\text{obs}} > 0$.

$p_{\min}$ indicates the probability of observing such a deviation by chance, taking into account the number of selections and event classes tested.
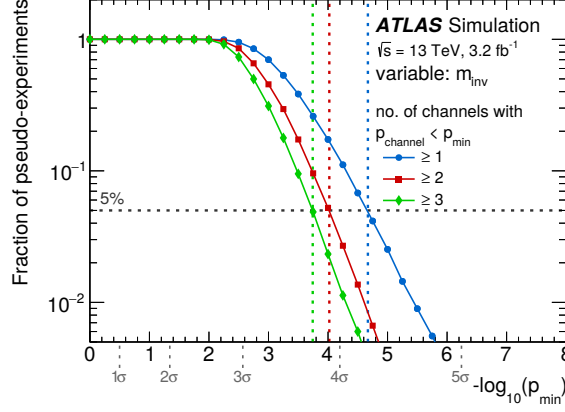

Figure 1: The fractions of pseudo-experiments ($P_{\exp,i}(p_{\min})$) in the m_{inv} scan, which have at least one, two or three p_{channel}-values smaller than a given threshold ($p_{\min}$). Pseudo-datasets are generated from the SM expectation. Dotted lines are drawn at $P_{\exp,i} = 5\%$ and at the corresponding $-\log_{10}(p_{\min})$-values.

To illustrate this, Figure 1 shows three cumulative distributions of p_{channel}-values from pseudo-experiments. The number of event classes (686) and the m_{inv} distributions used to generate these pseudo-experiments coincide with the example application in Section 3. The distribution in Figure 1 with circular markers is the fraction of pseudo-experiments with at least one p_{channel}-value smaller than $p_{\min}$. For example, about 15% of the pseudo-experiments have at least one p_{channel}-value smaller than $p_{\min} = 10^{-4}$. Therefore, the estimated probability ($P_{\exp,i}$) of obtaining a single p_{channel}-value ($i = 1$) smaller than 10^{-4} from data in the absence of a signal is about 15%, or $P_{\exp,1}(10^{-4}) = 0.15$. To estimate the probability of observing deviations of a given size in at least two or three different event classes, the second or third smallest p_{channel}-value of a pseudo-experiment is compared with a given $p_{\min}$ threshold. From Figure 1 it follows for instance that 2% of the pseudo-experiments have at least three p_{channel}-values smaller than 10^{-4}. Consequently, the probability of obtaining a third smallest p_{channel}-value smaller than 10^{-4} from data in the absence of a signal is about 2%, or $P_{\exp,3}(10^{-4}) = 0.02$

In Figure 1 a horizontal dotted line is drawn at a fraction of pseudo-experiments of 5% and corresponding vertical dotted lines are drawn at the three $p_{\min}$ thresholds. The observation of one, two or three p_{channel}-values in data below the corresponding $p_{\min}$ threshold, i.e. an observation with a $P_{\exp,i} < 0.05$, promotes the selections that yielded these deviations to signal regions that can be tested in a new dataset.

2.5 Step 5: Evaluation of the sensitivity

The sensitivity of the procedure to a priori unspecified BSM signals can be evaluated with two different methods that either use a modified background estimation through the removal of SM processes or in which signal contributions are added to the pseudo-data sample.

In the first method, a rare SM process (with either a low cross-section or a low reconstruction efficiency) is removed from the background model. The search algorithm is applied again to test the data or 'signal' pseudo-experiments generated from the unmodified SM expectation, against the modified background

expectation. The data samples would be expected to reveal excesses relative to the modified background prediction.

In the second method, pseudo-experiments are used to test the sensitivity of the analysis to benchmark signal models of new physics. The prediction of a model is added to the SM prediction, and this modified expectation is used to generate 'signal' pseudo-experiments. The search algorithm is applied to the pseudo-experiments and the distribution of p_{channel}-values is derived.

To provide a figure of merit for the sensitivity of the analysis, the fraction of 'signal' pseudo-experiments with $P_{\text{exp},i} < 5\%$ for $i = 1, 2, 3$ is computed.

2.6 Step 6: Results

Finding one or more deviations in the data with $P_{\text{exp},i} < 5\%$ triggers a dedicated analysis that uses the data selection in which the deviation is observed as a signal region (step 7). If no significant deviations are found, the outcome of the analysis technique includes information such as: the number of events and expectation per event class, a comparison of the data with the SM expectation in the distributions of observables considered, the scan results (i.e. the location and the local p_0-value of the largest deviation per event class) and the comparison with the expectation from pseudo-experiments.

2.7 Step 7 (only in the case of $P_{\text{exp},i} < 5\%$): Dedicated analysis of deviation

Dedicated analysis on original dataset   Deviations are investigated using methods similar to those of a conventional analysis. In particular, the background prediction is determined using control selections to control and validate the background modelling. Such a procedure further constrains the background expectation and uncertainty, and reduces the dependence on simulation.

Dedicated analysis on an independent dataset   If a deviation persists in a dedicated analysis using the original dataset, the data selection in which the deviation is observed defines a data-derived signal region that is tested in an independent new dataset with a similar or larger integrated luminosity. At this point, a particular model of new physics can be used to interpret the result of testing the data-derived signal region. Since the signal region is known, the corresponding data can be excluded ('blinded') from the analysis until the very end to minimize any possible bias in the analysis. Additionally, since only a few optimized hypothesis tests are performed on the independent dataset, the large look-elsewhere effect due to the large number of hypothesis tests performed in step 3 is not present in the dedicated analysis of the signal region(s).

2.8 Advantages and disadvantages

The features of this strategy lead to several advantages and disadvantages that are outlined below.

Advantages:

- It can find unexpected signals for new physics due to the large number of event classes and phase-space regions probed, which may otherwise remain uninvestigated.

- A relatively small excess in two or three independent data selections, each of which is not big enough to trigger a dedicated analysis by itself ($P_{\mathrm{exp},1} > 5\%$), can trigger one in combination ($P_{\mathrm{exp},2,3} < 5\%$).

- The approach is broad, and the resulting distributions can be used to probe the overall description of the data by the event generators for many SM processes.

- The probability of a deviation occuring in *any* of the many different event classes under study can be determined with pseudo-experiments, resulting in a truly global interpretation of the probability of finding a deviation within an experiment such as ATLAS.

Disadvantages:

- The outcome depends on the MC-based description of physics processes and simulations of the detector response. Event classes in which the majority of the events contain misreconstructed objects are typically poorly modelled by MC simulation and might need to be excluded from the analysis. Although step 2 validates the description of the data by the MC simulation, there is still a possibility of triggering false positives due to an MC mismodelling in a corner of phase space. Step 7 aims to minimize this by reducing the dependence on MC simulations in a dedicated analysis performed for each significant deviation. In future implementations a better background model could be constructed with the help of control regions or data-derived fitting functions. This might allow the detection of excesses which are small compared to the uncertainties in the MC-based description of the SM processes.

- Since this analysis is not optimized for a specific class of BSM signals, a dedicated analysis optimized for a given BSM signal achieves a larger sensitivity to that signal. The enormous parameter space of possible signals makes an optimized search for each of them impossible.

- The large number of data selections introduce a large look-elsewhere effect, which reduces the significance of a real signal. Step 7 circumvents this problem since the final discovery significance is determined with a dedicated analysis of one or a few data selection(s) and a statistically independent dataset. This can yield an improved signal sensitivity if the background uncertainty can be constrained in the dedicated analysis.

- Despite being broad, the procedure might miss a certain signal because it does not show a localized excess in one of the studied distributions. As an example this strategy is largely insensitive to BSM processes resulting in small overall normalization differences in large cross-section processes such as multijet production. This might be overcome with better observables or modified algorithms, which may then be sensitive to such signals.

3 Application of the strategy to ATLAS data

This section describes the application of the strategy outlined in the previous section to the 13 TeV *pp* collision data recorded by the ATLAS experiment in 2015.

3.1 Step 1: Data selection and Monte Carlo simulation

3.1.1 ATLAS detector and dataset

The ATLAS detector [11] is a multipurpose particle physics detector with a forward-backward symmetric cylindrical geometry and a coverage of nearly 4π in solid angle.[3] The inner tracking detector (ID) consists of silicon pixel and microstrip detectors covering the pseudorapidity region $|\eta| < 2.5$, surrounded by a straw-tube transition radiation tracker which enhances electron identification in the region $|\eta| < 2.0$. Between Run 1 and Run 2, a new inner pixel layer, the insertable B-layer [12], was inserted at a mean sensor radius of 3.3 cm. The inner detector is surrounded by a thin superconducting solenoid providing an axial 2 T magnetic field and by a fine-granularity lead/liquid-argon (LAr) electromagnetic calorimeter covering $|\eta| < 3.2$. A steel/scintillator-tile calorimeter provides hadronic coverage in the central pseudorapidity range ($|\eta| < 1.7$). The endcap and forward calorimeter coverage ($1.5 < |\eta| < 4.9$) is completed by LAr active layers with either copper or tungsten as the absorber material. An extensive muon spectrometer with an air-core toroid magnet system surrounds the calorimeters. Three layers of high-precision tracking chambers provide coverage in the range $|\eta| < 2.7$, while dedicated fast chambers provide a muon trigger in the region $|\eta| < 2.4$. The ATLAS trigger system consists of a hardware-based level-1 trigger followed by a software-based high-level trigger [13].

The data used in this analysis were collected by the ATLAS detector during 2015 in pp collisions at the LHC with a centre-of-mass energy of 13 TeV and a 25 ns bunch crossing interval. After applying quality criteria for the beam, data and detector, the available dataset corresponds to an integrated luminosity of 3.2 fb^{-1}. In this dataset, each event includes an average of approximately 14 additional inelastic pp collisions in the same bunch crossing (pile-up).

Candidate events are required to have a reconstructed vertex [14], with at least two associated tracks with $p_T > 400$ MeV. The vertex with the highest sum of squared transverse momenta of the tracks is considered to be the primary vertex.

3.1.2 Monte Carlo samples

Monte Carlo simulated event samples [15] are used to describe SM background processes and to model possible signals. The ATLAS detector is simulated either by a software system based on GEANT4 [16] or by a faster simulation based on a parameterization of the calorimeter response and GEANT4 for the other detector systems. To account for additional pp interactions from the same or nearby bunch crossings, a set of minimum-bias interactions generated using PYTHIA 8.186 [17], the MSTW2008LO [18] parton distribution function (PDF) set and the A2 set of tuned parameters (tune) [19] was superimposed onto the hard-scattering events to reproduce the observed distribution of the average number of interactions per bunch crossing. In all MC samples, except those produced by SHERPA [20], the EVTGEN v1.2.0 program [21] was used to model the properties of the bottom and charm hadron decays. The SM MC programs are listed in Table 1 and a detailed explanation can be found in Appendix A.1.

---

[3] ATLAS uses a right-handed coordinate system with its origin at the nominal interaction point in the centre of the detector. The positive x-axis is defined by the direction from the interaction point to the centre of the LHC ring, with the positive y-axis pointing upwards, while the beam direction defines the z-axis. Cylindrical coordinates (r, ϕ) are used in the transverse plane, ϕ being the azimuthal angle around the z-axis. The pseudorapidity η is defined in terms of the polar angle θ by $\eta = -\ln\tan(\theta/2)$. The angular distance is defined as $\Delta R = \sqrt{(\Delta\eta)^2 + (\Delta\phi)^2}$. Rapidity is defined as $y = 0.5 \cdot \ln[(E + p_z)/(E - p_z)]$ where E denotes the energy and p_z is the component of the momentum along the beam direction.

Table 1: A summary of the MC samples used in the analysis to model SM background processes. For each sample the corresponding generator, matrix element (ME) accuracy, parton shower, cross-section normalization accuracy, PDF set and tune are indicated. Details are given in Appendix A.1. Samples with 'data' in the 'cross-section normalization' column are scaled to data as described in Section 3.2.3. Z refers to γ^*/Z.

Physics process	Generator	ME accuracy	Parton shower	Cross-section normalization	PDF set	Tune
$W\,(\to\ell\nu)$ + jets	Sherpa 2.1.1	0,1,2j@NLO + 3,4j@LO	Sherpa 2.1.1	NNLO	NLO CT10	Sherpa default
$Z\,(\to\ell^+\ell^-)$ + jets	Sherpa 2.1.1	0,1,2j@NLO + 3,4j@LO	Sherpa 2.1.1	NNLO	NLO CT10	Sherpa default
$Z/W\,(\to q\bar{q})$ + jets	Sherpa 2.1.1	1,2,3,4j@LO	Sherpa 2.1.1	NNLO	NLO CT10	Sherpa default
$Z/W + \gamma$	Sherpa 2.1.1	0,1,2,3j@LO	Sherpa 2.1.1	NLO	NLO CT10	Sherpa default
$Z/W + \gamma\gamma$	Sherpa 2.1.1	0,1,2,3j@LO	Sherpa 2.1.1	NLO	NLO CT10	Sherpa default
γ + jets	Sherpa 2.1.1	0,1,2,3,4j@LO	Sherpa 2.1.1	data	NLO CT10	Sherpa default
$\gamma\gamma$ + jets	Sherpa 2.1.1	0,1,2j@LO	Sherpa 2.1.1	data	NLO CT10	Sherpa default
$\gamma\gamma\gamma$ + jets	MG5_aMC@NLO 2.3.3	0,1j@LO	Pythia 8.212	LO	NNPDF23LO	A14
$t\bar{t}$	Powheg-Box v2	NLO	Pythia 6.428	NNLO+NNLL	NLO CT10	Perugia 2012
$t\bar{t} + W$	MG5_aMC@NLO 2.2.2	0,1,2j@LO	Pythia 8.186	NLO	NNPDF2.3LO	A14
$t\bar{t} + Z$	MG5_aMC@NLO 2.2.2	0,1j@LO	Pythia 8.186	NLO	NNPDF2.3LO	A14
$t\bar{t} + WW$	MG5_aMC@NLO 2.2.2	LO	Pythia 8.186	NLO	NNPDF2.3LO	A14
$t\bar{t} + \gamma$	MG5_aMC@NLO 2.2.2	LO	Pythia 8.186	LO	NNPDF2.3LO	A14
$t\bar{t} + b\bar{b}$	Sherpa 2.2.0	NLO	Sherpa 2.2.0	NLO	NLO CT10f4	Sherpa default
Single-top (t-channel)	Powheg-Box v1	NLO	Pythia 6.428	app. NNLO	NLO CT10f4	Perugia 2012
Single-top (s- and Wt-channel)	Powheg-Box v2	NLO	Pythia 6.428	app. NNLO	NLO CT10	Perugia 2012
tZ	MG5_aMC@NLO 2.2.2	LO	Pythia 8.186	LO	NNPDF2.3LO	A14
3-top	MG5_aMC@NLO 2.2.2	LO	Pythia 8.186	LO	NNPDF2.3LO	A14
4-top	MG5_aMC@NLO 2.2.2	LO	Pythia 8.186	NLO	NNPDF2.3LO	A14
WW	Sherpa 2.1.1	0j@NLO + 1,2,3j@LO	Sherpa 2.1.1	NLO	NLO CT10	Sherpa default
WZ	Sherpa 2.1.1	0j@NLO + 1,2,3j@LO	Sherpa 2.1.1	NLO	NLO CT10	Sherpa default
ZZ	Sherpa 2.1.1	0,1j@NLO + 2,3j@LO	Sherpa 2.1.1	NLO	NLO CT10	Sherpa default
Multijets	Pythia 8.186	LO	Pythia 8.186	data	NNPDF2.3LO	A14
Higgs (ggF/VBF)	Powheg-Box v2	NLO	Pythia 8.186	NNLO	NLO CT10	AZNLO
Higgs ($t\bar{t}H$)	MG5_aMC@NLO 2.2.2	NLO	Herwig++	NNLO	NLO CT10	UEEE5
Higgs (W/ZH)	Pythia 8.186	LO	Pythia 8.186	NNLO	NNPDF2.3LO	A14
Tribosons	Sherpa 2.1.1	0,1,2j@LO	Sherpa 2.1.1	NLO	NLO CT10	Sherpa default

In addition to the SM background processes, two possible signals are considered as benchmarks. The first benchmark model considered is the production of a new heavy neutral gauge boson of spin 1 (Z'), as predicted by many extensions of the SM. Here, the specific case of the sequential extension of the SM gauge group (SSM) [22, 23] is considered, for which the couplings are the same as for the SM Z boson. This process was generated at leading order (LO) using PYTHIA 8.212 with the NNPDF23LO [24] PDF set and the A14 tune [25], as a Drell–Yan process, for five different resonant masses, covering the range from 2 TeV to 4 TeV, in steps of 0.5 TeV. The considered decays of Z' bosons are inclusive, covering the full range of lepton and quark pairs. Interference effects with SM Drell–Yan production are not included, and the Z' boson is required to decay into fermions only.

The second signal considered is the supersymmetric [26–31] production of gluino pairs through strong interactions. The gluinos are assumed to decay promptly into a pair of top quarks and an almost massless neutralino via an off-shell top squark $\tilde{g} \rightarrow tt\tilde{\chi}_1^0$. Samples for this process were generated at LO with up to two additional partons using MG5_aMC@NLO 2.2.2 [32] with the CTEQ6L1 [33] PDF set, interfaced to PYTHIA 8.186 with the A14 tune. The matching with the parton shower was done using the CKKW-L [34] prescription, with a matching scale set to one quarter of the pair-produced resonance mass. The signal cross-sections were calculated at next-to-leading order (NLO) in the strong coupling constant, adding the resummation of soft gluon emission at next-to-leading-logarithm (NLL) accuracy [35–37].

3.1.3 Object reconstruction

Reconstructed physics objects considered in the analysis are: prompt and isolated electrons (e), muons (μ) and photons (γ), as well as b-jets (b) and light (non-b-tagged) jets (j) reconstructed with the anti-k_t algorithm [38] with radius parameter $R = 0.4$, and large missing transverse momentum (E_T^{miss}). Table 2 lists the reconstructed physics objects along with their p_T and pseudorapidity requirements. Jets and electrons misidentified as hadronically decaying τ-leptons are difficult to model with the MC-based approach used in this analysis. Therefore, the identification of hadronically decaying τ-leptons is not considered; they are mostly reconstructed as light jets. Details of the object reconstruction can be found in Appendix B.

Table 2: The physics objects used for classifying the events, with their corresponding label, minimum p_T requirement, and pseudorapidity requirement.

Object	Label	p_T (min) [GeV]	Pseudorapidity
Isolated electron	e	25	$|\eta| < 1.37$ or $1.52 < |\eta| < 2.47$
Isolated muon	μ	25	$|\eta| < 2.7$
Isolated photon	γ	50	$|\eta| < 1.37$ or $1.52 < |\eta| < 2.37$
b-tagged jet	b	60	$|\eta| < 2.5$
Light (non-b-tagged) jet	j	60	$|\eta| < 2.8$
Missing transverse momentum	E_T^{miss}	200	

After object identification, overlaps between object candidates are resolved using the distance variable $\Delta R_y = \sqrt{(\Delta y)^2 + (\Delta \phi)^2}$. If an electron and a muon share the same ID track, the electron is removed. Any jet within a distance $\Delta R_y = 0.2$ of an electron candidate is discarded, unless the jet has a value of the b-tagging MV2c20 discriminant [39, 40] larger than that corresponding to approximately 85% b-tagging efficiency, in which case the electron is discarded since it probably originated from a semileptonic b-hadron decay. Any remaining electron within $\Delta R_y = 0.4$ of a jet is discarded. Muons within $\Delta R_y = 0.4$ of

a jet are also removed. However, if the jet has fewer than three associated tracks, the muon is kept and the jet is discarded instead to avoid inefficiencies for high-energy muons undergoing significant energy loss in the calorimeter. If a photon candidate is found within $\Delta R_y = 0.4$ of a jet, the jet is discarded. Photons within a cone of size $\Delta R_y = 0.4$ around an electron or muon candidate are discarded.

The missing transverse momentum (with magnitude E_T^{miss}) is defined as the negative vector sum of the transverse momenta of all selected and calibrated physics objects (electrons, photons, muons and jets) in the event, with an additional soft-term [41]. The soft-term is constructed from all tracks that are not associated with any physics object, but are associated with the primary vertex.

3.1.4 Event selection and classification

The events are divided into mutually exclusive classes that are labelled with the number and type of reconstructed objects listed in Table 2. The division can be regarded as a classification according to the most important features of the event. The classification includes all possible final-state configurations and object multiplicities, e.g. if a data event with seven reconstructed muons and no other objects is found, it is classified in a '7-muon' event class (7μ). Similarly an event with missing transverse momentum, two muons, one photon and four jets is classified and considered in the corresponding event class denoted $E_T^{miss}2\mu1\gamma4j$.

All events contributing to a particular event class are also required to be selected by a trigger from a corresponding class of triggers by imposing a hierarchy in the event selection. The flow diagram in Figure 2 gives a graphical representation of the trigger and offline event selection, based on the class of the event. Since the thresholds for the single-photon and single-jet triggers are higher than the p_T requirements in the photon and jet object selection, an additional reconstruction-level p_T cut is imposed to avoid trigger inefficiencies. For the other triggers, the p_T requirements in the object definitions exceed the trigger thresholds by a sufficient margin to avoid additional trigger inefficiencies. Events with $E_T^{miss} > 200$ GeV are required to pass the E_T^{miss} trigger, otherwise they are rejected and not considered for further event selection. If the event has $E_T^{miss} < 200$ GeV but contains an electron with $p_T > 25$ GeV it is required to pass the single-electron trigger. However, events with more than one electron with $p_T > 25$ GeV or with an additional muon with $p_T > 25$ GeV can be selected by the dielectron trigger or electron-muon trigger respectively if the event fails to pass the single-electron trigger. Events with a muon with $p_T > 25$ GeV but no reconstructed electrons or large E_T^{miss} are required to pass the single-muon trigger. If the event has more than one muon with $p_T > 25$ GeV and fails to pass the single-muon trigger, it can additionally be selected by the dimuon trigger. Remaining events with a photon with $p_T > 140$ GeV or two photons with $p_T > 50$ GeV are required to pass the single-photon or diphoton trigger, respectively. Finally, any remaining event with no large E_T^{miss}, leptons, or photons, but containing a jet with $p_T > 500$ GeV is required to pass the single-jet trigger.

In addition to the thresholds imposed by the trigger, a further selection is applied to event classes with $E_T^{miss} < 200$ GeV containing one lepton or one electron and one muon and possibly additional photons or jets ($1\mu + X$, $1e + X$ and $1\mu1e + X$), to reduce the overall data volume. In these event classes, one lepton is required to have $p_T > 100$ GeV if the event has less than three jets with $p_T > 60$ GeV.

To suppress sources of fake E_T^{miss}, additional requirements are imposed on events to be classified in E_T^{miss} categories. The ratio of E_T^{miss} to m_{eff} is required to be greater than 0.2, and the minimum azimuthal separation between the E_T^{miss} direction and the three leading reconstructed jets (if present) has to be greater than 0.4, otherwise the event is rejected.
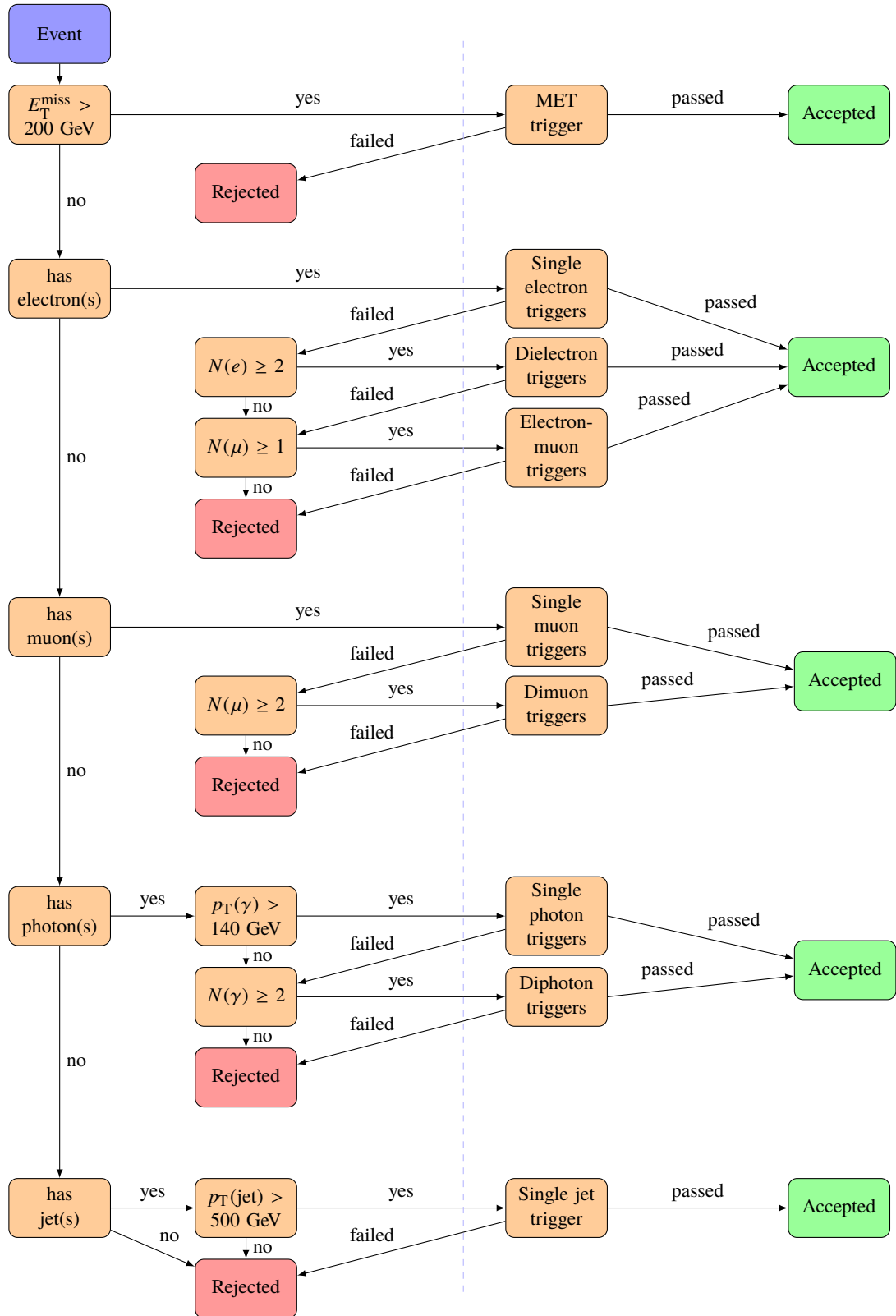
Figure 2: Flow diagram for the trigger and offline event selection strategy. The offline requirements are shown on the left of the dashed line and the trigger requirements are shown on the right of the dashed line.

3.2 Step 2: Systematic uncertainties and validation

3.2.1 Systematic uncertainties

Experimental uncertainties The dominant experimental systematic uncertainties in the SM expectation for the different event classes are the jet energy scale (JES) and resolution (JER) [42] and the scale and resolution of the E_T^miss soft-term. The uncertainty related to the modelling of E_T^miss in the simulation is estimated by propagating the uncertainties in the energy and momentum scale of each of the objects entering the calculation, with an additional uncertainty in the resolution and scale of the soft-term [41]. The uncertainties in the b-tagging scale factors are determined in data samples enriched in top quark decays, and in simulated events [39]. Leptonic decays of J/ψ mesons and Z bosons in data and simulation are exploited to estimate the uncertainties in lepton reconstruction, identification, momentum/energy scale and resolution, and isolation criteria [43–45]. Photon reconstruction and identification efficiencies are evaluated from samples of $Z \to ee$ and $Z + \gamma$ events [45, 46]. The luminosity measurement was calibrated during dedicated beam-separation scans, using the same methodology as that described in Ref. [47]. The uncertainty of this measurement is found to be 2.1%.

In total, 35 sources of experimental uncertainties are identified pertaining to one or more physics objects considered. For each source the one-standard-deviation (1σ) confidence interval (CI) is propagated to a 1σ CI around the nominal SM expectation. The total experimental uncertainty of the SM expectation is obtained from the sum in quadrature of these 35 1σ CIs and the uncertainty of the luminosity measurement.

Theoretical modelling uncertainties Two different sources of uncertainty in the theoretical modelling of the SM production processes are considered. A first uncertainty is assigned to account for our knowledge of the cross-sections for the inclusive processes. A second uncertainty is used to cover the modelling of the shape of the differential cross-sections. In order to derive the modelling uncertainties, either variations of the QCD factorization, renormalization, resummation and merging scales are used or comparisons of the nominal MC samples with alternative ones are used. For some SM processes additional modelling uncertainties are included. Appendix A.2 describes all theoretical uncertainties considered for the various SM processes. The total uncertainty is taken as the sum in quadrature of the two components and the statistical uncertainty of the MC prediction.

3.2.2 Validation procedures

The evaluated SM processes, together with their standard selection cuts and the studied validation distributions, are detailed in Table 3. These validation distributions rely on inclusive selections to probe the general agreement between data and simulation and are evaluated in restricted ranges where large new-physics contributions have been excluded by previous direct searches.

There are some cases in which the validation procedure finds modelling problems and MC background corrections are needed (multijets, $\gamma(\gamma)$ + jets). In other cases, the affected event classes are excluded from the analysis as their SM expectation mostly arises from object misidentification (e.g. jets reconstructed as electrons) which is poorly modelled in MC simulation. The excluded classes are: $1e1j$, $1e2j$, $1e3j$, $1e4j$, $1e1b$, $1e1b1j$, $1e1b2j$, $1e1b3j$. Event classes containing a single object, as well as those containing only E_T^miss and a lepton are also discarded from the analysis.

Table 3: A summary of the SM processes and their inclusive selections used to validate the background modelling. For each selection the p_T, η, and ϕ distributions of the objects used in the selection and of additional jets are included as validation distributions by default. Additional validation distributions are listed per selection. In all cases, 'jet(s)' refers to both b-tagged and non-b-tagged jets, except where 'b-jet' is mentioned explicitly. H_T(jets) is defined as the scalar p_T sum of all the jets in the event. Some selections rely on the transverse mass ($m_T(\ell, E_T^{miss})$) which is defined as $[2\, p_T(\ell)\, E_T^{miss}\, (1 - \cos \Delta\phi(\ell, E_T^{miss}))]^{1/2}$. $N((b\text{-})\text{jets})$ is the number of (b-)jets in an event. For the distance variables ΔR and $\Delta\phi$, the two instances of the objects with the minimum distance between them are used. The H_T(jets), $m_T(\ell, E_T^{miss})$, $p_T(\ell\ell)$ and m_{inv} validation distributions are evaluated in restricted ranges where large new-physics contributions have been excluded by previous direct searches. Same-flavour opposite-charge sign lepton pairs are referred to as SFOS pairs.

Physics process	Event selection	Additional validation distributions
$W(\to \ell\nu)$ + jets	1 lepton, $E_T^{miss} > 25$ GeV and $m_T(\ell, E_T^{miss}) > 50$ GeV	$N(\text{jets})$ $N(b\text{-jets})$ $m_T(\ell, E_T^{miss})$ $H_T(\text{jets})$ $\Delta R(\ell, \text{jet})$ $\Delta\phi(\ell, E_T^{miss})$ $\Delta\phi(\text{jet}, E_T^{miss})$
	& $N(\text{jets}) \geq 3$	$H_T(\text{jets})$
	& $N(b\text{-jets}) \geq 1$	$m_T(\ell, E_T^{miss})$
	& $N(b\text{-jets}) \geq 2$	$m_T(\ell, E_T^{miss})$
$Z(\to \ell\ell)$ + jets	1 SFOS pair $66 < m_{inv}(\ell\ell) < 116$ GeV	$N(\text{jets})$ $N(b\text{-jets})$ $m_{inv}(\ell\ell)$ $p_T(\ell\ell)$ $H_T(\text{jets})$ $\Delta R(\ell, \ell)$ $\Delta R(\ell, \text{jet})$
	& $N(\text{jets}) \geq 2$	$H_T(\text{jets})$
	& $N(b\text{-jets}) \geq 1$	$m_{inv}(\ell\ell)$ $p_T(\ell\ell)$
	& $N(b\text{-jets}) \geq 2$	$m_{inv}(\ell\ell)$ $p_T(\ell\ell)$
$W + \gamma(\gamma)$	same selection as $W(\to \ell\nu)$ + jets and 1(2) additional photon(s)	same distributions as $W(\to \ell\nu)$ + jets and $\Delta R(\ell, \gamma)$
$Z + \gamma(\gamma)$	same selection as $Z(\to \ell\ell)$ + jets and 1(2) additional photon(s)	same distributions as $Z(\to \ell\ell)$ + jets and $\Delta R(\ell, \gamma)$
$\gamma(\gamma)$ + jets	1(2) photon(s), no leptons and at least 1(0) jet(s)	$N(\text{jets})$ $N(b\text{-jets})$ $H_T(\text{jets})$ $m_{inv}(\gamma\gamma)$ $\Delta R(\gamma, \gamma)$ $\Delta R(\gamma, \text{jet})$
$t\bar{t} \to$ $W(\to jj)+$ $W(\to \ell\nu)+$ $b\bar{b}$	1 lepton, at least 2 b-jets and at least 2 light jets $50 < m_{inv}(jj) < 110$ GeV electron channel: $m_T(e, E_T^{miss}) > 50$ GeV muon channel: $m_T(\mu, E_T^{miss}) > 60$ GeV $E_T^{miss} > 40$ GeV	$N(\text{jets})$ $N(b\text{-jets})$ $m_{inv}(jj)$ $m_T(\ell, E_T^{miss})$ $\Delta R(\text{jet}, \text{jet})$ $\Delta R(\ell, \text{jet})$
Diboson		
WW	1 electron and 1 muon of opposite charge and no jets $E_T^{miss} > 50$ GeV	
WZ	1 SFOS pair ($\ell\ell$) and 1 lepton of different flavour (ℓ') $66 < m_{inv}(\ell\ell) < 116$ GeV $E_T^{miss} > 50$ GeV and $m_T(\ell', E_T^{miss}) > 50$ GeV	$m_{inv}(\ell\ell)$ (SFOS pair(s)) $p_T(\ell\ell)$ (SFOS pair(s)) $m_T(\ell', E_T^{miss})$ $\Delta R(\ell, \ell)$ $\Delta\phi(\ell, E_T^{miss})$
ZZ	2 SFOS pairs $66 < m_{inv}(\ell\ell) < 116$ GeV (both SFOS pairs)	
Multijets	at least 2 jets no leptons or photons	$N(\text{jets})$ $N(b\text{-jets})$ $\Delta R(\text{jet}, \text{jet})$ E_T^{miss}/m_{eff}

3.2.3 Corrections to the MC background

The MC samples for multijet and γ + jets production, while giving a good description of kinematic variables, predict an overall cross-section and a jet multiplicity distribution that disagrees with data. Following step 2, correction procedures were applied.

In classes containing only j and b the multijet MC samples are scaled to data with normalization factors ranging between approximately 0.8 and 1.2. The normalization factors are derived separately in each exclusive jet multiplicity class by equating the expected total number of events to the observed number of events. If a channel contains less than five data events, no modifications are made.

For γ + jets event classes the same rescaling procedure is applied to classes with exactly one photon, no leptons or $E_{\mathrm{T}}^{\mathrm{miss}}$, and any number of jets.

The SHERPA 2.1.1 MC generator has a known deficiency in the modelling of $E_{\mathrm{T}}^{\mathrm{miss}}$ due to too large forward jet activity. This results in a visible mismodelling of the $E_{\mathrm{T}}^{\mathrm{miss}}$ distribution in event classes with two photons, which also affects the m_{eff} distribution. To correct for this mismodelling a reweighting [48] is applied to the background events containing two real photons ($\gamma\gamma$ + jets). The diphoton MC events are reweighted as a function of $E_{\mathrm{T}}^{\mathrm{miss}}$ and of the number of selected jets to match the respective distributions in the data for the inclusive diphoton sample in the range $E_{\mathrm{T}}^{\mathrm{miss}} < 100$ GeV. In no other event classes was the mismodeling large enough to warrant such a procedure.

3.2.4 Comparison of the event yields with the MC prediction

After classification, 704 event classes are found with at least one data event or an SM expectation greater than 0.1 events. The data and the background predictions from MC simulation for these classes are shown in Figure 3 and Appendix C. Agreement is observed between data and the prediction in most of the event classes. In events classes having more than two b-jets and where the SM expectation is dominated by $t\bar{t}$ production, the nominal SM expectation is systematically slightly below the data. Data events are found in 528 out of 704 event classes. These include events with up to four leptons (muons and/or electrons), three photons, twelve jets and eight b-jets. There are 18 event classes with an SM expectation of less than 0.1 events; no more than two data events are observed in any of these, and they are not considered further in the analysis. The remaining 686 classes are retained for statistical analysis.

3.3 Step 3: Sensitive variables and search algorithm

In order to quantitatively determine the level of agreement between the data and the SM expectation, and to identify regions of possible deviations, this analysis uses an algorithm for multiple hypothesis testing. The algorithm locates a single region of largest deviation for specific observables in each event class.

In the following, an algorithm derived from the algorithm used in Ref. [5] is applied to the 2015 dataset.
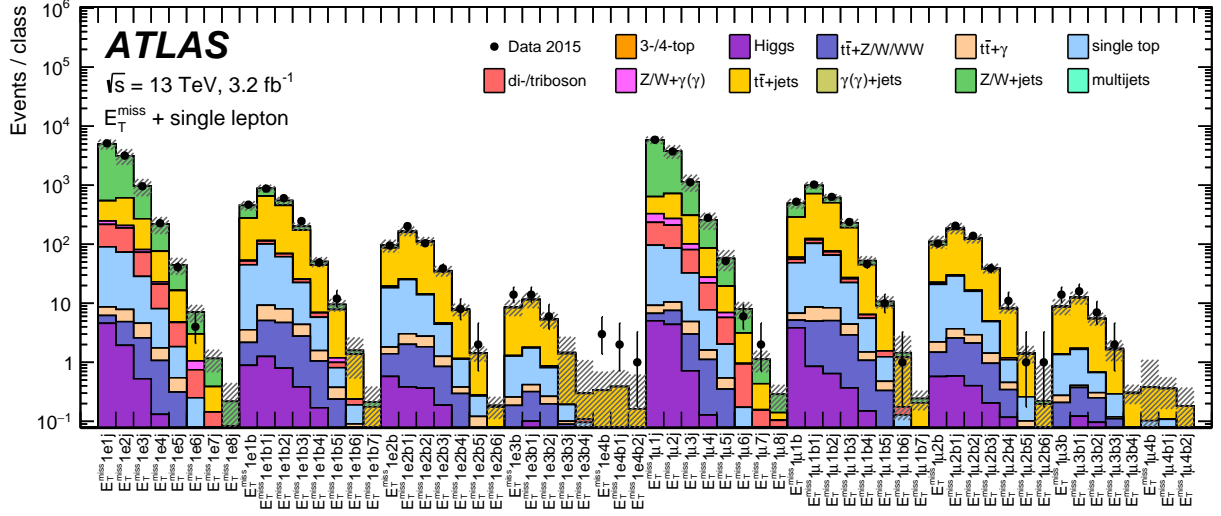
Figure 3: The number of events in data, and for the different SM background predictions considered, for classes with large E_T^{miss}, one lepton and (b-)jets (no photons). The classes are labelled according to the multiplicity and type (e, μ, γ, j, b, E_T^{miss}) of the reconstructed objects for the given event class. The hatched bands indicate the total uncertainty of the SM prediction. This figure shows 60 out of 704 event classes, the remaining event classes can be found in Figures 11–23 of Appendix C.

3.3.1 Choice of variables

For each event class, the m_{eff} and m_{inv} distributions are considered in the form of histograms. The invariant mass is computed from all visible objects in the event, with no attempt to use the E_T^{miss} information. These variables have been widely used in searches for new physics, and are sensitive to a large range of possible signals, manifesting either as bumps, deficits or wide excesses. Several other commonly used kinematic variables have also been studied for various models, but were not found to significantly increase the sensitivity. The approach is however not limited to these variables, as discussed in Section 2.

For each histogram, the bin widths $h(x)$ as a function of the abscissa x are determined using:

$$h(x) = \sqrt{\sum_{i=1}^{N_{objects}} k^2 \sigma_i^2(x/2)}$$

where $N_{objects}$ is the number of objects in the event class, $\sigma_i(x/2)$ is the expected detector resolution for the p_T of object i evaluated at $p_T = x/2$ and $\eta = 0$, and k is the width of the bin in standard deviations. An exception to this is the missing transverse momentum resolution ($\sigma_{E_T^{miss}}$), which is a function of $\sum E_T$, where $\sum E_T$ is approximated by the effective mass minus the E_T^{miss} object requirement: $\sigma_{E_T^{miss}} (\sum E_T = x - 200 \text{ GeV})$. The E_T^{miss} object is only considered in the binning of the effective mass histograms. A $\pm 1\sigma$ interval is used for the bin width ($k = 2$) for all objects except for photons and electrons, for which a $\pm 3\sigma$ interval is used ($k = 6$) to avoid having too finely binned histograms with few MC events. This results in variable bin widths with values ranging from 20 GeV to about 2000 GeV. For a given event class, the scan starts at a value of the scanned observable larger than two times the sum of the minimum p_T requirement of each contributing object considered (e.g. 100 GeV for a 2μ class). This minimises spurious deviations which might arise from insufficiently well modelled threshold regions.

17

3.3.2 Algorithm to search for deviations of the data from the expectation

The algorithm identifies the single region with the largest upward or downward deviation in a distribution, provided in the form of a histogram, as the region of interest (ROI). The total number of independent bins is 36936, leading to 518320 combinations of contiguous bins (regions[4]) with an SM expectation larger than 0.01 events. For each region with an SM expectation larger than 0.01, the statistical estimator p_0 is calculated as defined in Eqs. (1)–(3). Here, p_0 is to be interpreted as a local p_0-value. The region of largest deviation found by the algorithm is the region with the smallest p_0-value. Such a method is able to find narrow resonances and single outstanding bins, as well as signals spread over large regions of phase space in distributions of any shape.

To illustrate the operation of the algorithm, six example distributions are presented. Figure 4(a) shows the invariant mass distribution of the event class with one photon, three light jets and large missing transverse momentum ($E_{\mathrm{T}}^{\mathrm{miss}}1\gamma3j$), which has the smallest p_{channel}-value in the m_{inv} scan. Figure 4(b) shows the effective mass distribution of the event class with one muon, one electron, four b-jets and two light jets ($1\mu1e4b2j$), which has the smallest p_{channel}-value in the m_{eff} scan. Figure 4(c) shows the invariant mass distribution of the event class with one electron, one photon, two b-jets and two light jets ($1e1\gamma2b2j$). Figure 4(d) shows the effective mass distribution of the event class with six light jets ($6j$). Figure 4(e) shows the invariant mass distribution of the event class with two muons, a light jet and large missing transverse momentum ($E_{\mathrm{T}}^{\mathrm{miss}}2\mu1j$) and Figure 4(f) shows the effective mass distribution of the event class with three light jets and large missing transverse momentum ($E_{\mathrm{T}}^{\mathrm{miss}}3j$). The regions with the largest deviation found by the search algorithm in these distributions, an excess in Figures 4(a), 4(b), 4(c) and 4(f), and a deficit in Figures 4(d) and 4(e), are indicated by vertical dashed lines.

To minimize the impact of few MC events, 213992 regions where the background prediction has a total relative uncertainty of over 100% are discarded by the algorithm. Discarding a region forces the algorithm to consider a different or larger region in the event class, or if no region in the event class satisfies the condition, to discard the entire event class.[5] For all discarded regions with $N_{\mathrm{obs}} > 3$ a p_0-value is calculated. If the p_0-value is smaller than the p_{channel}-value (or if there is no ROI and hence no p_{channel}-value), it is evaluated manually by comparing it with the distribution of p_{channel}-values from the scan. This is done for 27 event classes among which the smallest p_0-value observed in a discarded region is 0.01. To model the analysis of discarded regions in pseudo-experiments, regions are allowed to have larger uncertainties if they fulfil the $N_{\mathrm{obs}} > 3$ criterion.

In addition to monitoring regions discarded due to a total uncertainty in excess of 100%, regions discarded due to $N_{\mathrm{SM}} < 0.01$ but with $N_{\mathrm{obs}} > 3$ would also be monitored individually; however, no such region has been observed.

Tables 4 and 5 list the three event classes with the largest deviations in the m_{inv} and m_{eff} scans respectively. The largest deviation reported by a dedicated search using the same dataset was observed in an inclusive diphoton data selection at a diphoton mass of around 750 GeV with a local significance of 3.9σ [49]. Due to the different event selections and background estimates the excess has a lower significance in this analysis. The excess was not confirmed in a dedicated analysis with 2016 data [50].

---

[4] A histogram of n bins has 1 region of n contiguous bins, 2 regions of $n-1$ contiguous bins, etc. down to n regions of single bins. Therefore, it has $\sum_{i=1}^{n} i = n(n+1)/2$ regions. When combining bins, background uncertainties are conservatively treated as correlated among the bins.

[5] In the m_{inv} and m_{eff} scan respectively, 72 and 87 event classes are discarded since they have no ROI.
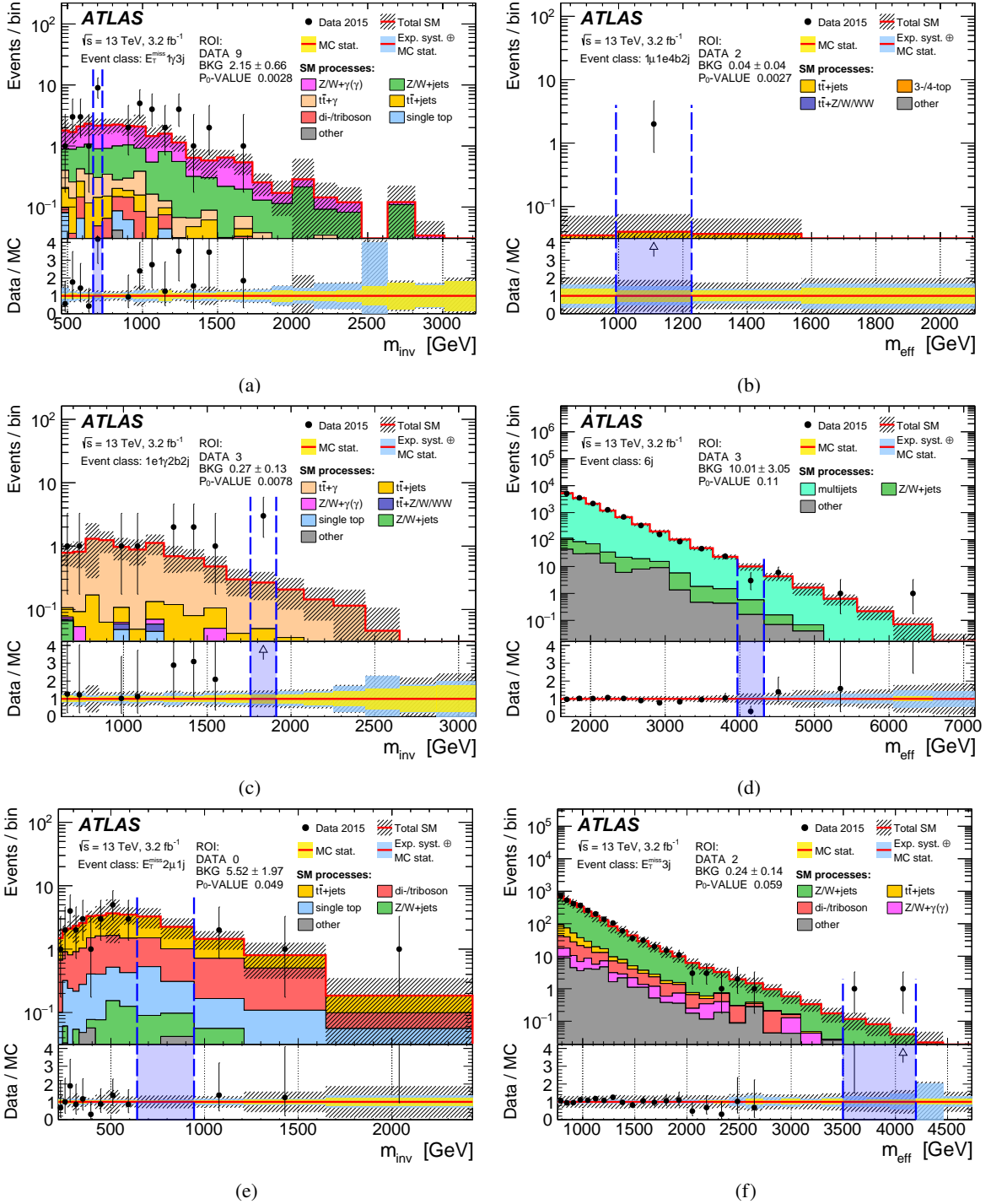
Figure 4: Example distributions showing the region of interest (ROI), i.e. the region with the smallest p_0-value, between the vertical dashed lines. (a) $E_T^{miss}1\gamma3j$ channel, which has the largest deviation in the m_{inv} scan. (b) $1\mu1e4b2j$ channel, which has the largest deviation in the m_{eff} scan. (c) An upward fluctuation in the m_{inv} distribution of the $1e1\gamma2b2j$ channel. (d) A downward fluctuation in the m_{eff} distribution of the $6j$ channel. (e) A downward fluctuation in the m_{inv} distribution of the $E_T^{miss}2\mu1j$ channel. (f) An upward fluctuation in the m_{eff} distribution of the $E_T^{miss}3j$ channel. The hatched band includes all systematic and statistical uncertainties from MC simulations. In the ratio plots the inner solid uncertainty band shows the statistical uncertainty from MC simulations, the middle solid band includes the experimental systematic uncertainty, and the hatched band includes the theoretical systematic uncertainty.

19

Table 4: List of the three channels with the smallest p_{channel}-values in the scan of the m_{inv} distributions.

Channel	p_{channel} $(\cdot 10^{-3})$	N_{obs}	$N_{\text{SM}} \pm \delta N_{\text{SM}}$	Region [GeV]
	Largest deviations in m_{inv} scan			
$E_{\text{T}}^{\text{miss}}\,1\gamma\,3j$	2.81	9	2.15 ± 0.66	670–732
$1\mu\,1e\,4b\,2j$	2.91	2	0.042 ± 0.037	1227–1569
$1e\,1b\,4j$	3.44	160	105 ± 14	726–809

Table 5: List of the three channels with the smallest p_{channel}-values in the scan of the m_{eff} distributions.

Channel	p_{channel} $(\cdot 10^{-3})$	N_{obs}	$N_{\text{SM}} \pm \delta N_{\text{SM}}$	Region [GeV]
	Largest deviations in m_{eff} scan			
$1\mu\,1e\,4b\,2j$	2.66	2	0.040 ± 0.036	992–1227
$1\mu\,1\gamma\,5j$	3.98	4	0.45 ± 0.18	750–895
$3b\,1j$	4.87	4	0.42 ± 0.24	3401–3923

3.4 Step 4: Generation of pseudo-experiments

As described in Section 2.4, pseudo-experiments are generated to derive the probability of finding a p_0-value of a given size, for a given observable and algorithm. The p_{channel}-value distributions of the pseudo-experiments and their statistical properties can be compared with the p_{channel}-value distribution obtained from data. Correlations in the uncertainties of the SM expectation affect this probability and their effect is taken into account in the generation of pseudo-data as outlined in the following.

For the experimental uncertainties, each of the 35 sources of uncertainty is varied independently by drawing a value at random from a Gaussian pdf. This value is assumed to be 100% correlated across all bins and event classes. The uncertainty in the normalization of the various backgrounds is also considered as 100% correlated. Likewise, theoretical shape uncertainties, including those estimated from scale variations or the differences with alternative generators, are assumed to be 100% correlated, with the exception of the uncertainties which are used for some SM processes with small cross-sections. The latter uncertainties are assumed to be uncorrelated, both between event classes and between bins of the same event class. Scale variations are applied in the generation of pseudo-experiments by varying the renormalization, factorization, resummation and merging scales independently. The values for each scale of a given pseudo-experiment are 100% correlated between all bins and event classes. The scales are correlated between processes of the same type which are generated with a similar generator set-up, i.e. scales are correlated among the $W/Z/\gamma$ + jets processes, among all the diboson processes, among the $t\bar{t} + W/Z$ processes, and among the single-top processes.

Changing the size of the theoretical uncertainties by a factor of two leads to a change of less than 5% in the $-\log_{10}(p_{\text{min}})$ thresholds at which a dedicated analysis is triggered. The correlation assumptions in the theoretical uncertainties were also tested. Figure 5 shows the effect of changing the correlation assumption for all theoretical shape uncertainties that are nominally taken as 100% correlated. This test decorrelates the bin-by-bin variations due to the theoretical shape uncertainties in the pseudo-data while retaining the correlation when summing over selected bins in the scan, thus testing the impact of an incorrect assumption in the correlation model. By comparing the nominal assumption of 100% correlation with

a 50% correlated component, and a fully uncorrelated assumption, the threshold at which a dedicated analysis is triggered is changed by a negligible amount.
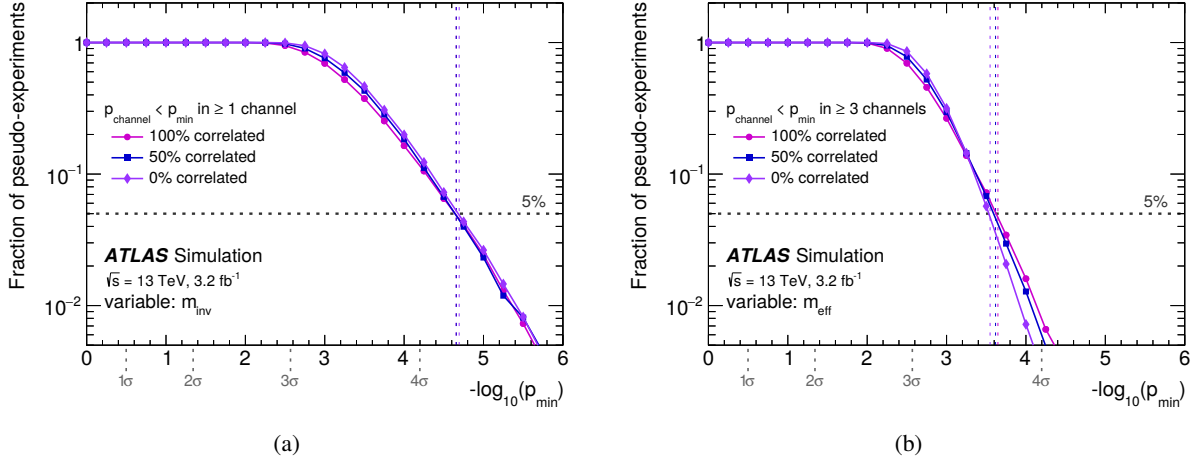

Figure 5: A comparison of different correlation assumptions for scale variations: 100% correlated; 50% correlated and 50% uncorrelated; and 100% uncorrelated. The fractions of pseudo-experiments in the scan of the m_{inv} distribution having at least one p_{channel}-value smaller than p_{min} are shown on the left (a), while the fractions in the scan of the m_{eff} distribution having at least three p_{channel}-values smaller than p_{min} are shown on the right (b).

3.5 Step 5: Evaluation of the sensitivity of the strategy

3.5.1 Sensitivity to Standard Model processes

The sensitivity of the procedure is evaluated with two different methods that either use a modified background estimation through the removal of SM processes or in which signal contributions are added to the pseudo-data sample. As a figure of merit, the fraction of 'signal' pseudo-experiments with $P_{\mathrm{exp},i} < 5\%$ for $i = 1, 2, 3$ is computed.

Figure 6 shows how removing the WZ process from the background prediction affects the three smallest expected p_{channel}-values. In Figures 6(a) and 6(b), the dashed curves show the nominal expected p_{channel} distribution obtained from pseudo-experiments. These define the p_{min} thresholds for which $P_{\mathrm{exp},i} < 5\%$ and vertical dashed lines are drawn at the threshold values. The solid lines show the p_{channel} distributions obtained by testing pseudo-experiments generated from the SM prediction against the modified background prediction which has the WZ diboson process removed. It can be observed that in this case the m_{eff} scan is more sensitive; the fraction of 'signal' pseudo-experiments with $P_{\mathrm{exp},i} < 5\%$ is at least 80% in all three cases $i = 1, 2, 3$.

Additionally, in Figures 6(a) and 6(b), the three smallest p_{channel}-values observed in the data are shown by arrows, both when tested against the full SM prediction (dashed) and when tested against the modified prediction (solid). For all three cases ($i = 1, 2, 3$), $P_{\mathrm{exp},i} < 5\%$ is found again. This means that a dedicated analysis would be performed for the three event classes in which the p_{channel}-values are observed, i.e. 3μ, $1\mu 2e1j$, and $2\mu 1e1j$, likely resulting in the discovery of an unexpected signal due to WZ production. Figures 6(c) and 6(d) shows the m_{eff} distributions of the data with the full SM prediction and the modified prediction respectively. This test uses the conclusion from Section 3.6 and is performed in retrospect. In
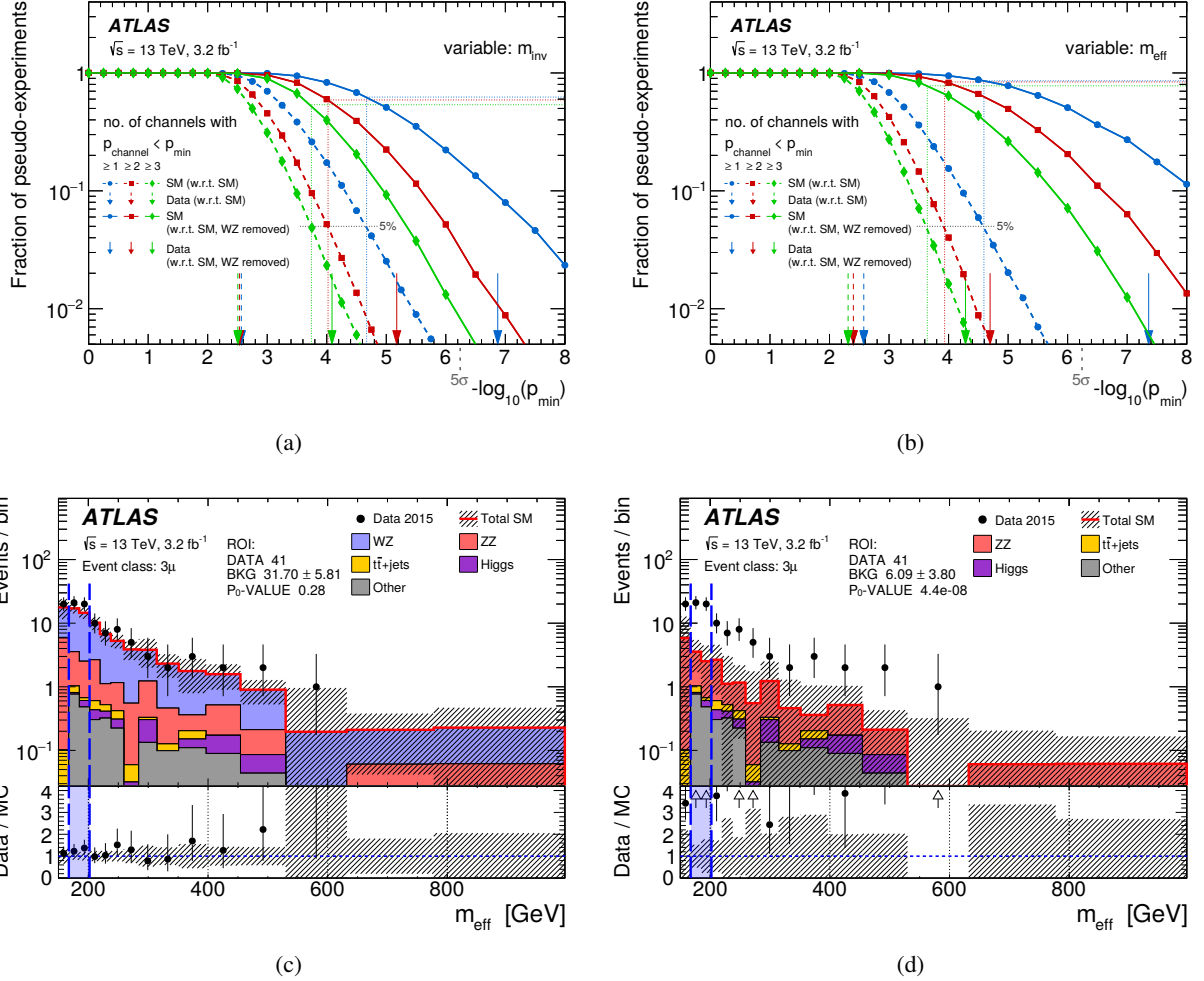
Figure 6: The fraction of pseudo-experiments which have at least one, two and three p_{channel}-values below a given p_{min}, given for both the pseudo-experiments generated from the nominal SM expectation and tested against the nominal expectation (dashed) and for those tested against the modified expectation ('SM, WZ removed') in which the WZ diboson process is removed (solid). The m_{inv} scan is shown in (a) and the m_{eff} scan in (b). The scan results of the data tested against the modified background prediction are indicated with solid arrows. For reference the scan results under the SM hypothesis are plotted as dashed arrows. The largest deviation after removing the WZ process from the background expectation is found in the m_{eff} distribution of the 3μ event class. The distributions of the data and the expectation with both WZ included and WZ removed are shown in (c) and (d) respectively.

the case of a significant deviation, this test would be performed with pseudo-data to assess the sensitivity of the search to a missing background.
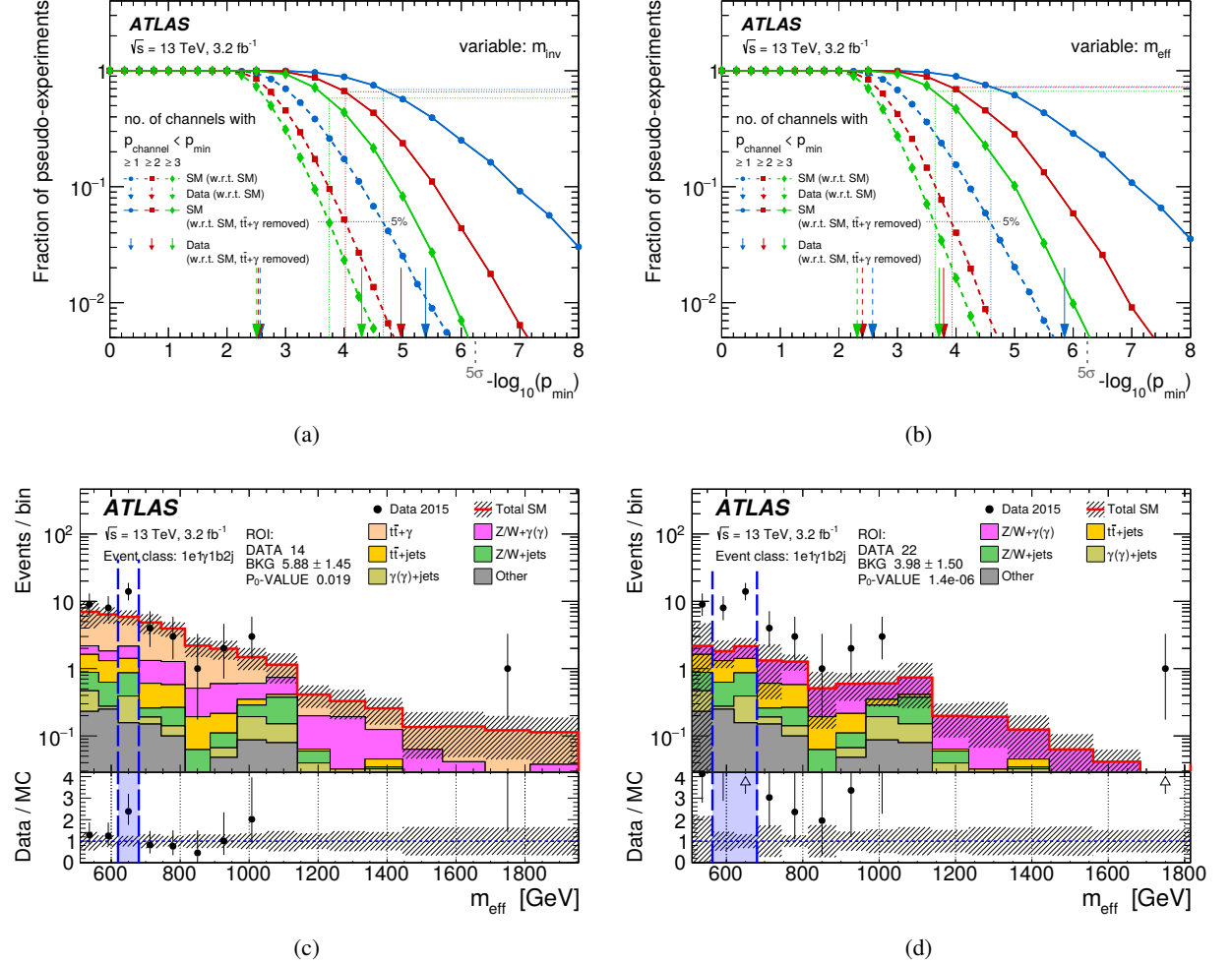

(a)

(b)

(c)

(d)

Figure 7: The fraction of pseudo-experiments which have at least one, two and three p_{channel}-values below a given p_{min}, given for both the pseudo-experiments generated from the nominal SM expectation and tested against the nominal expectation (dashed) and for those tested against the modified expectation ('SM, $t\bar{t}\gamma$ removed') in which the $t\bar{t}\gamma$ process is removed (solid). The m_{inv} scan is shown in (a) and the m_{eff} scan in (b). The scan results of the data tested against the modified background prediction are indicated with solid arrows. For reference the scan results under the SM hypothesis are plotted as dashed arrows. The largest deviation after removing the $t\bar{t}\gamma$ process from the background expectation is found in the m_{eff} distribution of the $1e1\gamma1b2j$ event class. The distributions of the data and the expectation with both $t\bar{t}\gamma$ included and $t\bar{t}\gamma$ removed are shown in (c) and (d) respectively.

Figure 7 shows the effect of removing the $t\bar{t} + \gamma$ process. Again the m_{eff} scan is slightly more sensitive, and at least 70% of 'signal' pseudo-experiments have $P_{\text{exp},i} < 5\%$ in all three cases $i = 1, 2, 3$. In the data, $P_{\text{exp},i} < 5\%$ is found again for all three cases ($i = 1, 2, 3$). A dedicated analysis would be performed for the three classes $1\mu1\gamma2b1j$, $1e1\gamma2b2j$, and $1\mu1\gamma1b3j$, likely resulting in the discovery of an unexpected signal due to $t\bar{t} + \gamma$ production.

It is interesting to note that these discoveries would have been made without a priori knowledge of the existence of these processes.

23

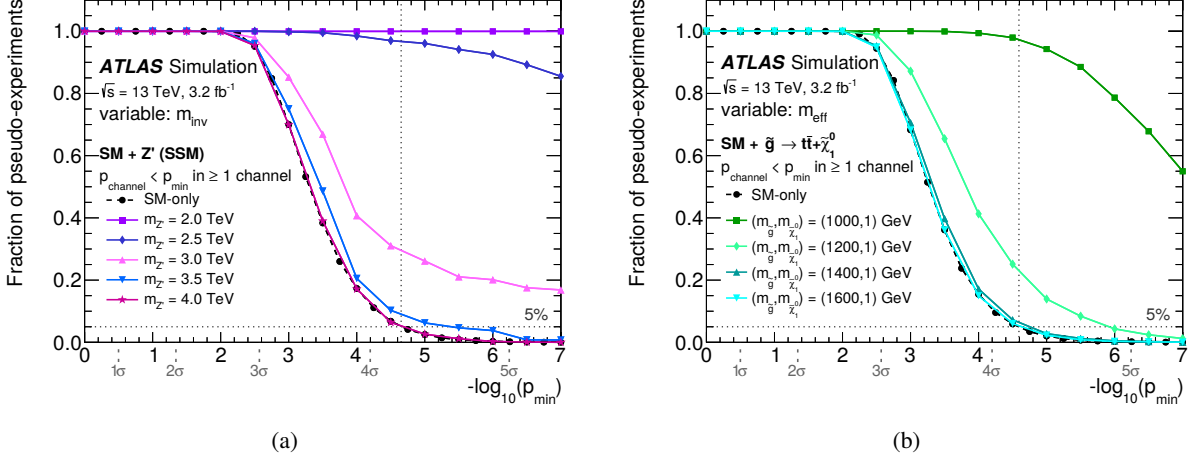### 3.5.2 Sensitivity to new-physics signals

Figure 8: The fraction of pseudo-experiments in which a deviation is found with a $p_{channel}$-value smaller than a given p_{min}. Distributions are shown for pseudo-experiments generated from the SM expectation (circular markers), and after injecting signals of (a) inclusive Z' decays or (b) gluino pairs with $\tilde{g} \to t\bar{t}\tilde{\chi}_1^0$ decays and various masses. The line corresponding to the injection of a Z' boson with a mass of 4 TeV and a gluino with a mass of 1600 GeV overlap with the line obtained from the SM-only pseudo-experiments due to the small signal cross-section.

Figure 8 shows the sensitivity for the two benchmark signals considered as a function of the mass of the produced particle. For the Z' model, where the mass of the resonance can be reconstructed from its decay products, the sensitivity to the signal is found to be the largest in the scan of the m_{inv} distribution. Gluinos undergo a cascade decay process to the lightest neutralino, which is undetected and leads to missing transverse momentum. It is not possible to fully reconstruct an event from gluino pair production due to the presence of neutralinos in the final state. The sensitivity to the gluino signal is therefore found to be the largest in the m_{eff} scan, where a broad excess at large values of this quantity is expected.

Exclusion and discovery sensitivity have to be carefully distinguished when the results of this search are compared with model-based searches. An exclusion sensitivity at the 95% CL in a dedicated search roughly corresponds to a single class having a p_0-value for a discovery test smaller than 0.05. Consequently, the sensitivity to a benchmark signal corresponding to a given particle mass should be compared with the discovery sensitivity of other searches for a Z' boson or gluino.

As previously described, a deviation for which $P_{exp,i} < 5\%$ promotes the selection to a signal region for a dedicated analysis. By applying this sensitivity criterion, it can be seen in Figure 8 that this search is sensitive to a Z' boson with a mass of about 2.5 TeV as more than 90% of the signal-injected pseudo-experiments show a deviation for which $P_{exp,1} < 5\%$. Similar sensitivity is expected for a gluino with a mass of about 1 TeV. The probability of discovering a new-physics signal in a new dataset with a dedicated search in the selected event classes is estimated in the next section.

3.5.3 Sensitivity of a second independent dataset

In step 7 a dedicated analysis of a deviation is performed on an independent dataset. The sensitivity of step 7 is evaluated with pseudo-experiments.

A first pseudo-experiment emulates the original dataset on which this analysis is performed. The scan algorithm is applied after which eight different cases can be distinguished where $P_{\mathrm{exp},i}$ is either larger or smaller than 5% for $i = 1, 2, 3$. In seven cases at least one $P_{\mathrm{exp},i} < 5\%$ and a new independent pseudo-experiment is generated to emulate a new independent dataset with the same integrated luminosity. The one, two or three data selections for which $P_{\mathrm{exp},i} < 5\%$ are applied to the second pseudo-experiment to obtain the p_0-values for these selections. Although the systematic uncertainties may be reduced by applying data-driven estimates of the background, they were assumed to have the same size in the second pseudo-experiment to make a conservative estimate. The systematic uncertainties are also expected to be partially correlated between two datasets but here they were assumed to be uncorrelated.

In four of the seven cases $P_{\mathrm{exp},1} < 5\%$ and these cases are grouped together into a 'one signal region' class. This class shows the sensitivity when there would be only a single data-derived signal region. The case where only $P_{\mathrm{exp},3} < 5\%$ is called the 'three signal region' class. The two remaining cases where $P_{\mathrm{exp},2} < 5\%$ define the 'two signal region' class. These classes show cases when a data-derived signal region is found only by a combination of two and three regions.
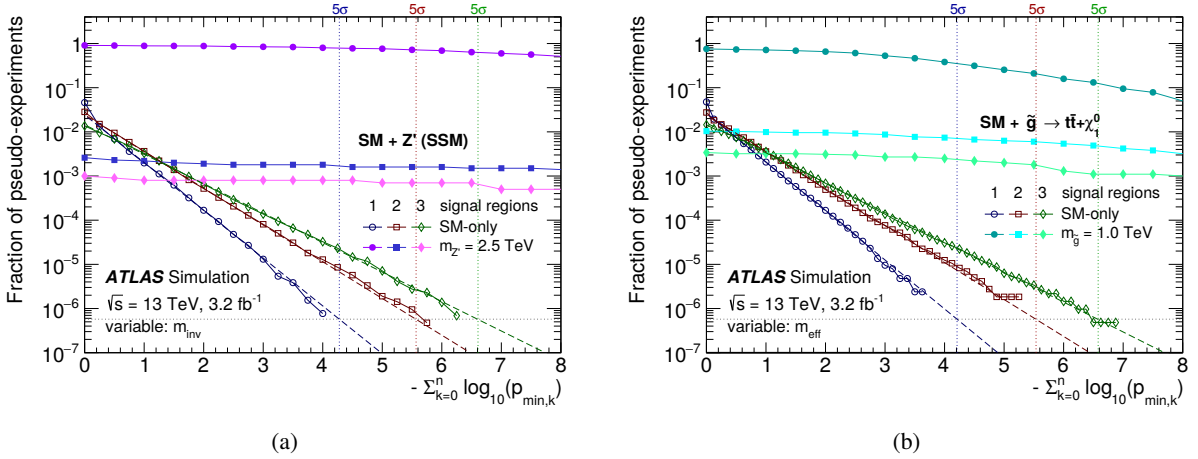

(a)   (b)

Figure 9: The fraction of cases in which the first pseudo-experiment has $P_{\mathrm{exp},i} < 5\%$ and triggers a second pseudo-experiment which yields a value for $-\sum_{k=1}^{n} \log_{10}(p_{0k})$ smaller than a given value ($-\sum_{k=1}^{n} \log_{10}(p_{\min,k})$). Here n denotes the minimum number of event classes (1, 2 or 3) for which $P_{\mathrm{exp},i} < 0.05$. The distribution is shown for pseudo-experiments generated from the SM expectation, and from an SM-plus-signal expectation of (a) inclusive decays of a Z' boson with mass $m_{Z'} = 2.5$ TeV or (b) gluino pairs with mass $m_{\tilde{g}} = 1.0$ TeV and $\tilde{g} \to t\bar{t}\tilde{\chi}_1^0$ decays. The signal region tested in the follow-up pseudo-experiment is defined by the preceding pseudo-experiment. The 5σ thresholds are obtained by extrapolating the SM-only fractions to $5.7 \cdot 10^{-7}$ and are indicated at the top of the figure for $n = 1$ (left), $n = 2$ (middle) or $n = 3$ (right) event classes.

For each of the three classes ($n = 1, 2, 3$) the statistical estimator $\prod_{k=1}^{n} p_{0k}$ is computed. Figure 9 shows, as a function of the estimator in the logarithmic form $-\sum_{k=1}^{n} \log_{10}(p_{0k})$ the fraction of cases in which the first pseudo-experiment has $P_{\mathrm{exp},i} < 5\%$ and triggers a second pseudo-experiment which yields a value for $-\sum_{k=1}^{n} \log_{10}(p_{0k})$ above a threshold given by the value on the horizontal axis. This is done for pseudo-experiments generated from the SM expectation (SM-only) and for pseudo-experiments generated from the SM expectation plus Z' or gluino signal contributions. The 5σ lines are derived from the fractions given by the SM-only lines, as these correspond to the probability of false positives which defines the level of significance. It should be noted that the SM-only lines with circular markers start at a fraction of 0.05 by construction of the $P_{\mathrm{exp},i} < 5\%$ definition. The $n = 2$ and $n = 3$ lines show the gain in sensitivity when

a deviation in one or two channels, respectively, is not large enough to define a data-derived signal region. It does not show the gain in sensitivity from considering multiple channels when a single channel defines a signal region. Signals which produce one or more large deviations therefore lower the number of cases in the $n = 2$ and 3 categories, while signals producing deviations close to the $P_{\exp,i} < 5\%$ threshold (e.g. for higher Z' masses) would raise the number of cases in the $n = 2$ and 3 categories. A Z' boson with a mass of 2.5 TeV would yield a discovery in almost all cases.

In the case of a 1.0 TeV gluino the sensitivity is about 5σ. The sensitivity increases to about 1.1 TeV if the integrated luminosity of the two datasets combined is increased to about 10 fb^{-1} by doubling the size of the second dataset to 6.4 fb^{-1}. ATLAS has determined the discovery sensitivity of the dedicated searches for gluinos decaying to quarks, a W boson and a neutralino. This dedicated search estimates a local significance (i.e. not corrected for trial factors of the dedicated searches) of 5σ with a luminosity of 10 fb^{-1} for gluinos with a mass of 1.35 TeV assuming a systematic uncertainty of 25% [51].

It should be noted that, with this strategy, these signals are found without any a priori assumptions about the model, including the mass and the decay chain of the gluinos or the Z' boson. It can therefore be concluded that this procedure could also be sensitive to possible unexpected signals for new physics.

3.6 Step 6: Results

In step 6 the p_{channel}-values found in the analysis of the 2015 ATLAS data are interpreted by comparing them with the p_{channel}-values found in the pseudo-experiments.
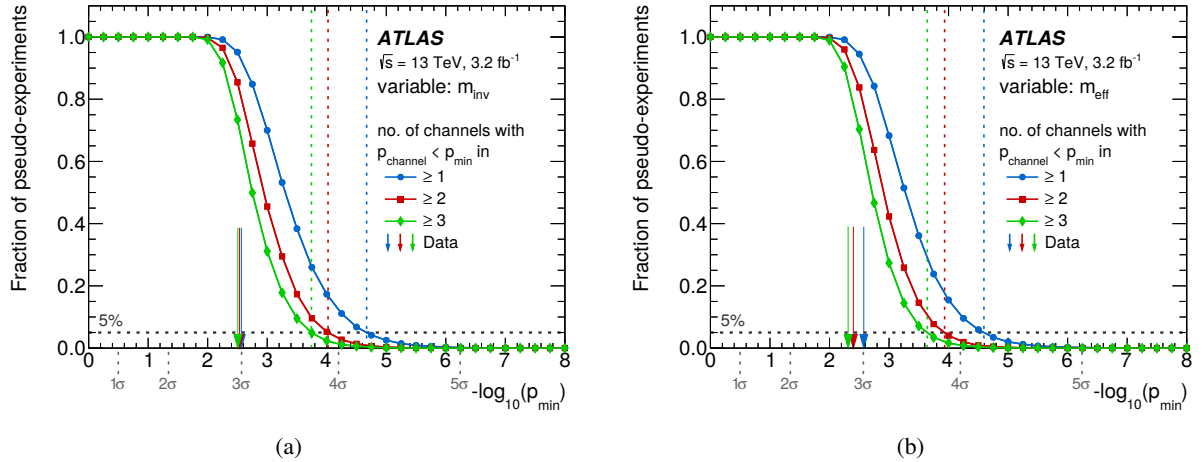

Figure 10: The fractions of pseudo-experiments ($P_{\exp,i}(p_{\min})$) which have at least one, two or three p_{channel}-values (circular, square, and rhombic markers respectively) smaller than a given threshold ($p_{\min}$) in the scans of (a) the m_{inv} distributions, and of (b) the m_{eff} distributions. The coloured arrows represent the three smallest p_{channel}-values observed in data. Dashed lines are drawn at $P_{\exp,i} = 5\%$ and at the $p_{\min}$-values corresponding to 1σ, 2σ, 3σ, 4σ and 5σ local significances.

Figure 10 shows the fractions of pseudo-experiments that have at least one, two or three p_{channel}-values below a given threshold ($p_{\min}$) in the scans of the m_{inv} and the m_{eff} distributions. The statistical tests in both distributions for the three leading p_{channel}-values are all consistent at the $P_{\exp,i} > 50\%$ level with the SM expectation of p_{channel}-values obtained from pseudo-experiments. Changing the size of the theoretical

shape uncertainties by a factor of two leads to a change in the three smallest p_{channel}-values of a factor of two. It therefore does not lead to an appreciable change in the result.

In conclusion, no significant deviations are found in the 2015 dataset and consequently no dedicated analysis using data-derived signal regions (step 7) is initiated.

4 Conclusions

A strategy for a model-independent general search to find potential indications of new physics is presented. Events are classified according to their final state into many event classes. For each event class an automated search algorithm tests whether the data is compatible with the Monte Carlo simulated Standard Model expectation in various distributions sensitive to the effects of new physics. For each distribution the search algorithm is repeated on many pseudo-experiments to make a frequentist estimate of the statistical significance of the three largest deviations. A data selection in which a significant deviation is observed defines a data-derived signal region which will be tested on a new dataset in a dedicated analysis with an improved background model.

The strategy has been applied to the data collected by the ATLAS experiment at the LHC during 2015, corresponding to a total of 3.2 fb^{-1} of 13 TeV pp collisions. In this dataset, exclusive event classes containing electrons, muons, photons, b-tagged jets, non-b-tagged jets and missing transverse momentum have been scanned for deviations from the MC-based SM prediction in the distributions of the effective mass and the invariant mass. Sensitivity studies with various toy signals ($t\bar{t} + \gamma$, WZ, gluino, and Z' production) have shown that the strategy could discover signals for new physics without an a priori knowledge of the existence of the processes.

No significant deviations are found in the 2015 dataset and consequently no dedicated analysis using data-derived signal regions is performed. The strategy discussed in this paper will be useful to search for signals of unknown particles and interactions in the subsequent Run 2 datasets.

Acknowledgements

Appendix

A Details of the Monte Carlo samples

A.1 Monte Carlo programs and settings

Samples of multijet production were simulated with $2 \rightarrow 2$ matrix elements (ME) at leading order (LO) using the PYTHIA 8.186 generator [17]. The A14 [25] set of shower and multiple parton interactions parameters (tune) was used together with the NNPDF2.3LO PDF set [24]. Alternative multijet samples with $2 \rightarrow 2$ ME at LO were generated with HERWIG++ 2.7.1 [53] with the UEEE5 underlying-event tune and the CTEQ6L1 [33] PDF set, and with SHERPA 2.1.1 [20] with ME for $2 \rightarrow 2$ and $2 \rightarrow 3$ partons at LO merged using the ME+PSLO prescription. All SHERPA samples use the CT10 [54] PDF set and the SHERPA parton shower [55] with a dedicated shower tuning developed by the SHERPA authors.

Events containing leptonic decays of a W or Z bosons with associated jets (W/Z + jets) were simulated using the SHERPA 2.1.1 generator [56]. Matrix elements were calculated using the Comix [57] and Open-Loops [58] generators. They include up to two partons at NLO and four partons at leading order (LO), merged using the ME+PS@NLO prescription [59]. Samples with W and Z decaying hadronically are also generated with SHERPA 2.1.1 including up to four partons at LO. The W/Z + jets events were normalized to their inclusive next-to-next-to-leading-order (NNLO) cross-sections [60, 61]. Simulated samples of massive vector bosons produced in association with one or two real photons were also generated with SHERPA 2.1.1 with a ME calculated at LO for up to three partons. They are scaled to their NLO cross-sections computed with MCFM [62, 63].

Samples of prompt photon production in association with jets (γ + jets) were generated using SHERPA 2.1.1. For these samples up to four real parton emissions are included at LO. Events containing two prompt photons ($\gamma\gamma$ + jets) were also generated with SHERPA 2.1.1. Matrix elements were calculated with up to two partons at LO. The gluon-induced box process is also included. These samples were scaled to data following the procedure described in Section 3.2.3.

Top-quark pair production events, and single top quarks in the Wt- and s-channels, were simulated using the POWHEG-BOX v2 [64] generator with the CT10 PDF set, as detailed in Ref. [65]. The top quark mass was set to 172.5 GeV. The h_{damp} parameter, which regulates the transverse momentum of the first extra emission beyond the Born configuration and thus controls the p_T of the $t\bar{t}$ system, was set to the mass of the top quark. Electroweak t-channel single-top-quark events were generated using the POWHEG-BOX v1 generator. This generator uses the four-flavour scheme for the NLO matrix-element calculations together with the fixed four-flavour PDF set CT10f4. For all top-quark processes, top-quark spin correlations are preserved (for the single-top t-channel, top quarks were decayed using MadSpin [66]). An alternative sample of $t\bar{t}$ was generated with the SHERPA 2.1.1 generator, including up to one additional parton at NLO and up to four additional partons at LO accuracy, interfaced to the parton shower using the ME+PS@NLO prescription. The parton shower (PS), fragmentation, and the underlying event of the POWHEG-BOX samples were simulated using PYTHIA 6.428 [67] with the CTEQ6L1 PDF set and the corresponding Perugia 2012 tune (P2012) [68]. The $t\bar{t}$ and single-top-quark events were normalized to the NNLO cross-section including the resummation of soft gluon emission at next-to-next-to-logarithm accuracy [69–71] using Top++2.0 [72]. Both the default and the alternative $t\bar{t}$ samples were corrected to reproduce the NNLO prediction [73, 74] of the top quark p_T and the p_T of the $t\bar{t}$ system. The contribution of $t\bar{t} + b\bar{b}$ was

generated separately with Sherpa 2.1.1 at NLO; the calculation was performed in the four-flavour scheme and with the CT10f4 PDF set.

Diboson samples were generated with the Sherpa 2.1.1 generator, and are described in Ref. [75]. The matrix elements contain the WW, WZ and ZZ processes and all other diagrams with four or six electroweak vertices (such as same-electric-charge W boson production in association with two jets, $W^{\pm}W^{\pm}jj$). Fully leptonic triboson processes (WWW, WWZ, WZZ and ZZZ) with on-shell bosons and up to six charged leptons were also simulated using Sherpa 2.1.1. The ME for the ZZ processes were calculated at NLO for up to one additional parton; final states with two and three additional partons were calculated at LO. The WZ and WW processes were calculated at NLO with up to three extra partons at LO using the ME+PS@NLO prescription. The WW final states were generated without bottom quarks in the hard-scattering process, to avoid contributions from top-quark-mediated processes. The triboson processes were calculated with the same configuration and with up to two extra partons at LO. The generator cross-sections were used for the normalization of these backgrounds.

Samples of top quark production in association with vector bosons [76] (W, Z, γ and WW, including the non-resonant γ^*/Z contributions) were generated at LO with MG5_aMC@NLO 2.2.2 [32] interfaced to Pythia 8.186, with up to two ($t\bar{t}W$), one ($t\bar{t}Z$) or no ($t\bar{t}WW$, $t\bar{t}\gamma$) extra partons included in the matrix element. The A14 tune was used together with the NNPDF2.3LO PDF set. The $t\bar{t}\gamma$ sample uses a fixed QCD renormalization and factorization scale of $2m_t$, and the top decay was performed in MG5_aMC@NLO to account for hard photon radiation from the top decay products. The same generator was also used to simulate the tZ, 3-top and 4-top quarks processes. The $t\bar{t}W$, $t\bar{t}Z$, $t\bar{t}WW$ and 4-top samples were normalized to their NLO cross-sections [32] while the LO cross-section from the generator was used for tZ and 3-top quarks.

The Higgs boson mass was set to 125 GeV and all SM Higgs boson decay modes were considered. The production of the SM Higgs boson in the gluon–gluon fusion (ggF) and vector-boson fusion (VBF) channels was modelled using the Powheg-Box v2 generator with the CT10 PDF set. It was interfaced to Pythia 8.186 with the CTEQ6L1 PDF set and the AZNLO tune [77]. Production of a Higgs boson in association with a pair of top quarks was simulated using MG5_aMC@NLO 2.2.2 interfaced to Herwig++ 2.7.1 [78] for showering and hadronization. The UEEE5 underlying-event tune was used together with the CT10 (matrix element) and CTEQ6L1 (parton shower) PDF sets. Simulated samples of SM Higgs boson production in association with a W or Z boson were produced with Pythia 8.186, using the A14 tune and the NNPDF2.3LO PDF set. Events were normalized to their most accurate cross-sections calculations (typically NNLO) [79].

To avoid double counting, events with a hard photon from final-state radiation were removed from the multijet, $t\bar{t}$ and W/Z + jets samples.

A.2 Theoretical uncertainties

The inclusive W and Z cross-sections are known at NNLO, with an uncertainty of about 5% [60, 61]. Modelling uncertainties for W + jets and Z + jets are determined by varying the renormalization, factorization and resummation scales in the ME by factors 0.5 and 2, together with a change of the merging scale from 20 GeV to 15 GeV or 30 GeV.

For top quark pair or single-top production, processes known to NNLO+NNLL [72] or approximate NNLO [69–71], respectively, the cross-section uncertainty is 7%. The modelling uncertainty for $t\bar{t}$ is

determined by comparing the nominal Powheg+Pythia NLO+PS sample with an alternative sample generated with Sherpa including up to two partons at NLO and four at LO accuracy in the ME. The single-top quark uncertainty is estimated by varying the renormalization and factorization scales, and by changing the h_{damp} parameter and the shower tune of the Powheg+Pythia sample. An uncertainty in the interference between the Wt and $t\bar{t}$ production is estimated by comparing the nominal Wt sample, where all doubly resonant NLO Wt diagrams are removed, with a sample where the cross-section contribution from Feynman diagrams containing two top quarks is subtracted [80].

Diboson cross-sections (WW, WZ and ZZ) are calculated at NLO, and a 6% uncertainty, evaluated with the MCFM program [62, 63], is applied to their cross-sections. Their modelling uncertainty is evaluated analogously to V + jets by varying the scales used to perform the calculation. For $W + \gamma$ and $Z + \gamma$ samples, which are computed at LO, a 20% uncertainty in the cross-section is assumed, with a further 20% modelling uncertainty assigned in accord with the measurement in Ref. [81].

The cross-sections for top-quark pair production in association with one or two vector bosons are calculated at NLO and an uncertainty of 15% is used [32]. Their modelling uncertainty is evaluated from variations of the renormalization and factorization scales, together with a change in the merging scale. For $t\bar{t} + \gamma$, an additional 12% uncertainty in the normalization is assumed, while a uniform 30% uncertainty is assigned to the modelling.

Multijet and γ + jets processes are scaled to data following the procedure described in Section 3.2.2. Therefore, no uncertainty is applied to their normalization. For multijets the maximum bin-by-bin difference between the Pythia 8 nominal sample and alternative samples generated with Sherpa and Herwig++ is considered as a shape uncertainty. In addition the standard deviation of the 100 replica sets of the NNPDF2.3LO PDF is used. The modelling uncertainty for γ + jets is estimated from scale variations with the same methodology as for the V + jets samples. The uncertainty in the $\gamma\gamma$ + jets modelling is instead taken to be 30% from parton-level comparisons of samples with varied scales.

A conservative uncertainty of 20% [79] is assumed for Higgs production in the ggF, VBF and VH channels. A further uncertainty of 20% is assigned as a shape uncertainty.

For the subdominant triboson (including $V + \gamma\gamma$), ttH, 3-top, 4-top and tZ production processes a 50% uncertainty is assigned to the event yields, similarly to Ref. [82]. Uncertainties associated with the PDFs are found to be negligible in all but the multijet samples, for which they have been explicitly estimated.

B Details of the object reconstruction

Electron candidates are reconstructed from an isolated electromagnetic calorimeter energy deposit matched to an ID track and are required to have $|\eta| < 2.47$, a transverse momentum $p_T > 10$ GeV, and to pass a loose likelihood-based identification requirement [44, 83]. The likelihood input variables include measurements of calorimeter shower shapes and measurements of track properties from the ID. The candidate electrons are selected if the matched tracks have a transverse impact parameter significance relative to the reconstructed primary vertex of $|d_0|/\sigma(d_0) < 5$. Candidates within the transition region between the barrel and endcap electromagnetic calorimeters, $1.37 < |\eta| < 1.52$, are removed.

Muon candidates are reconstructed in the region $|\eta| < 2.7$ from muon spectrometer tracks matched to ID tracks. The muon candidates are selected if they have a transverse momentum above 10 GeV and pass the medium identification requirements defined in Ref. [43], based on selections on the number of hits in the

different ID and muon spectrometer subsystems, and the significance of the charge to momentum ratio q/p.

All candidate leptons (electrons and muons) are used for the object overlap removal, as discussed in Section 3.1.3. Tighter requirements on the lepton candidates are imposed, which are then referred to as 'signal' electrons or muons and are used further in the analysis, i.e. to establish the accuracy of the background modelling processes or to classify the events. Signal electrons must satisfy a tight likelihood-based identification requirement [44, 83]. Signal muons must fulfil the requirement of $|d_0|/\sigma(d_0) < 3$. The track associated with a signal lepton must have a longitudinal impact parameter relative to the reconstructed primary vertex, z_0, satisfying $|z_0 \cdot \sin\theta| < 0.5$ mm. Isolation requirements are applied to both the signal electrons and muons. The calorimeter isolation is computed as the sum of the energies of calorimeter energy clusters in a cone of size $\Delta R = 0.2$ around the lepton. Track isolation is defined as the scalar sum of the p_T of tracks within a variable-size cone around the lepton, in a cone of size $\Delta R = 0.2$ (0.3) for electron (muon) transverse momenta $p_T < 50$ GeV ($p_T < 33$ GeV) and of size $\Delta R = 10$ GeV$/p_T$ for $p_T > 50$ GeV ($p_T > 33$ GeV). The efficiency of these criteria increases with the lepton transverse momentum, reaching 95% at 25 GeV and 99% at 60 GeV, as determined in a control sample of Z decays into leptons selected with a tag-and-probe technique [43, 44]. Corrections are applied to the MC samples to match the leptons' trigger, reconstruction and isolation efficiencies in data.

Photon candidates are reconstructed from an isolated electromagnetic calorimeter energy deposit and are required to satisfy the tight identification criteria described in Refs. [46, 84]. Furthermore, photons are required to have $p_T > 25$ GeV and $|\eta| < 2.37$, excluding the barrel–endcap calorimeter transition in the range $1.37 < |\eta| < 1.52$. Photons must further satisfy isolation criteria based on both track and calorimeter information [46]. After correcting for contributions from pile-up, the energy within a cone of $\Delta R = 0.4$ around the cluster barycentre is required to be less than 2.45 GeV $+ 0.022 \times p_T^\gamma$, where p_T^γ is the transverse momentum of the photon candidate. The energy of tracks in a cone of $\Delta R = 0.2$ should be less than $0.05 \times p_T^\gamma$.

Jet candidates are reconstructed with the anti-k_t algorithm [38] implemented in the FastJet package [85] with a radius parameter of $R = 0.4$, using as input three-dimensional energy clusters in the calorimeter [86] calibrated to the electromagnetic scale. The reconstructed jets are then calibrated to the jet energy scale (JES) derived from simulation and in situ corrections based on 13 TeV data [42, 87]. For all jets the expected average energy contribution from pile-up clusters is subtracted according to the jet area prescription [88]. Quality criteria are imposed to identify jets arising from non-collision sources or detector noise and any event containing such a jet is removed [89]. All jet candidates are required to have $p_T > 20$ GeV and $|\eta| < 2.8$.

Identification of jets containing b-hadrons (b-tagging) is performed with a multivariate discriminant, MV2c20, making use of track impact parameters, the b- and c-hadron flight paths inside the jet and reconstructed secondary vertices [39, 40]. The algorithm working point used corresponds to a 77% average efficiency obtained for b-jets in simulated $t\bar{t}$ events. The rejection factors for light-quark jets, c-quark jets and hadronically decaying τ-leptons in simulated $t\bar{t}$ events are approximately 140, 4.5 and 10, respectively [40]. Jets with $|\eta| < 2.5$ which satisfy this b-tagging requirement are identified as b-jet candidates. To compensate for differences between data and MC simulation in the b-tagging efficiencies and mistag rates, correction factors are applied to the simulated samples [40].

C Event yields for all event classes

Figure 11: The number of events in data, and for the different SM background predictions considered, for classes with at least one photon and (b-)jets (no leptons or E_T^{miss}). The classes are labelled according to the multiplicity and type (e, μ, γ, j, b, E_T^{miss}) of the reconstructed objects for the given event class. In event classes with four or more data events, the γ + jets and $\gamma\gamma$ + jets MC samples are scaled to data in the single-photon and diphoton event classes respectively. The hatched bands indicate the total uncertainty of the SM prediction.

Figure 12: The number of events in data, and for the different SM background predictions considered, for classes with one electron and (b-)jets (no muons, photons or E_T^{miss}). The classes are labelled according to the multiplicity and type (e, μ, γ, j, b, E_T^{miss}) of the reconstructed objects for the given event class. The hatched bands indicate the total uncertainty of the SM prediction.

Figure 13: The number of events in data, and for the different SM background predictions considered, for classes with one muon and (b-)jets (no electrons, photons or E_T^{miss}). The classes are labelled according to the multiplicity and type (e, μ, γ, j, b, E_T^{miss}) of the reconstructed objects for the given event class. The hatched bands indicate the total uncertainty of the SM prediction.

Figure 14: The number of events in data, and for the different SM background predictions considered, for classes with one muon, one electron and (b-)jets (no photons or E_T^{miss}). The classes are labelled according to the multiplicity and type (e, μ, γ, j, b, E_T^{miss}) of the reconstructed objects for the given event class. The hatched bands indicate the total uncertainty of the SM prediction.
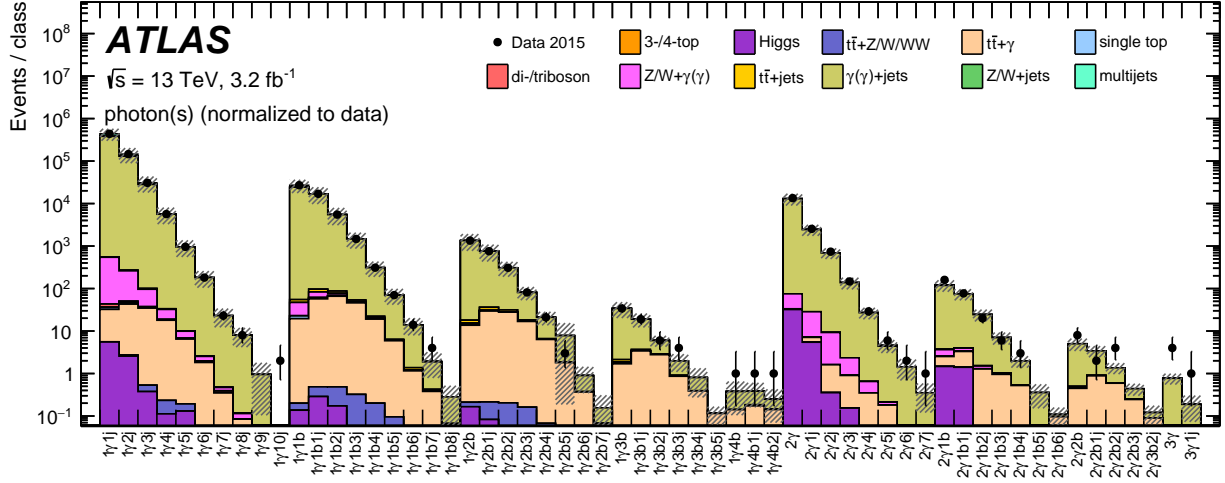

Figure 15: The number of events in data, and for the different SM background predictions considered, for classes with two same-flavour leptons and (b-)jets (no photons or E_T^{miss}). The classes are labelled according to the multiplicity and type (e, μ, γ, j, b, E_T^{miss}) of the reconstructed objects for the given event class. The hatched bands indicate the total uncertainty of the SM prediction.

Figure 16: The number of events in data, and for the different SM background predictions considered, for classes with three or four leptons and (b-)jets (no photons or E_T^{miss}). The classes are labelled according to the multiplicity and type (e, μ, γ, j, b, E_T^{miss}) of the reconstructed objects for the given event class. The hatched bands indicate the total uncertainty of the SM prediction.
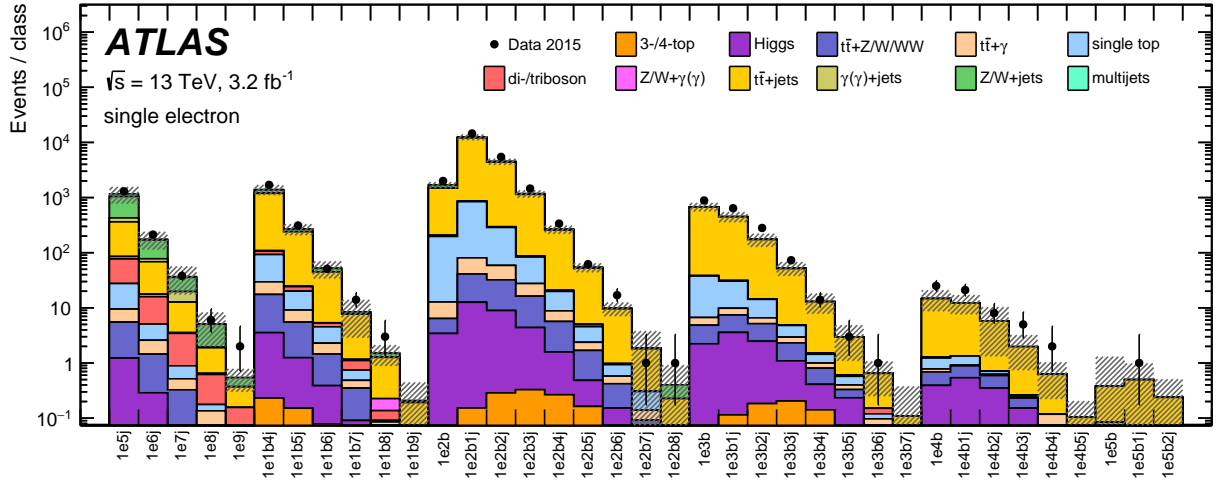

Figure 17: The number of events in data, and for the different SM background predictions considered, for classes with one lepton, at least one photon and (b-)jets (no E_T^{miss}). The classes are labelled according to the multiplicity and type (e, μ, γ, j, b, E_T^{miss}) of the reconstructed objects for the given event class. The hatched bands indicate the total uncertainty of the SM prediction.
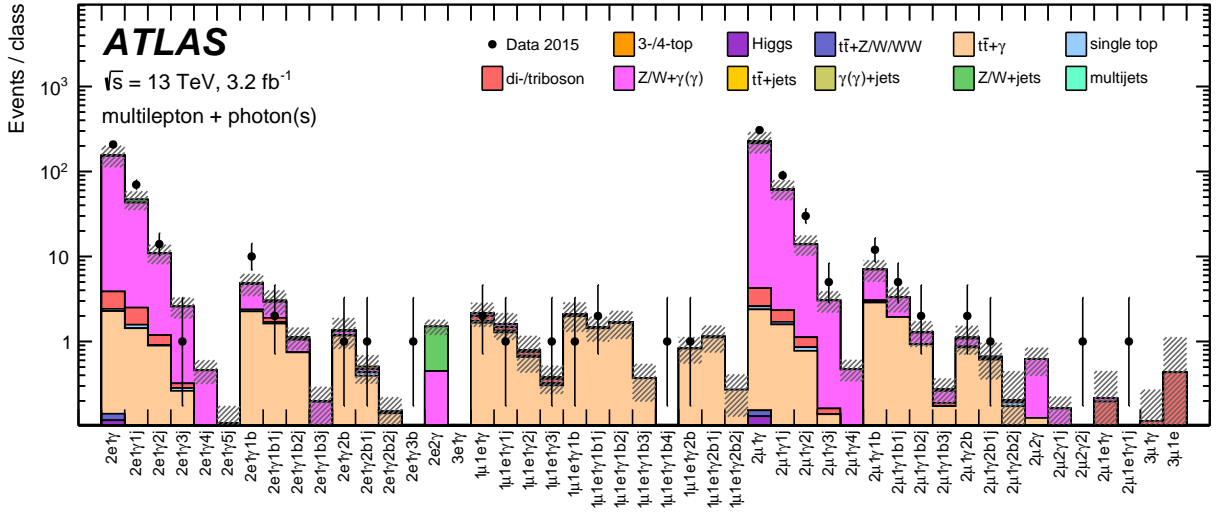
Figure 18: The number of events in data, and for the different SM background predictions considered, for classes with at least two leptons, at least one photon and (b-)jets (no E_T^{miss}). The classes are labelled according to the multiplicity and type (e, μ, γ, j, b, E_T^{miss}) of the reconstructed objects for the given event class. The hatched bands indicate the total uncertainty of the SM prediction.
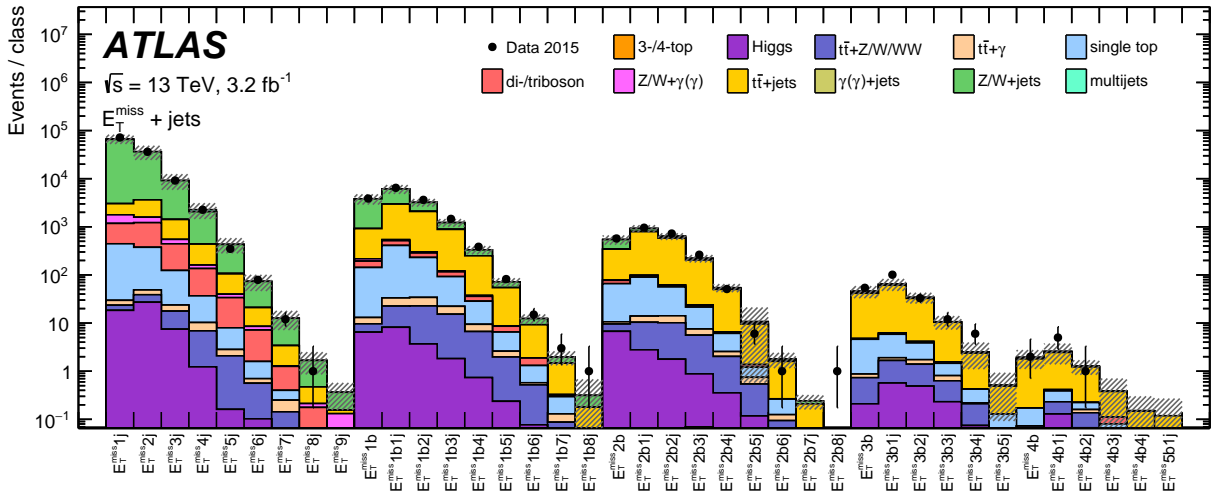
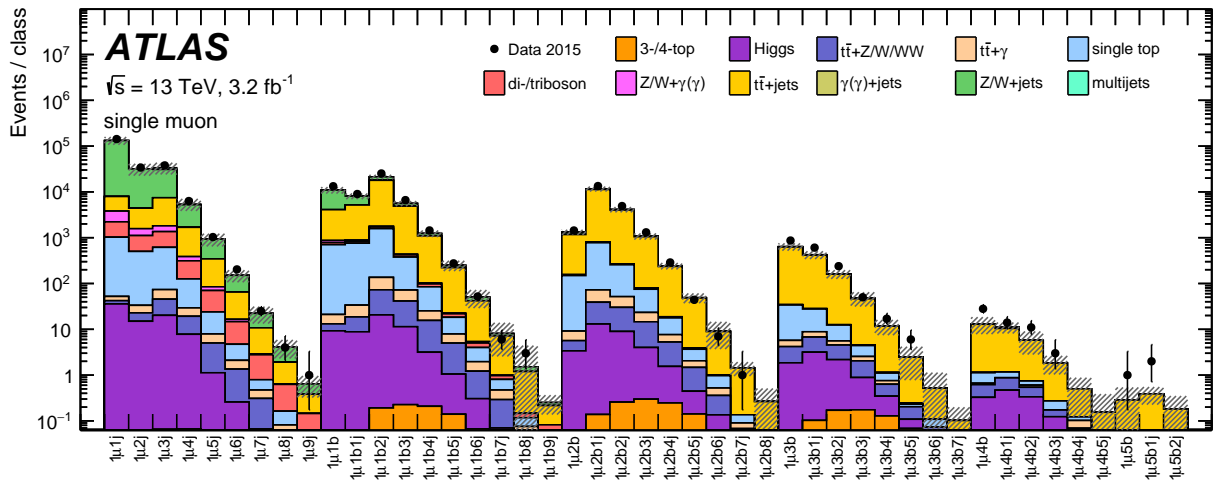Figure 19: The number of events in data, and for the different SM background predictions considered, for classes with large E_T^{miss} and (b-)jets (no leptons or photons). The classes are labelled according to the multiplicity and type (e, μ, γ, j, b, E_T^{miss}) of the reconstructed objects for the given event class. The hatched bands indicate the total uncertainty of the SM prediction.
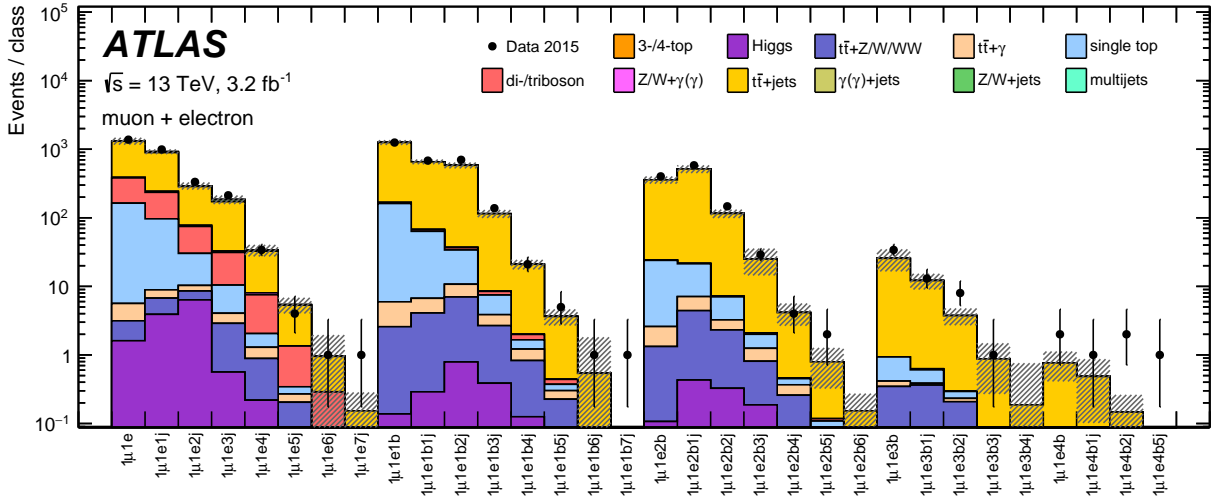
Figure 20: The number of events in data, and for the different SM background predictions considered, for classes with large E_T^{miss}, at least one photon, leptons and (b-)jets. The classes are labelled according to the multiplicity and type (e, μ, γ, j, b, E_T^{miss}) of the reconstructed objects for the given event class. The hatched bands indicate the total uncertainty of the SM prediction.
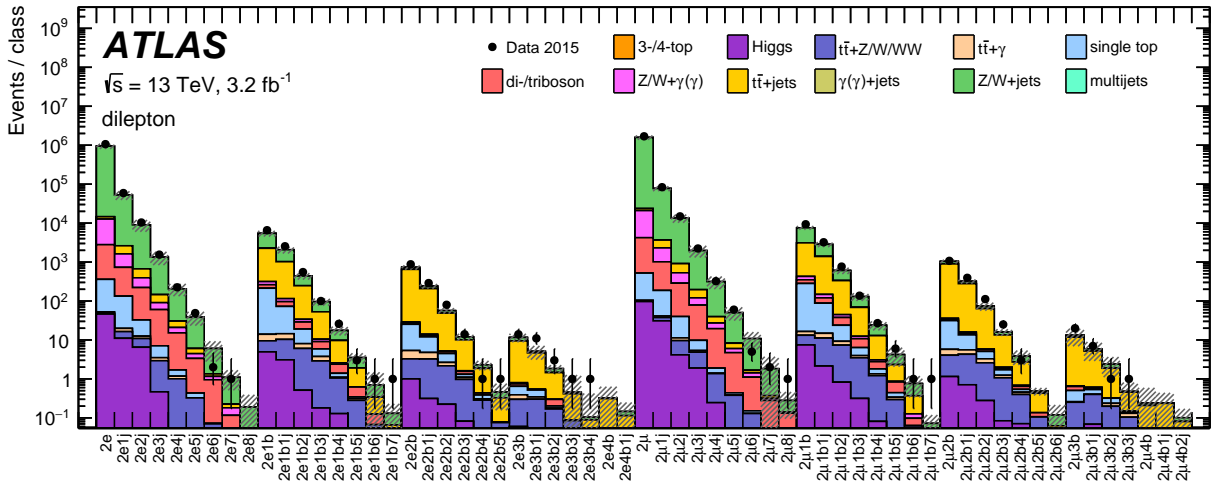

Figure 21: The number of events in data, and for the different SM background predictions considered, for classes with large E_T^{miss}, one muon, one electron and (b-)jets (no photons). The classes are labelled according to the multiplicity and type (e, μ, γ, j, b, E_T^{miss}) of the reconstructed objects for the given event class. The hatched bands indicate the total uncertainty of the SM prediction.

Figure 22: The number of events in data, and for the different SM background predictions considered, for classes with large $E_{\mathrm{T}}^{\mathrm{miss}}$, at least one pair of same flavour leptons and (b-)jets (no photons). The classes are labelled according to the multiplicity and type (e, μ, γ, j, b, $E_{\mathrm{T}}^{\mathrm{miss}}$) of the reconstructed objects for the given event class. The hatched bands indicate the total uncertainty of the SM prediction.

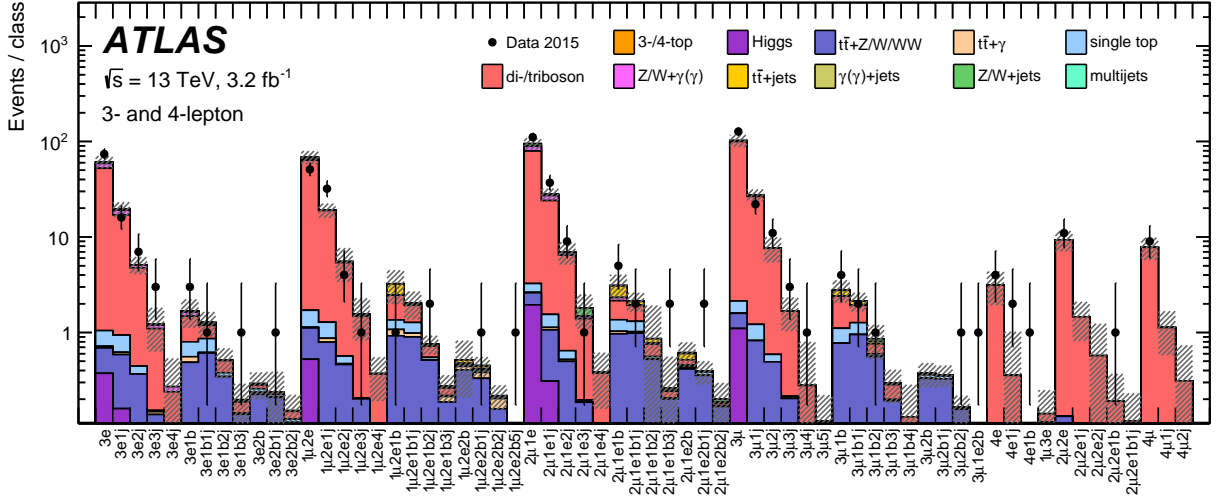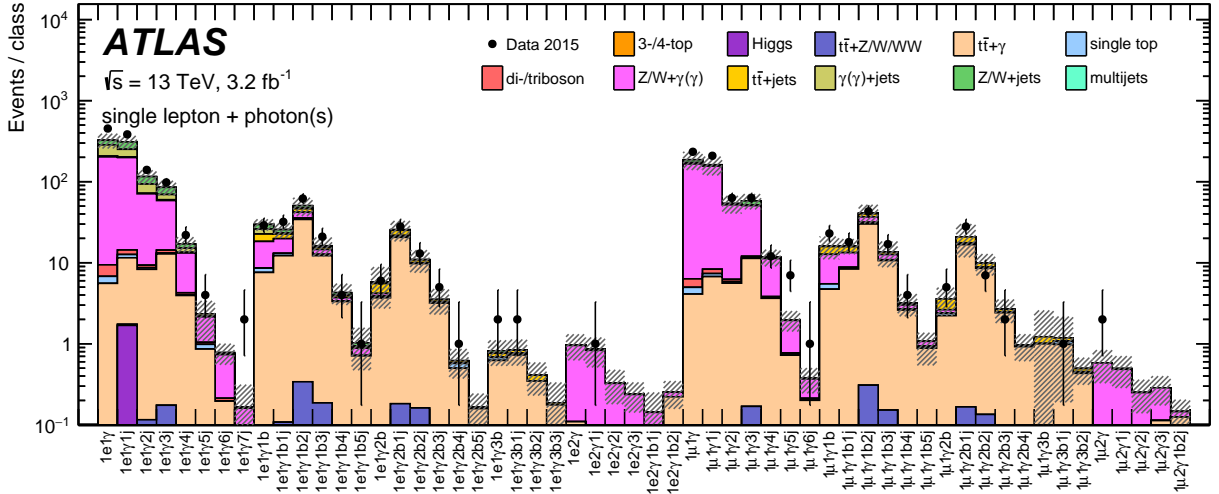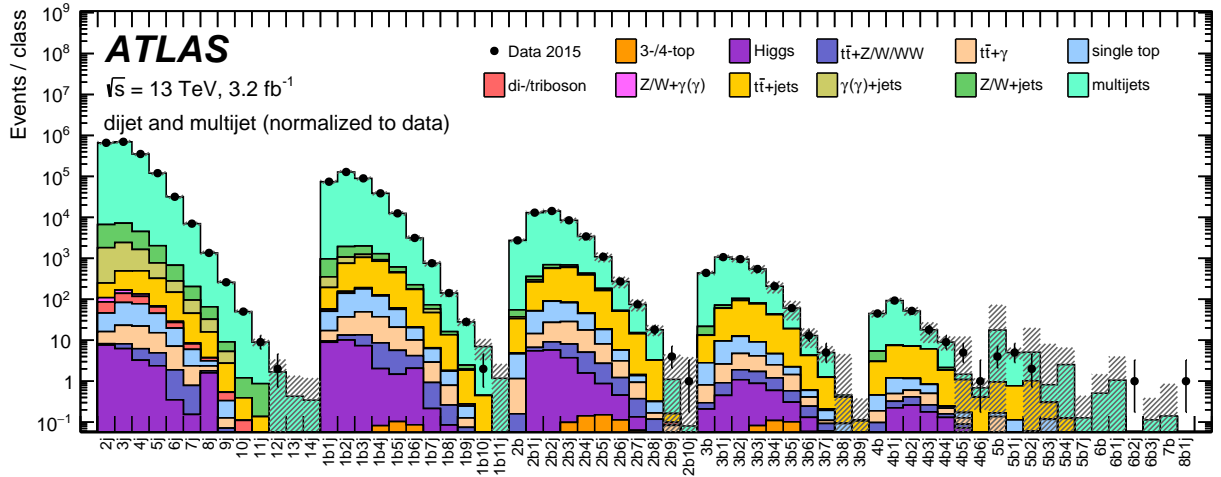Figure 23: The number of events in data, and for the different SM background predictions considered, for classes with (b-)jets (no $E_{\mathrm{T}}^{\mathrm{miss}}$, leptons or photons). The classes are labelled according to the multiplicity and type (e, μ, γ, j, b, $E_{\mathrm{T}}^{\mathrm{miss}}$) of the reconstructed objects for the given event class. In event classes with four or more data events, the multijet MC sample is scaled to data. The hatched bands indicate the total uncertainty of the SM prediction.

References

[1] D0 Collaboration, *Search for new physics in eµX data at DØ using SLEUTH: A quasi-model-independent search strategy for new physics*, Phys. Rev. D **62** (2000) 092004, arXiv: `hep-ex/0006011`.

[2] D0 Collaboration, *Quasi-model-independent search for new physics at large transverse momentum*, Phys. Rev. D **64** (2001) 012004, arXiv: `hep-ex/0011067`.

[3] D0 Collaboration, *Quasi-Model-Independent Search for New High p_T Physics at DO*, Phys. Rev. Lett. **86** (2001) 3712, arXiv: `hep-ex/0011071`.

[4] D0 Collaboration, *Model independent search for new phenomena in $p\bar{p}$ collisions at $\sqrt{s}$ = 1.96 TeV*, Phys. Rev. D **85** (2012) 092015, arXiv: `1108.5362 [hep-ex]`.

[5] H1 Collaboration, *A general search for new phenomena in ep scattering at HERA*, Phys. Lett. B **602** (2004) 14, arXiv: `hep-ex/0408044`.

[6] H1 Collaboration, *A general search for new phenomena at HERA*, Phys. Lett. B **674** (2009) 257, arXiv: `0901.0507 [hep-ex]`.

[7] CDF Collaboration, *Model-independent and quasi-model-independent search for new physics at CDF*, Phys. Rev. D **78** (2008) 012002, arXiv: `0712.1311 [hep-ex]`.

[8] CDF Collaboration, *Global search for new physics with 2.0 fb^{-1} at CDF*, Phys. Rev. D **79** (2009) 011101, arXiv: `0809.3781 [hep-ex]`.

[9] S. Brandt, C. Peyrou, R. Sosnowski and A. Wroblewski, *The principal axis of jets – an attempt to analyse high-energy collisions as two-body processes*, Phys. Lett. **12** (1964) 57.

[10] E. Farhi, *Quantum Chromodynamics Test for Jets*, Phys. Rev. Lett. **39** (1977) 1587.

[11] ATLAS Collaboration, *The ATLAS Experiment at the CERN Large Hadron Collider*, JINST **3** (2008) S08003.

[12] ATLAS Collaboration, *ATLAS Insertable B-Layer Technical Design Report*, (2010), URL: `https://cds.cern.ch/record/1291633`, *ATLAS Insertable B-Layer Technical Design Report Addendum*, ATLAS-TDR-19-ADD-1, 2012, URL: `https://cds.cern.ch/record/1451888`.

[13] ATLAS Collaboration, *Performance of the ATLAS Trigger System in 2015*, Eur. Phys. J. C **77** (2017) 317, arXiv: `1611.09661 [hep-ex]`.

[14] ATLAS Collaboration, *Vertex Reconstruction Performance of the ATLAS Detector at $\sqrt{s}$ = 13 TeV*, ATL-PHYS-PUB-2015-026, 2015, URL: `https://cds.cern.ch/record/2037717`.

[15] ATLAS Collaboration, *The ATLAS Simulation Infrastructure*, Eur. Phys. J. C **70** (2010) 823, arXiv: `1005.4568 [physics.ins-det]`.

[16] S. Agostinelli et al., *GEANT4 a simulation toolkit*, Nucl. Instrum. Meth. A **506** (2003) 250.

[17] T. Sjöstrand, S. Mrenna and P. Z. Skands, *A brief introduction to PYTHIA 8.1*, Comput. Phys. Commun. **178** (2008) 852, arXiv: `0710.3820 [hep-ph]`.

[18] A. Martin, W. Stirling, R. Thorne and G. Watt, *Parton distributions for the LHC*,
Eur. Phys. J. C **63** (2009) 189, arXiv: 0901.0002 [hep-ph].

[19] ATLAS Collaboration, *Summary of ATLAS Pythia 8 tunes*, ATL-PHYS-PUB-2012-003, 2012,
URL: https://cds.cern.ch/record/1474107.

[20] T. Gleisberg et al., *Event generation with SHERPA 1.1*, JHEP **02** (2009) 007,
arXiv: 0811.4622 [hep-ph].

[21] D. J. Lange, *The EvtGen particle decay simulation package*,
Nucl. Instrum. Meth. A **462** (2001) 152.

[22] D. London and J. L. Rosner, *Extra gauge bosons in E_6*, Phys. Rev. D **34** (1986) 1530.

[23] P. Langacker, *The physics of heavy Z' gauge bosons*, Rev. Mod. Phys. **81** (2009) 1199,
arXiv: 0801.1345 [hep-ph].

[24] R. D. Ball et al., *Parton distributions with LHC data*, Nucl. Phys. B **867** (2013) 244,
arXiv: 1207.1303 [hep-ph].

[25] ATLAS Collaboration, *ATLAS Pythia 8 tunes to 7 TeV data*, ATL-PHYS-PUB-2014-021, 2014,
URL: https://cds.cern.ch/record/1966419.

[26] Yu. A. Golfand and E. P. Likhtman,
Extension of the Algebra of Poincare Group Generators and Violation of p Invariance,
JETP Lett. **13** (1971) 323, [Pisma Zh. Eksp. Teor. Fiz. **13** (1971) 452].

[27] D. V. Volkov and V. P. Akulov, *Is the Neutrino a Goldstone Particle?*, Phys. Lett. B **46** (1973) 109.

[28] J. Wess and B. Zumino, *Supergauge Transformations in Four-Dimensions*,
Nucl. Phys. B **70** (1974) 39.

[29] J. Wess and B. Zumino, *Supergauge Invariant Extension of Quantum Electrodynamics*,
Nucl. Phys. B **78** (1974) 1.

[30] S. Ferrara and B. Zumino, *Supergauge Invariant Yang-Mills Theories*,
Nucl. Phys. B **79** (1974) 413.

[31] A. Salam and J. Strathdee, *Super-symmetry and non-Abelian gauges*, Phys. Lett. B **51** (1974) 353.

[32] J. Alwall et al., *The automated computation of tree-level and next-to-leading order differential
cross sections, and their matching to parton shower simulations*, JHEP **07** (2014) 079,
arXiv: 1405.0301 [hep-ph].

[33] J. Pumplin et al.,
New Generation of Parton Distributions with Uncertainties from Global QCD Analysis,
JHEP **07** (2002) 012, arXiv: hep-ph/0201195.

[34] L. Lonnblad and S. Prestel, *Matching tree-level matrix elements with interleaved showers*,
JHEP **03** (2012) 019, arXiv: 1109.4829 [hep-ph].

[35] W. Beenakker, M. Kramer, T. Plehn, M. Spira and P. M. Zerwas,
Stop production at hadron colliders, Nucl. Phys. B **515** (1998) 3, arXiv: hep-ph/9710451.

[36] W. Beenakker et al., *Supersymmetric top and bottom squark production at hadron colliders*,
JHEP **08** (2010) 098, arXiv: 1006.4771 [hep-ph].

[37] W. Beenakker et al., *Squark and gluino hadroproduction*, Int. J. Mod. Phys. A **26** (2011) 2637,
arXiv: 1105.1110 [hep-ph].

[38] M. Cacciari, G. P. Salam and G. Soyez, *The anti-k_t jet clustering algorithm*, JHEP **04** (2008) 063, arXiv: `0802.1189 [hep-ph]`.

[39] ATLAS Collaboration, *Performance of b-jet identification in the ATLAS experiment*, JINST **11** (2016) P04008, arXiv: `1512.01094 [hep-ex]`.

[40] ATLAS Collaboration, *Expected performance of the ATLAS b-tagging algorithms in Run-2*, ATL-PHYS-PUB-2015-022, 2015, URL: `https://cds.cern.ch/record/2037697`.

[41] ATLAS Collaboration, *Performance of missing transverse momentum reconstruction with the ATLAS detector using proton–proton collisions at $\sqrt{s}$ = 13 TeV*, (2018), arXiv: `1802.08168 [hep-ex]`.

[42] ATLAS Collaboration, *Jet energy scale measurements and their systematic uncertainties in proton–proton collisions at $\sqrt{s}$ = 13 TeV with the ATLAS detector*, Phys. Rev. D **96** (2017) 072002, arXiv: `1703.09665 [hep-ex]`.

[43] ATLAS Collaboration, *Muon reconstruction performance of the ATLAS detector in proton–proton collision data at $\sqrt{s}$ = 13 TeV*, Eur. Phys. J. C **76** (2016) 292, arXiv: `1603.05598 [hep-ex]`.

[44] ATLAS Collaboration, *Electron efficiency measurements with the ATLAS detector using the 2015 LHC proton–proton collision data*, ATLAS-CONF-2016-024, 2016, URL: `https://cds.cern.ch/record/2157687`.

[45] ATLAS Collaboration, *Electron and photon energy calibration with the ATLAS detector using data collected in 2015 at $\sqrt{s}$ = 13 TeV*, ATL-PHYS-PUB-2016-015, 2016, URL: `https://cds.cern.ch/record/2203514`.

[46] ATLAS Collaboration, *Photon identification in 2015 ATLAS data*, ATL-PHYS-PUB-2016-014, 2016, URL: `https://cds.cern.ch/record/2203125`.

[47] ATLAS Collaboration, *Luminosity determination in pp collisions at $\sqrt{s}$ = 8 TeV using the ATLAS detector at the LHC*, Eur. Phys. J. C **76** (2016) 653, arXiv: `1608.03953 [hep-ex]`.

[48] ATLAS Collaboration, *Search for supersymmetry in a final state containing two photons and missing transverse momentum in $\sqrt{s}$ = 13 TeV pp collisions at the LHC using the ATLAS detector*, Eur. Phys. J. C **76** (2016) 517, arXiv: `1606.09150 [hep-ex]`.

[49] ATLAS Collaboration, *Search for resonances in diphoton events at $\sqrt{s}$ = 13 TeV with the ATLAS detector*, JHEP **09** (2016) 001, arXiv: `1606.03833 [hep-ex]`.

[50] ATLAS Collaboration, *Search for new phenomena in high-mass diphoton final states using 37 fb^{-1} of proton–proton collisions collected at $\sqrt{s}$ = 13 TeV with the ATLAS detector*, Phys. Lett. B **775** (2017) 105, arXiv: `1707.04147 [hep-ex]`.

[51] ATLAS Collaboration, *Expected sensitivity studies for gluino and squark searches using the early LHC 13 TeV Run-2 dataset with the ATLAS experiment*, ATL-PHYS-PUB-2015-005, 2015, URL: `https://atlas.web.cern.ch/Atlas/GROUPS/PHYSICS/PUBNOTES/ATL-PHYS-PUB-2015-005`.

[52] ATLAS Collaboration, *ATLAS Computing Acknowledgements*, ATL-GEN-PUB-2016-002, URL: `https://cds.cern.ch/record/2202407`.

[53] G. Corcella et al., *HERWIG 6: an event generator for hadron emission reactions with interfering gluons (including supersymmetric processes)*, JHEP **01** (2001) 010, arXiv: `hep-ph/0011363`.

[54] H.-L. Lai et al., *New parton distributions for collider physics*, Phys. Rev. D **82** (2010) 074024, arXiv: 1007.2241 [hep-ph].

[55] S. Schumann and F. Krauss,
A parton shower algorithm based on Catani-Seymour dipole factorisation, JHEP **03** (2008) 038, arXiv: 0709.1027 [hep-ph].

[56] ATLAS Collaboration, *Monte Carlo Generators for the Production of a W or Z/γ* Boson in Association with Jets at ATLAS in Run 2*, ATL-PHYS-PUB-2016-003, 2016, URL: https://cds.cern.ch/record/2120133.

[57] T. Gleisberg and S. Höche, *Comix, a new matrix element generator*, JHEP **12** (2008) 039, arXiv: 0808.3674 [hep-ph].

[58] F. Cascioli, P. Maierhöfer and S. Pozzorini, *Scattering Amplitudes with Open Loops*, Phys. Rev. Lett. **108** (2012) 111601, arXiv: 1111.5206 [hep-ph].

[59] S. Höche, F. Krauss, M. Schönherr and F. Siegert,
QCD matrix elements + parton showers. The NLO case, JHEP **04** (2013) 027, arXiv: 1207.5030 [hep-ph].

[60] R. Gavin, Y. Li, F. Petriello and S. Quackenbush,
FEWZ 2.0: A code for hadronic Z production at next-to-next-to-leading order, Comput. Phys. Commun. **182** (2011) 2388, arXiv: 1011.3540 [hep-ph].

[61] R. Gavin, Y. Li, F. Petriello and S. Quackenbush, *W physics at the LHC with FEWZ 2.1*, Comput. Phys. Commun. **184** (2013) 208, arXiv: 1201.5896 [hep-ph].

[62] J. M. Campbell and R. K. Ellis, *Update on vector boson pair production at hadron colliders*, Phys. Rev. D **60** (1999) 113006, arXiv: hep-ph/9905386.

[63] J. M. Campbell, R. K. Ellis and C. Williams, *Vector boson pair production at the LHC*, JHEP **07** (2011) 018, arXiv: 1105.0020 [hep-ph].

[64] S. Alioli, P. Nason, C. Oleari and E. Re, *A general framework for implementing NLO calculations in shower Monte Carlo programs: the POWHEG BOX*, JHEP **10** (2010) 043, arXiv: 1002.2581 [hep-ph].

[65] ATLAS Collaboration,
Simulation of top-quark production for the ATLAS experiment at $\sqrt{s}$ = 13 TeV, ATL-PHYS-PUB-2016-004, 2016, URL: https://cds.cern.ch/record/2120417.

[66] P. Artoisenet, R. Frederix, O. Mattelaer and R. Rietkerk,
Automatic spin-entangled decays of heavy resonances in Monte Carlo simulations, JHEP **03** (2013) 015, arXiv: 1212.3460 [hep-ph].

[67] T. Sjöstrand, S. Mrenna and P. Skands, *PYTHIA 6.4 physics and manual*, JHEP **05** (2006) 026, arXiv: hep-ph/0603175.

[68] P. Z. Skands, *Tuning Monte Carlo generators: The Perugia tunes*, Phys. Rev. D **82** (2010) 074018, arXiv: 1005.3457 [hep-ph].

[69] N. Kidonakis,
Two-loop soft anomalous dimensions for single top quark associated production with a W^- or H^-, Phys. Rev. D **82** (2010) 054018, arXiv: 1005.4451 [hep-ph].

[70] N. Kidonakis,
Next-to-next-to-leading logarithm resummation for s-channel single top quark production,
Phys. Rev. D **81** (2010) 054028, arXiv: `1001.5034 [hep-ph]`.

[71] N. Kidonakis, *Next-to-next-to-leading-order collinear and soft gluon corrections for t-channel single top quark production*, Phys. Rev. D **83** (2011) 091503, arXiv: `1103.2792 [hep-ph]`.

[72] M. Czakon and A. Mitov,
Top++: A program for the calculation of the top-pair cross-section at hadron colliders,
Comput. Phys. Commun. **185** (2014) 2930, arXiv: `1112.5675 [hep-ph]`.

[73] M. Czakon, D. Heymes and A. Mitov,
High-Precision Differential Predictions for Top-Quark Pairs at the LHC,
Phys. Rev. Lett. **116** (2016) 082003, arXiv: `1511.00549 [hep-ph]`.

[74] M. Czakon, D. Heymes and A. Mitov,
Dynamical scales for multi-TeV top-pair production at the LHC, JHEP **04** (2017) 071,
arXiv: `1606.03350 [hep-ph]`.

[75] ATLAS Collaboration, *Multi-boson simulation for* 13 *TeV ATLAS analyses*,
ATL-PHYS-PUB-2016-002, 2016, URL: `https://cds.cern.ch/record/2119986`.

[76] ATLAS Collaboration,
Modelling of the $t\bar{t}H$ and $t\bar{t}V(V = W, Z)$ processes for $\sqrt{s}$ = 13 TeV ATLAS analyses,
ATL-PHYS-PUB-2016-005, 2016, URL: `https://cds.cern.ch/record/2120826`.

[77] ATLAS Collaboration, *Measurement of the Z/γ^* boson transverse momentum distribution in pp collisions at $\sqrt{s}$ = 7 TeV with the ATLAS detector*, JHEP **09** (2014) 145,
arXiv: `1406.3660 [hep-ex]`.

[78] M. Bahr et al., *Herwig++ Physics and Manual*, Eur. Phys. J. C **58** (2008) 639,
arXiv: `0803.0883 [hep-ph]`.

[79] LHC Higgs Cross Section Working Group,
Handbook of LHC Higgs Cross Sections: 2. Differential Distributions, CERN-2012-002,
arXiv: `1201.3084 [hep-ph]`.

[80] S. Frixione, E. Laenen, P. Motylinski, B. R. Webber and C. D. White,
Single-top hadroproduction in association with a W boson, JHEP **07** (2008) 029,
arXiv: `0805.3067 [hep-ph]`.

[81] ATLAS Collaboration, *Measurements of $W\gamma$ and $Z\gamma$ production in pp collisions at $\sqrt{s}$ = 7 TeV with the ATLAS detector at the LHC*, Phys. Rev. D **87** (2013) 112003,
arXiv: `1302.1283 [hep-ex]`, Erratum: Phys. Rev. D **91** (2015) 119901.

[82] ATLAS Collaboration, *Search for supersymmetry at $\sqrt{s}$ = 13 TeV in final states with jets and two same-sign leptons or three leptons with the ATLAS detector*, Eur. Phys. J. C **76** (2016) 259,
arXiv: `1602.09058 [hep-ex]`.

[83] ATLAS Collaboration, *Electron efficiency measurements with the ATLAS detector using 2012 LHC proton–proton collision data*, Eur. Phys. J. C **77** (2017) 195, arXiv: `1612.01456 [hep-ex]`.

[84] ATLAS Collaboration, *Measurement of the photon identification efficiencies with the ATLAS detector using LHC Run-1 data*, (2016), arXiv: `1606.01813 [hep-ex]`.

[85] M. Cacciari, G. P. Salam and G. Soyez, *FastJet user manual*, Eur. Phys. J. C **72** (2012) 1896,
arXiv: `1111.6097 [hep-ph]`.

[86] ATLAS Collaboration,
Topological cell clustering in the ATLAS calorimeters and its performance in LHC Run 1,
Eur. Phys. J. C **77** (2017) 490, arXiv: 1603.02934 [hep-ex].

[87] ATLAS Collaboration, *Monte Carlo Calibration and Combination of In-situ Measurements of Jet Energy Scale, Jet Energy Resolution and Jet Mass in ATLAS*, ATLAS-CONF-2015-037, 2015,
URL: https://cds.cern.ch/record/2044941.

[88] ATLAS Collaboration, *Performance of pile-up mitigation techniques for jets in pp collisions at $\sqrt{s} = 8$ TeV using the ATLAS detector*, Eur. Phys. J. C **76** (2016) 581,
arXiv: 1510.03823 [hep-ex].

[89] ATLAS Collaboration,
Selection of jets produced in 13 *TeV proton–proton collisions with the ATLAS detector*,
ATLAS-CONF-2015-029, 2015, URL: https://cds.cern.ch/record/2037702.

The ATLAS Collaboration

M. Aaboud[34d], G. Aad[99], B. Abbott[124], O. Abdinov[13,*], B. Abeloos[128], S.H. Abidi[165], O.S. AbouZeid[143], N.L. Abraham[153], H. Abramowicz[159], H. Abreu[158], Y. Abulaiti[6], B.S. Acharya[64a,64b,o], S. Adachi[161], L. Adamczyk[81a], J. Adelman[119], M. Adersberger[112], T. Adye[141], A.A. Affolder[143], Y. Afik[158], C. Agheorghiesei[27c], J.A. Aguilar-Saavedra[136f,136a], F. Ahmadov[77,ag], G. Aielli[71a,71b], S. Akatsuka[83], T.P.A. Åkesson[94], E. Akilli[52], A.V. Akimov[108], G.L. Alberghi[23b,23a], J. Albert[174], P. Albicocco[49], M.J. Alconada Verzini[86], S. Alderweireldt[117], M. Aleksa[35], I.N. Aleksandrov[77], C. Alexa[27b], G. Alexander[159], T. Alexopoulos[10], M. Alhroob[124], B. Ali[138], G. Alimonti[66a], J. Alison[36], S.P. Alkire[145], C. Allaire[128], B.M.M. Allbrooke[153], B.W. Allen[127], P.P. Allport[21], A. Aloisio[67a,67b], A. Alonso[39], F. Alonso[86], C. Alpigiani[145], A.A. Alshehri[55], M.I. Alstaty[99], B. Alvarez Gonzalez[35], D. Álvarez Piqueras[172], M.G. Alviggi[67a,67b], B.T. Amadio[18], Y. Amaral Coutinho[78b], L. Ambroz[131], C. Amelung[26], D. Amidei[103], S.P. Amor Dos Santos[136a,136c], S. Amoroso[35], C. Anastopoulos[146], L.S. Ancu[52], N. Andari[21], T. Andeen[11], C.F. Anders[59b], J.K. Anders[20], K.J. Anderson[36], A. Andreazza[66a,66b], V. Andrei[59a], S. Angelidakis[37], I. Angelozzi[118], A. Angerami[38], A.V. Anisenkov[120b,120a], A. Annovi[69a], C. Antel[59a], M.T. Anthony[146], M. Antonelli[49], D.J.A. Antrim[169], F. Anulli[70a], M. Aoki[79], L. Aperio Bella[35], G. Arabidze[104], Y. Arai[79], J.P. Araque[136a], V. Araujo Ferraz[78b], R. Araujo Pereira[78b], A.T.H. Arce[47], R.E. Ardell[91], F.A. Arduh[86], J-F. Arguin[107], S. Argyropoulos[75], A.J. Armbruster[35], L.J. Armitage[90], O. Arnaez[165], H. Arnold[118], M. Arratia[31], O. Arslan[24], A. Artamonov[109,*], G. Artoni[131], S. Artz[97], S. Asai[161], N. Asbah[44], A. Ashkenazi[159], E.M. Asimakopoulou[170], L. Asquith[153], K. Assamagan[29], R. Astalos[28a], R.J. Atkin[32a], M. Atkinson[171], N.B. Atlay[148], K. Augsten[138], G. Avolio[35], R. Avramidou[58a], B. Axen[18], M.K. Ayoub[15a], G. Azuelos[107,au], A.E. Baas[59a], M.J. Baca[21], H. Bachacou[142], K. Bachas[65a,65b], M. Backes[131], P. Bagnaia[70a,70b], M. Bahmani[82], H. Bahrasemani[149], J.T. Baines[141], M. Bajic[39], O.K. Baker[181], P.J. Bakker[118], D. Bakshi Gupta[93], E.M. Baldin[120b,120a], P. Balek[178], F. Balli[142], W.K. Balunas[133], E. Banas[82], A. Bandyopadhyay[24], S. Banerjee[179,k], A.A.E. Bannoura[180], L. Barak[159], W.M. Barbe[37], E.L. Barberio[102], D. Barberis[53b,53a], M. Barbero[99], T. Barillari[113], M-S. Barisits[74], J. Barkeloo[127], T. Barklow[150], N. Barlow[31], R. Barnea[158], S.L. Barnes[58c], B.M. Barnett[141], R.M. Barnett[18], Z. Barnovska-Blenessy[58a], A. Baroncelli[72a], G. Barone[26], A.J. Barr[131], L. Barranco Navarro[172], F. Barreiro[96], J. Barreiro Guimarães da Costa[15a], R. Bartoldus[150], A.E. Barton[87], P. Bartos[28a], A. Basalaev[134], A. Bassalat[128], R.L. Bates[55], S.J. Batista[165], J.R. Batley[31], M. Battaglia[143], M. Bauce[70a,70b], F. Bauer[142], K.T. Bauer[169], H.S. Bawa[150,m], J.B. Beacham[122], M.D. Beattie[87], T. Beau[132], P.H. Beauchemin[168], P. Bechtle[24], H.C. Beck[51], H.P. Beck[20,r], K. Becker[131], M. Becker[97], C. Becot[121], A. Beddall[12d], A.J. Beddall[12a], V.A. Bednyakov[77], M. Bedognetti[118], C.P. Bee[152], T.A. Beermann[35], M. Begalli[78b], M. Begel[29], A. Behera[152], J.K. Behr[44], A.S. Bell[92], G. Bella[159], L. Bellagamba[23b], A. Bellerive[33], M. Bellomo[158], K. Belotskiy[110], N.L. Belyaev[110], O. Benary[159,*], D. Benchekroun[34a], M. Bender[112], N. Benekos[10], Y. Benhammou[159], E. Benhar Noccioli[181], J. Benitez[75], D.P. Benjamin[47], M. Benoit[52], J.R. Bensinger[26], S. Bentvelsen[118], L. Beresford[131], M. Beretta[49], D. Berge[44], E. Bergeaas Kuutmann[170], N. Berger[5], L.J. Bergsten[26], J. Beringer[18], S. Berlendis[56], N.R. Bernard[100], G. Bernardi[132], C. Bernius[150], F.U. Bernlochner[24], T. Berry[91], P. Berta[97], C. Bertella[15a], G. Bertoli[43a,43b], I.A. Bertram[87], C. Bertsche[44], G.J. Besjes[39], O. Bessidskaia Bylund[43a,43b], M. Bessner[44], N. Besson[142], A. Bethani[98], S. Bethke[113], A. Betti[24], A.J. Bevan[90], J. Beyer[113], R.M.B. Bianchi[135], O. Biebel[112], D. Biedermann[19], R. Bielski[98], K. Bierwagen[97], N.V. Biesuz[69a,69b], M. Biglietti[72a], T.R.V. Billoud[107], M. Bindi[51], A. Bingul[12d], C. Bini[70a,70b], S. Biondi[23b,23a], T. Bisanz[51], C. Bittrich[46], D.M. Bjergaard[47], J.E. Black[150], K.M. Black[25], R.E. Blair[6], T. Blazek[28a], I. Bloch[44], C. Blocker[26], A. Blue[55], U. Blumenschein[90], Dr. Blunier[144a],

G.J. Bobbink[118], V.S. Bobrovnikov[120b,120a], S.S. Bocchetta[94], A. Bocci[47], C. Bock[112], D. Boerner[180],
D. Bogavac[112], A.G. Bogdanchikov[120b,120a], C. Bohm[43a], V. Boisvert[91], P. Bokan[170,y], T. Bold[81a],
A.S. Boldyrev[111], A.E. Bolz[59b], M. Bomben[132], M. Bona[90], J.S. Bonilla[127], M. Boonekamp[142],
A. Borisov[140], G. Borissov[87], J. Bortfeldt[35], D. Bortoletto[131], V. Bortolotto[61a,61b,61c], D. Boscherini[23b],
M. Bosman[14], J.D. Bossio Sola[30], J. Boudreau[135], E.V. Bouhova-Thacker[87], D. Boumediene[37],
C. Bourdarios[128], S.K. Boutle[55], A. Boveia[122], J. Boyd[35], I.R. Boyko[77], A.J. Bozson[91], J. Bracinik[21],
N. Brahimi[99], A. Brandt[8], G. Brandt[180], O. Brandt[59a], F. Braren[44], U. Bratzler[162], B. Brau[100],
J.E. Brau[127], W.D. Breaden Madden[55], K. Brendlinger[44], A.J. Brennan[102], L. Brenner[44], R. Brenner[170],
S. Bressler[178], D.L. Briglin[21], T.M. Bristow[48], D. Britton[55], D. Britzger[59b], I. Brock[24], R. Brock[104],
G. Brooijmans[38], T. Brooks[91], W.K. Brooks[144b], E. Brost[119], J.H Broughton[21],
P.A. Bruckman de Renstrom[82], D. Bruncko[28b], A. Bruni[23b], G. Bruni[23b], L.S. Bruni[118], S. Bruno[71a,71b],
B.H. Brunt[31], M. Bruschi[23b], N. Bruscino[135], P. Bryant[36], L. Bryngemark[44], T. Buanes[17], Q. Buat[35],
P. Buchholz[148], A.G. Buckley[55], I.A. Budagov[77], F. Buehrer[50], M.K. Bugge[130], O. Bulekov[110],
D. Bullock[8], T.J. Burch[119], S. Burdin[88], C.D. Burgard[118], A.M. Burger[5], B. Burghgrave[119], K. Burka[82],
S. Burke[141], I. Burmeister[45], J.T.P. Burr[131], D. Büscher[50], V. Büscher[97], E. Buschmann[51], P. Bussey[55],
J.M. Butler[25], C.M. Buttar[55], J.M. Butterworth[92], P. Butti[35], W. Buttinger[35], A. Buzatu[155],
A.R. Buzykaev[120b,120a], G. Cabras[23b,23a], S. Cabrera Urbán[172], D. Caforio[138], H. Cai[171], V.M.M. Cairo[2],
O. Cakir[4a], N. Calace[52], P. Calafiura[18], A. Calandri[99], G. Calderini[132], P. Calfayan[63], G. Callea[40b,40a],
L.P. Caloba[78b], S. Calvente Lopez[96], D. Calvet[37], S. Calvet[37], T.P. Calvet[152], M. Calvetti[69a,69b],
R. Camacho Toro[36], S. Camarda[35], P. Camarri[71a,71b], D. Cameron[130], R. Caminal Armadans[100],
C. Camincher[56], S. Campana[35], M. Campanelli[92], A. Camplani[66a,66b], A. Campoverde[148],
V. Canale[67a,67b], M. Cano Bret[58c], J. Cantero[125], T. Cao[159], Y. Cao[171], M.D.M. Capeans Garrido[35],
I. Caprini[27b], M. Caprini[27b], M. Capua[40b,40a], R.M. Carbone[38], R. Cardarelli[71a], F.C. Cardillo[50],
I. Carli[139], T. Carli[35], G. Carlino[67a], B.T. Carlson[135], L. Carminati[66a,66b], R.M.D. Carney[43a,43b],
S. Caron[117], E. Carquin[144b], S. Carrá[66a,66b], G.D. Carrillo-Montoya[35], D. Casadei[21], M.P. Casado[14,g],
A.F. Casha[165], M. Casolino[14], D.W. Casper[169], R. Castelijn[118], V. Castillo Gimenez[172],
N.F. Castro[136a,136e], A. Catinaccio[35], J.R. Catmore[130], A. Cattai[35], J. Caudron[24], V. Cavaliere[29],
E. Cavallaro[14], D. Cavalli[66a], M. Cavalli-Sforza[14], V. Cavasinni[69a,69b], E. Celebi[12b], F. Ceradini[72a,72b],
L. Cerda Alberich[172], A.S. Cerqueira[78a], A. Cerri[153], L. Cerrito[71a,71b], F. Cerutti[18], A. Cervelli[23b,23a],
S.A. Cetin[12b], A. Chafaq[34a], D Chakraborty[119], S.K. Chan[57], W.S. Chan[118], Y.L. Chan[61a], P. Chang[171],
J.D. Chapman[31], D.G. Charlton[21], C.C. Chau[33], C.A. Chavez Barajas[153], S. Che[122], A. Chegwidden[104],
S. Chekanov[6], S.V. Chekulaev[166a], G.A. Chelkov[77,at], M.A. Chelstowska[35], C. Chen[58a], C.H. Chen[76],
H. Chen[29], J. Chen[58a], J. Chen[38], S. Chen[133], S.J. Chen[15c], X. Chen[15b,as], Y. Chen[80], Y-H. Chen[44],
H.C. Cheng[103], H.J. Cheng[15d], A. Cheplakov[77], E. Cheremushkina[140], R. Cherkaoui El Moursli[34e],
E. Cheu[7], K. Cheung[62], L. Chevalier[142], V. Chiarella[49], G. Chiarelli[69a], G. Chiodini[65a], A.S. Chisholm[35],
A. Chitan[27b], I. Chiu[161], Y.H. Chiu[174], M.V. Chizhov[77], K. Choi[63], A.R. Chomont[37], S. Chouridou[160],
Y.S. Chow[118], V. Christodoulou[92], M.C. Chu[61a], J. Chudoba[137], A.J. Chuinard[101], J.J. Chwastowski[82],
L. Chytka[126], D. Cinca[45], V. Cindro[89], I.A. Cioară[24], A. Ciocio[18], F. Cirotto[67a,67b], Z.H. Citron[178],
M. Citterio[66a], A. Clark[52], M.R. Clark[38], P.J. Clark[48], R.N. Clarke[18], C. Clement[43a,43b], Y. Coadou[99],
M. Cobal[64a,64c], A. Coccaro[53b,53a], J. Cochran[76], L. Colasurdo[117], B. Cole[38], A.P. Colijn[118], J. Collot[56],
P. Conde Muiño[136a,136b], E. Coniavitis[50], S.H. Connell[32b], I.A. Connelly[98], S. Constantinescu[27b],
G. Conti[35], F. Conventi[67a,av], A.M. Cooper-Sarkar[131], F. Cormier[173], K.J.R. Cormier[165],
M. Corradi[70a,70b], E.E. Corrigan[94], F. Corriveau[101,ae], A. Cortes-Gonzalez[35], M.J. Costa[172],
D. Costanzo[146], G. Cottin[31], G. Cowan[91], B.E. Cox[98], J. Crane[98], K. Cranmer[121], S.J. Crawley[55],
R.A. Creager[133], G. Cree[33], S. Crépé-Renaudin[56], F. Crescioli[132], M. Cristinziani[24], V. Croft[121],
G. Crosetti[40b,40a], A. Cueto[96], T. Cuhadar Donszelmann[146], A.R. Cukierman[150], M. Curatolo[49],
J. Cúth[97], S. Czekierda[82], P. Czodrowski[35], M.J. Da Cunha Sargedas De Sousa[136a,136b], C. Da Via[98],

W. Dabrowski[81a], T. Dado[28a,y], S. Dahbi[34e], T. Dai[103], O. Dale[17], F. Dallaire[107], C. Dallapiccola[100],
M. Dam[39], G. D'amen[23b,23a], J.R. Dandoy[133], M.F. Daneri[30], N.P. Dang[179,k], N.D Dann[98],
M. Danninger[173], V. Dao[35], G. Darbo[53b], S. Darmora[8], O. Dartsi[5], A. Dattagupta[127], T. Daubney[44],
S. D'Auria[55], W. Davey[24], C. David[44], T. Davidek[139], D.R. Davis[47], E. Dawe[102], I. Dawson[146], K. De[8],
R. De Asmundis[67a], A. De Benedetti[124], S. De Castro[23b,23a], S. De Cecco[132], N. De Groot[117],
P. de Jong[118], H. De la Torre[104], F. De Lorenzi[76], A. De Maria[51,t], D. De Pedis[70a], A. De Salvo[70a],
U. De Sanctis[71a,71b], A. De Santo[153], K. De Vasconcelos Corga[99], J.B. De Vivie De Regie[128],
C. Debenedetti[143], D.V. Dedovich[77], N. Dehghanian[3], I. Deigaard[118], M. Del Gaudio[40b,40a],
J. Del Peso[96], D. Delgove[128], F. Deliot[142], C.M. Delitzsch[7], M. Della Pietra[67a,67b], D. Della Volpe[52],
A. Dell'Acqua[35], L. Dell'Asta[25], M. Delmastro[5], C. Delporte[128], P.A. Delsart[56], D.A. DeMarco[165],
S. Demers[181], M. Demichev[77], S.P. Denisov[140], D. Denysiuk[118], L. D'Eramo[132], D. Derendarz[82],
J.E. Derkaoui[34d], F. Derue[132], P. Dervan[88], K. Desch[24], C. Deterre[44], K. Dette[165], M.R. Devesa[30],
P.O. Deviveiros[35], A. Dewhurst[141], S. Dhaliwal[26], F.A. Di Bello[52], A. Di Ciaccio[71a,71b], L. Di Ciaccio[5],
W.K. Di Clemente[133], C. Di Donato[67a,67b], A. Di Girolamo[35], B. Di Micco[72a,72b], R. Di Nardo[35],
K.F. Di Petrillo[57], A. Di Simone[50], R. Di Sipio[165], D. Di Valentino[33], C. Diaconu[99], M. Diamond[165],
F.A. Dias[39], T. Dias Do Vale[136a], M.A. Diaz[144a], J. Dickinson[18], E.B. Diehl[103], J. Dietrich[19],
S. Díez Cornell[44], A. Dimitrievska[18], J. Dingfelder[24], P. Dita[27b], S. Dita[27b], F. Dittus[35], F. Djama[99],
T. Djobava[157b], J.I. Djuvsland[59a], M.A.B. Do Vale[78c], M. Dobre[27b], D. Dodsworth[26], C. Doglioni[94],
J. Dolejsi[139], Z. Dolezal[139], M. Donadelli[78d], J. Donini[37], M. D'Onofrio[88], J. Dopke[141], A. Doria[67a],
M.T. Dova[86], A.T. Doyle[55], E. Drechsler[51], E. Dreyer[149], T. Dreyer[51], M. Dris[10], Y. Du[58b],
J. Duarte-Campderros[159], F. Dubinin[108], A. Dubreuil[52], E. Duchovni[178], G. Duckeck[112],
A. Ducourthial[132], O.A. Ducu[107,x], D. Duda[118], A. Dudarev[35], A.C. Dudder[97], E.M. Duffield[18],
L. Duflot[128], M. Dührssen[35], C. Dülsen[180], M. Dumancic[178], A.E. Dumitriu[27b,e], A.K. Duncan[55],
M. Dunford[59a], A. Duperrin[99], H. Duran Yildiz[4a], M. Düren[54], A. Durglishvili[157b], D. Duschinger[46],
B. Dutta[44], D. Duvnjak[1], M. Dyndal[44], B.S. Dziedzic[82], C. Eckardt[44], K.M. Ecker[113], R.C. Edgar[103],
T. Eifert[35], G. Eigen[17], K. Einsweiler[18], T. Ekelof[170], M. El Kacimi[34c], R. El Kosseifi[99], V. Ellajosyula[99],
M. Ellert[170], F. Ellinghaus[180], A.A. Elliot[174], N. Ellis[35], J. Elmsheuser[29], M. Elsing[35], D. Emeliyanov[141],
Y. Enari[161], J.S. Ennis[176], M.B. Epland[47], J. Erdmann[45], A. Ereditato[20], S. Errede[171], M. Escalier[128],
C. Escobar[172], B. Esposito[49], O. Estrada Pastor[172], A.I. Etienvre[142], E. Etzion[159], H. Evans[63],
A. Ezhilov[134], M. Ezzi[34e], F. Fabbri[23b,23a], L. Fabbri[23b,23a], V. Fabiani[117], G. Facini[92],
R.M. Fakhrutdinov[140], S. Falciano[70a], P.J. Falke[5], S. Falke[5], J. Faltova[139], Y. Fang[15a], M. Fanti[66a,66b],
A. Farbin[8], A. Farilla[72a], E.M. Farina[68a,68b], T. Farooque[104], S. Farrell[18], S.M. Farrington[176],
P. Farthouat[35], F. Fassi[34e], P. Fassnacht[35], D. Fassouliotis[9], M. Faucci Giannelli[48], A. Favareto[53b,53a],
W.J. Fawcett[52], L. Fayard[128], O.L. Fedin[134,q], W. Fedorko[173], M. Feickert[41], S. Feigl[130], L. Feligioni[99],
C. Feng[58b], E.J. Feng[35], M. Feng[47], M.J. Fenton[55], A.B. Fenyuk[140], L. Feremenga[8], J. Ferrando[44],
A. Ferrari[170], P. Ferrari[118], R. Ferrari[68a], D.E. Ferreira de Lima[59b], A. Ferrer[172], D. Ferrere[52],
C. Ferretti[103], F. Fiedler[97], A. Filipčič[89], F. Filthaut[117], M. Fincke-Keeler[174], K.D. Finelli[25],
M.C.N. Fiolhais[136a,136c,b], L. Fiorini[172], C. Fischer[14], J. Fischer[180], W.C. Fisher[104], N. Flaschel[44],
I. Fleck[148], P. Fleischmann[103], R.R.M. Fletcher[133], T. Flick[180], B.M. Flierl[112], L.M. Flores[133],
L.R. Flores Castillo[61a], N. Fomin[17], G.T. Forcolin[98], A. Formica[142], F.A. Förster[14], A.C. Forti[98],
A.G. Foster[21], D. Fournier[128], H. Fox[87], S. Fracchia[146], P. Francavilla[69a,69b], M. Franchini[23b,23a],
S. Franchino[59a], D. Francis[35], L. Franconi[130], M. Franklin[57], M. Frate[169], M. Fraternali[68a,68b],
D. Freeborn[92], S.M. Fressard-Batraneanu[35], B. Freund[107], W.S. Freund[78b], D. Froidevaux[35],
J.A. Frost[131], C. Fukunaga[162], T. Fusayasu[114], J. Fuster[172], O. Gabizon[158], A. Gabrielli[23b,23a],
A. Gabrielli[18], G.P. Gach[81a], S. Gadatsch[52], S. Gadomski[52], P. Gadow[113], G. Gagliardi[53b,53a],
L.G. Gagnon[107], C. Galea[27b], B. Galhardo[136a,136c], E.J. Gallas[131], B.J. Gallop[141], P. Gallus[138],
G. Galster[39], R. Gamboa Goni[90], K.K. Gan[122], S. Ganguly[178], Y. Gao[88], Y.S. Gao[150,m], C. García[172],

J.E. García Navarro[172], J.A. García Pascual[15a], M. Garcia-Sciveres[18], R.W. Gardner[36], N. Garelli[150], V. Garonne[130], K. Gasnikova[44], A. Gaudiello[53b,53a], G. Gaudio[68a], I.L. Gavrilenko[108], A. Gavrilyuk[109], C. Gay[173], G. Gaycken[24], E.N. Gazis[10], C.N.P. Gee[141], J. Geisen[51], M. Geisen[97], M.P. Geisler[59a], K. Gellerstedt[43a,43b], C. Gemme[53b], M.H. Genest[56], C. Geng[103], S. Gentile[70a,70b], C. Gentsos[160], S. George[91], D. Gerbaudo[14], G. Gessner[45], S. Ghasemi[148], M. Ghneimat[24], B. Giacobbe[23b], S. Giagu[70a,70b], N. Giangiacomi[23b,23a], P. Giannetti[69a], S.M. Gibson[91], M. Gignac[143], M. Gilchriese[18], D. Gillberg[33], G. Gilles[180], D.M. Gingrich[3,au], M.P. Giordani[64a,64c], F.M. Giorgi[23b], P.F. Giraud[142], P. Giromini[57], G. Giugliarelli[64a,64c], D. Giugni[66a], F. Giuli[131], M. Giulini[59b], S. Gkaitatzis[160], I. Gkialas[9,j], E.L. Gkougkousis[14], P. Gkountoumis[10], L.K. Gladilin[111], C. Glasman[96], J. Glatzer[14], P.C.F. Glaysher[44], A. Glazov[44], M. Goblirsch-Kolb[26], J. Godlewski[82], S. Goldfarb[102], T. Golling[52], D. Golubkov[140], A. Gomes[136a,136b,136d], R. Goncalves Gama[78a], R. Gonçalo[136a], G. Gonella[50], L. Gonella[21], A. Gongadze[77], F. Gonnella[21], J.L. Gonski[57], S. González de la Hoz[172], S. Gonzalez-Sevilla[52], L. Goossens[35], P.A. Gorbounov[109], H.A. Gordon[29], B. Gorini[35], E. Gorini[65a,65b], A. Gorišek[89], A.T. Goshaw[47], C. Gössling[45], M.I. Gostkin[77], C.A. Gottardo[24], C.R. Goudet[128], D. Goujdami[34c], A.G. Goussiou[145], N. Govender[32b,c], C. Goy[5], E. Gozani[158], I. Grabowska-Bold[81a], P.O.J. Gradin[170], E.C. Graham[88], J. Gramling[169], E. Gramstad[130], S. Grancagnolo[19], V. Gratchev[134], P.M. Gravila[27f], C. Gray[55], H.M. Gray[18], Z.D. Greenwood[93,aj], C. Grefe[24], K. Gregersen[92], I.M. Gregor[44], P. Grenier[150], K. Grevtsov[44], J. Griffiths[8], A.A. Grillo[143], K. Grimm[150], S. Grinstein[14,z], Ph. Gris[37], J.-F. Grivaz[128], S. Groh[97], E. Gross[178], J. Grosse-Knetter[51], G.C. Grossi[93], Z.J. Grout[92], A. Grummer[116], L. Guan[103], W. Guan[179], J. Guenther[35], A. Guerguichon[128], F. Guescini[166a], D. Guest[169], O. Gueta[159], R. Gugel[50], B. Gui[122], T. Guillemin[5], S. Guindon[35], U. Gul[55], C. Gumpert[35], J. Guo[58c], W. Guo[103], Y. Guo[58a,s], Z. Guo[99], R. Gupta[41], S. Gurbuz[12c], G. Gustavino[124], B.J. Gutelman[158], P. Gutierrez[124], N.G. Gutierrez Ortiz[92], C. Gutschow[92], C. Guyot[142], M.P. Guzik[81a], C. Gwenlan[131], C.B. Gwilliam[88], A. Haas[121], C. Haber[18], H.K. Hadavand[8], N. Haddad[34e], A. Hadef[99], S. Hageböck[24], M. Hagihara[167], H. Hakobyan[182,*], M. Haleem[175], J. Haley[125], G. Halladjian[104], G.D. Hallewell[99], K. Hamacher[180], P. Hamal[126], K. Hamano[174], A. Hamilton[32a], G.N. Hamity[146], K. Han[58a,ai], L. Han[58a], S. Han[15d], K. Hanagaki[79,v], M. Hance[143], D.M. Handl[112], B. Haney[133], R. Hankache[132], P. Hanke[59a], E. Hansen[94], J.B. Hansen[39], J.D. Hansen[39], M.C. Hansen[24], P.H. Hansen[39], K. Hara[167], A.S. Hard[179], T. Harenberg[180], S. Harkusha[105], P.F. Harrison[176], N.M. Hartmann[112], Y. Hasegawa[147], A. Hasib[48], S. Hassani[142], S. Haug[20], R. Hauser[104], L. Hauswald[46], L.B. Havener[38], M. Havranek[138], C.M. Hawkes[21], R.J. Hawkings[35], D. Hayden[104], C. Hayes[152], C.P. Hays[131], J.M. Hays[90], H.S. Hayward[88], S.J. Haywood[141], M.P. Heath[48], T. Heck[97], V. Hedberg[94], L. Heelan[8], S. Heer[24], K.K. Heidegger[50], S. Heim[44], T. Heim[18], B. Heinemann[44,ap], J.J. Heinrich[112], L. Heinrich[121], C. Heinz[54], J. Hejbal[137], L. Helary[35], A. Held[173], S. Hellesund[130], S. Hellman[43a,43b], C. Helsens[35], R.C.W. Henderson[87], Y. Heng[179], S. Henkelmann[173], A.M. Henriques Correia[35], G.H. Herbert[19], H. Herde[26], V. Herget[175], Y. Hernández Jiménez[32c], H. Herr[97], G. Herten[50], R. Hertenberger[112], L. Hervas[35], T.C. Herwig[133], G.G. Hesketh[92], N.P. Hessey[166a], J.W. Hetherly[41], S. Higashino[79], E. Higón-Rodriguez[172], K. Hildebrand[36], E. Hill[174], J.C. Hill[31], K.H. Hiller[44], S.J. Hillier[21], M. Hils[46], I. Hinchliffe[18], M. Hirose[129], D. Hirschbuehl[180], B. Hiti[89], O. Hladik[137], D.R. Hlaluku[32c], X. Hoad[48], J. Hobbs[152], N. Hod[166a], M.C. Hodgkinson[146], A. Hoecker[35], M.R. Hoeferkamp[116], F. Hoenig[112], D. Hohn[24], D. Hohov[128], T.R. Holmes[36], M. Holzbock[112], M. Homann[45], S. Honda[167], T. Honda[79], T.M. Hong[135], B.H. Hooberman[171], W.H. Hopkins[127], Y. Horii[115], A.J. Horton[149], L.A. Horyn[36], J-Y. Hostachy[56], A. Hostiuc[145], S. Hou[155], A. Hoummada[34a], J. Howarth[98], J. Hoya[86], M. Hrabovsky[126], J. Hrdinka[35], I. Hristova[19], J. Hrivnac[128], A. Hrynevich[106], T. Hryn'ova[5], P.J. Hsu[62], S.-C. Hsu[145], Q. Hu[29], S. Hu[58c], Y. Huang[15a], Z. Hubacek[138], F. Hubaut[99], M. Huebner[24], F. Huegging[24], T.B. Huffman[131], E.W. Hughes[38], M. Huhtinen[35], R.F.H. Hunter[33], P. Huo[152], A.M. Hupe[33], N. Huseynov[77,ag], J. Huston[104], J. Huth[57], R. Hyneman[103], G. Iacobucci[52],

G. Iakovidis[29], I. Ibragimov[148], L. Iconomidou-Fayard[128], Z. Idrissi[34e], P. Iengo[35], R. Ignazzi[39],
O. Igonkina[118,ac], R. Iguchi[161], T. Iizawa[177], Y. Ikegami[79], M. Ikeno[79], D. Iliadis[160], N. Ilic[150],
F. Iltzsche[46], G. Introzzi[68a,68b], M. Iodice[72a], K. Iordanidou[38], V. Ippolito[70a,70b], M.F. Isacson[170],
N. Ishijima[129], M. Ishino[161], M. Ishitsuka[163], C. Issever[131], S. Istin[12c,an], F. Ito[167], J.M. Iturbe Ponce[61a],
R. Iuppa[73a,73b], H. Iwasaki[79], J.M. Izen[42], V. Izzo[67a], S. Jabbar[3], P. Jacka[137], P. Jackson[1], R.M. Jacobs[24],
V. Jain[2], G. Jäkel[180], K.B. Jakobi[97], K. Jakobs[50], S. Jakobsen[74], T. Jakoubek[137], D.O. Jamin[125],
D.K. Jana[93], R. Jansky[52], J. Janssen[24], M. Janus[51], P.A. Janus[81a], G. Jarlskog[94], N. Javadov[77,ag],
T. Javůrek[50], M. Javurkova[50], F. Jeanneau[142], L. Jeanty[18], J. Jejelava[157a,ah], A. Jelinskas[176], P. Jenni[50,d],
C. Jeske[176], S. Jézéquel[5], H. Ji[179], J. Jia[152], H. Jiang[76], Y. Jiang[58a], Z. Jiang[150], S. Jiggins[92],
J. Jimenez Pena[172], S. Jin[15c], A. Jinaru[27b], O. Jinnouchi[163], H. Jivan[32c], P. Johansson[146], K.A. Johns[7],
C.A. Johnson[63], W.J. Johnson[145], K. Jon-And[43a,43b], R.W.L. Jones[87], S.D. Jones[153], S. Jones[7],
T.J. Jones[88], J. Jongmanns[59a], P.M. Jorge[136a,136b], J. Jovicevic[166a], X. Ju[179], J.J. Junggeburth[113],
A. Juste Rozas[14,z], A. Kaczmarska[82], M. Kado[128], H. Kagan[122], M. Kagan[150], T. Kaji[177],
E. Kajomovitz[158], C.W. Kalderon[94], A. Kaluza[97], S. Kama[41], A. Kamenshchikov[140], L. Kanjir[89],
Y. Kano[161], V.A. Kantserov[110], J. Kanzaki[79], B. Kaplan[121], L.S. Kaplan[179], D. Kar[32c], K. Karakostas[10],
N. Karastathis[10], M.J. Kareem[166b], E. Karentzos[10], S.N. Karpov[77], Z.M. Karpova[77], V. Kartvelishvili[87],
A.N. Karyukhin[140], K. Kasahara[167], L. Kashif[179], R.D. Kass[122], A. Kastanas[151], Y. Kataoka[161],
C. Kato[161], A. Katre[52], J. Katzy[44], K. Kawade[80], K. Kawagoe[85], T. Kawamoto[161], G. Kawamura[51],
E.F. Kay[88], V.F. Kazanin[120b,120a], R. Keeler[174], R. Kehoe[41], J.S. Keller[33], E. Kellermann[94],
J.J. Kempster[21], J. Kendrick[21], O. Kepka[137], S. Kersten[180], B.P. Kerševan[89], R.A. Keyes[101],
M. Khader[171], F. Khalil-Zada[13], A. Khanov[125], A.G. Kharlamov[120b,120a], T. Kharlamova[120b,120a],
A. Khodinov[164], T.J. Khoo[52], V. Khovanskiy[109,*], E. Khramov[77], J. Khubua[157b], S. Kido[80], M. Kiehn[52],
C.R. Kilby[91], H.Y. Kim[8], S.H. Kim[167], Y.K. Kim[36], N. Kimura[64a,64c], O.M. Kind[19], B.T. King[88],
D. Kirchmeier[46], J. Kirk[141], A.E. Kiryunin[113], T. Kishimoto[161], D. Kisielewska[81a], V. Kitali[44],
O. Kivernyk[5], E. Kladiva[28b], T. Klapdor-Kleingrothaus[50], M.H. Klein[103], M. Klein[88], U. Klein[88],
K. Kleinknecht[97], P. Klimek[119], A. Klimentov[29], R. Klingenberg[45,*], T. Klingl[24], T. Klioutchnikova[35],
F.F. Klitzner[112], P. Kluit[118], S. Kluth[113], E. Kneringer[74], E.B.F.G. Knoops[99], A. Knue[50],
A. Kobayashi[161], D. Kobayashi[85], T. Kobayashi[161], M. Kobel[46], M. Kocian[150], P. Kodys[139], T. Koffas[33],
E. Koffeman[118], N.M. Köhler[113], T. Koi[150], M. Kolb[59b], I. Koletsou[5], T. Kondo[79], N. Kondrashova[58c],
K. Köneke[50], A.C. König[117], T. Kono[79,ao], R. Konoplich[121,ak], N. Konstantinidis[92], B. Konya[94],
R. Kopeliansky[63], S. Koperny[81a], K. Korcyl[82], K. Kordas[160], A. Korn[92], I. Korolkov[14],
E.V. Korolkova[146], O. Kortner[113], S. Kortner[113], T. Kosek[139], V.V. Kostyukhin[24], A. Kotwal[47],
A. Koulouris[10], A. Kourkoumeli-Charalampidi[68a,68b], C. Kourkoumelis[9], E. Kourlitis[146],
V. Kouskoura[29], A.B. Kowalewska[82], R. Kowalewski[174], T.Z. Kowalski[81a], C. Kozakai[161],
W. Kozanecki[142], A.S. Kozhin[140], V.A. Kramarenko[111], G. Kramberger[89], D. Krasnopevtsev[110],
M.W. Krasny[132], A. Krasznahorkay[35], D. Krauss[113], J.A. Kremer[81a], J. Kretzschmar[88], K. Kreutzfeldt[54],
P. Krieger[165], K. Krizka[18], K. Kroeninger[45], H. Kroha[113], J. Kroll[137], J. Kroll[133], J. Kroseberg[24],
J. Krstic[16], U. Kruchonak[77], H. Krüger[24], N. Krumnack[76], M.C. Kruse[47], T. Kubota[102], S. Kuday[4b],
J.T. Kuechler[180], S. Kuehn[35], A. Kugel[59a], F. Kuger[175], T. Kuhl[44], V. Kukhtin[77], R. Kukla[99],
Y. Kulchitsky[105], S. Kuleshov[144b], Y.P. Kulinich[171], M. Kuna[56], T. Kunigo[83], A. Kupco[137], T. Kupfer[45],
O. Kuprash[159], H. Kurashige[80], L.L. Kurchaninov[166a], Y.A. Kurochkin[105], M.G. Kurth[15d],
E.S. Kuwertz[174], M. Kuze[163], J. Kvita[126], T. Kwan[174], A. La Rosa[113], J.L. La Rosa Navarro[78d],
L. La Rotonda[40b,40a], F. La Ruffa[40b,40a], C. Lacasta[172], F. Lacava[70a,70b], J. Lacey[44], D.P.J. Lack[98],
H. Lacker[19], D. Lacour[132], E. Ladygin[77], R. Lafaye[5], B. Laforge[132], S. Lai[51], S. Lammers[63], W. Lampl[7],
E. Lançon[29], U. Landgraf[50], M.P.J. Landon[90], M.C. Lanfermann[52], V.S. Lang[44], J.C. Lange[14],
R.J. Langenberg[35], A.J. Lankford[169], F. Lanni[29], K. Lantzsch[24], A. Lanza[68a], A. Lapertosa[53b,53a],
S. Laplace[132], J.F. Laporte[142], T. Lari[66a], F. Lasagni Manghi[23b,23a], M. Lassnig[35], T.S. Lau[61a],

A. Laudrain[128], A.T. Law[143], P. Laycock[88], M. Lazzaroni[66a,66b], B. Le[102], O. Le Dortz[132],
E. Le Guirriec[99], E.P. Le Quilleuc[142], M. LeBlanc[7], T. LeCompte[6], F. Ledroit-Guillon[56], C.A. Lee[29],
G.R. Lee[144a], L. Lee[57], S.C. Lee[155], B. Lefebvre[101], M. Lefebvre[174], F. Legger[112], C. Leggett[18],
G. Lehmann Miotto[35], W.A. Leight[44], A. Leisos[160,w], M.A.L. Leite[78d], R. Leitner[139], D. Lellouch[178],
B. Lemmer[51], K.J.C. Leney[92], T. Lenz[24], B. Lenzi[35], R. Leone[7], S. Leone[69a], C. Leonidopoulos[48],
G. Lerner[153], C. Leroy[107], R. Les[165], A.A.J. Lesage[142], C.G. Lester[31], M. Levchenko[134], J. Levêque[5],
D. Levin[103], L.J. Levinson[178], M. Levy[21], D. Lewis[90], B. Li[58a,s], C-Q. Li[58a], H. Li[58b], L. Li[58c], Q. Li[15d],
Q.Y. Li[58a], S. Li[58d,58c], X. Li[58c], Y. Li[148], Z. Liang[15a], B. Liberti[71a], A. Liblong[165], K. Lie[61c],
A. Limosani[154], C.Y. Lin[31], K. Lin[104], S.C. Lin[156], T.H. Lin[97], R.A. Linck[63], B.E. Lindquist[152],
A.L. Lionti[52], E. Lipeles[133], A. Lipniacka[17], M. Lisovyi[59b], T.M. Liss[171,ar], A. Lister[173], A.M. Litke[143],
J.D. Little[8], B. Liu[76], B.L Liu[6], H.B. Liu[29], H. Liu[103], J.B. Liu[58a], J.K.K. Liu[131], K. Liu[132], M. Liu[58a],
P. Liu[18], Y.L. Liu[58a], Y.W. Liu[58a], M. Livan[68a,68b], A. Lleres[56], J. Llorente Merino[15a], S.L. Lloyd[90],
C.Y. Lo[61b], F. Lo Sterzo[41], E.M. Lobodzinska[44], P. Loch[7], F.K. Loebinger[98], A. Loesle[50], K.M. Loew[26],
T. Lohse[19], K. Lohwasser[146], M. Lokajicek[137], B.A. Long[25], J.D. Long[171], R.E. Long[87], L. Longo[65a,65b],
K.A. Looper[122], J.A. Lopez[144b], I. Lopez Paz[14], A. Lopez Solis[132], J. Lorenz[112], N. Lorenzo Martinez[5],
M. Losada[22], P.J. Lösel[112], X. Lou[44], X. Lou[15a], A. Lounis[128], J. Love[6], P.A. Love[87],
J.J. Lozano Bahilo[172], H. Lu[61a], N. Lu[103], Y.J. Lu[62], H.J. Lubatti[145], C. Luci[70a,70b], A. Lucotte[56],
C. Luedtke[50], F. Luehring[63], I. Luise[132], W. Lukas[74], L. Luminari[70a], B. Lund-Jensen[151], M.S. Lutz[100],
P.M. Luzi[132], D. Lynn[29], R. Lysak[137], E. Lytken[94], F. Lyu[15a], V. Lyubushkin[77], H. Ma[29], L.L. Ma[58b],
Y. Ma[58b], G. Maccarrone[49], A. Macchiolo[113], C.M. Macdonald[146], J. Machado Miguens[133,136b],
D. Madaffari[172], R. Madar[37], W.F. Mader[46], A. Madsen[44], N. Madysa[46], J. Maeda[80], S. Maeland[17],
T. Maeno[29], A.S. Maevskiy[111], V. Magerl[50], C. Maidantchik[78b], T. Maier[112], A. Maio[136a,136b,136d],
O. Majersky[28a], S. Majewski[127], Y. Makida[79], N. Makovec[128], B. Malaescu[132], Pa. Malecki[82],
V.P. Maleev[134], F. Malek[56], U. Mallik[75], D. Malon[6], C. Malone[31], S. Maltezos[10], S. Malyukov[35],
J. Mamuzic[172], G. Mancini[49], I. Mandić[89], J. Maneira[136a], L. Manhaes de Andrade Filho[78a],
J. Manjarres Ramos[46], K.H. Mankinen[94], A. Mann[112], A. Manousos[74], B. Mansoulie[142],
J.D. Mansour[15a], R. Mantifel[101], M. Mantoani[51], S. Manzoni[66a,66b], G. Marceca[30], L. March[52],
L. Marchese[131], G. Marchiori[132], M. Marcisovsky[137], C.A. Marin Tobon[35], M. Marjanovic[37],
D.E. Marley[103], F. Marroquim[78b], Z. Marshall[18], M.U.F Martensson[170], S. Marti-Garcia[172],
C.B. Martin[122], T.A. Martin[176], V.J. Martin[48], B. Martin dit Latour[17], M. Martinez[14,z],
V.I. Martinez Outschoorn[100], S. Martin-Haugh[141], V.S. Martoiu[27b], A.C. Martyniuk[92], A. Marzin[35],
L. Masetti[97], T. Mashimo[161], R. Mashinistov[108], J. Masik[98], A.L. Maslennikov[120b,120a], L.H. Mason[102],
L. Massa[71a,71b], P. Mastrandrea[5], A. Mastroberardino[40b,40a], T. Masubuchi[161], P. Mättig[180], J. Maurer[27b],
B. Maček[89], S.J. Maxfield[88], D.A. Maximov[120b,120a], R. Mazini[155], I. Maznas[160], S.M. Mazza[143],
N.C. Mc Fadden[116], G. Mc Goldrick[165], S.P. Mc Kee[103], A. McCarn[103], T.G. McCarthy[113],
L.I. McClymont[92], E.F. McDonald[102], J.A. Mcfayden[35], G. Mchedlidze[51], M.A. McKay[41],
K.D. McLean[174], S.J. McMahon[141], P.C. McNamara[102], C.J. McNicol[176], R.A. McPherson[174,ae],
Z.A. Meadows[100], S. Meehan[145], T. Megy[50], S. Mehlhase[112], A. Mehta[88], T. Meideck[56], B. Meirose[42],
D. Melini[172,h], B.R. Mellado Garcia[32c], J.D. Mellenthin[51], M. Melo[28a], F. Meloni[20], A. Melzer[24],
S.B. Menary[98], L. Meng[88], X.T. Meng[103], A. Mengarelli[23b,23a], S. Menke[113], E. Meoni[40b,40a],
S. Mergelmeyer[19], C. Merlassino[20], P. Mermod[52], L. Merola[67a,67b], C. Meroni[66a], F.S. Merritt[36],
A. Messina[70a,70b], J. Metcalfe[6], A.S. Mete[169], C. Meyer[133], J. Meyer[158], J-P. Meyer[142],
H. Meyer Zu Theenhausen[59a], F. Miano[153], R.P. Middleton[141], L. Mijović[48], G. Mikenberg[178],
M. Mikestikova[137], M. Mikuž[89], M. Milesi[102], A. Milic[165], D.A. Millar[90], D.W. Miller[36], A. Milov[178],
D.A. Milstead[43a,43b], A.A. Minaenko[140], I.A. Minashvili[157b], A.I. Mincer[121], B. Mindur[81a],
M. Mineev[77], Y. Minegishi[161], Y. Ming[179], L.M. Mir[14], A. Mirto[65a,65b], K.P. Mistry[133], T. Mitani[177],
J. Mitrevski[112], V.A. Mitsou[172], A. Miucci[20], P.S. Miyagawa[146], A. Mizukami[79], J.U. Mjörnmark[94],

T. Mkrtchyan[182], M. Mlynarikova[139], T. Moa[43a,43b], K. Mochizuki[107], P. Mogg[50], S. Mohapatra[38],
S. Molander[43a,43b], R. Moles-Valls[24], M.C. Mondragon[104], K. Mönig[44], J. Monk[39], E. Monnier[99],
A. Montalbano[149], J. Montejo Berlingen[35], F. Monticelli[86], S. Monzani[66a], R.W. Moore[3], N. Morange[128],
D. Moreno[22], M. Moreno Llácer[35], P. Morettini[53b], M. Morgenstern[118], S. Morgenstern[35], D. Mori[149],
T. Mori[161], M. Morii[57], M. Morinaga[177], V. Morisbak[130], A.K. Morley[35], G. Mornacchi[35], J.D. Morris[90],
L. Morvaj[152], P. Moschovakos[10], M. Mosidze[157b], H.J. Moss[146], J. Moss[150,n], K. Motohashi[163],
R. Mount[150], E. Mountricha[29], E.J.W. Moyse[100], S. Muanza[99], F. Mueller[113], J. Mueller[135],
R.S.P. Mueller[112], D. Muenstermann[87], P. Mullen[55], G.A. Mullier[20], F.J. Munoz Sanchez[98], P. Murin[28b],
W.J. Murray[176,141], A. Murrone[66a,66b], M. Muškinja[89], C. Mwewa[32a], A.G. Myagkov[140,al], J. Myers[127],
M. Myska[138], B.P. Nachman[18], O. Nackenhorst[45], K. Nagai[131], R. Nagai[79,ao], K. Nagano[79],
Y. Nagasaka[60], K. Nagata[167], M. Nagel[50], E. Nagy[99], A.M. Nairz[35], Y. Nakahama[115], K. Nakamura[79],
T. Nakamura[161], I. Nakano[123], R.F. Naranjo Garcia[44], R. Narayan[11], D.I. Narrias Villar[59a],
I. Naryshkin[134], T. Naumann[44], G. Navarro[22], R. Nayyar[7], H.A. Neal[103], P.Y. Nechaeva[108], T.J. Neep[142],
A. Negri[68a,68b], M. Negrini[23b], S. Nektarijevic[117], C. Nellist[51], M.E. Nelson[131], S. Nemecek[137],
P. Nemethy[121], M. Nessi[35,f], M.S. Neubauer[171], M. Neumann[180], P.R. Newman[21], T.Y. Ng[61c], Y.S. Ng[19],
H.D.N. Nguyen[99], T. Nguyen Manh[107], E. Nibigira[37], R.B. Nickerson[131], R. Nicolaidou[142],
J. Nielsen[143], N. Nikiforou[11], V. Nikolaenko[140,al], I. Nikolic-Audit[132], K. Nikolopoulos[21], P. Nilsson[29],
Y. Ninomiya[79], A. Nisati[70a], N. Nishu[58c], R. Nisius[113], I. Nitsche[45], T. Nitta[177], T. Nobe[161],
Y. Noguchi[83], M. Nomachi[129], I. Nomidis[33], M.A. Nomura[29], T. Nooney[90], M. Nordberg[35],
N. Norjoharuddeen[131], T. Novak[89], O. Novgorodova[46], R. Novotny[138], M. Nozaki[79], L. Nozka[126],
K. Ntekas[169], E. Nurse[92], F. Nuti[102], F.G. Oakham[33,au], H. Oberlack[113], T. Obermann[24], J. Ocariz[132],
A. Ochi[80], I. Ochoa[38], J.P. Ochoa-Ricoux[144a], K. O'Connor[26], S. Oda[85], S. Odaka[79], A. Oh[98], S.H. Oh[47],
C.C. Ohm[151], H. Ohman[170], H. Oide[53b,53a], H. Okawa[167], Y. Okumura[161], T. Okuyama[79], A. Olariu[27b],
L.F. Oleiro Seabra[136a], S.A. Olivares Pino[144a], D. Oliveira Damazio[29], J.L. Oliver[1], M.J.R. Olsson[36],
A. Olszewski[82], J. Olszowska[82], D.C. O'Neil[149], A. Onofre[136a,136e], K. Onogi[115], P.U.E. Onyisi[11],
H. Oppen[130], M.J. Oreglia[36], Y. Oren[159], D. Orestano[72a,72b], E.C. Orgill[98], N. Orlando[61b],
A.A. O'Rourke[44], R.S. Orr[165], B. Osculati[53b,53a,*], V. O'Shea[55], R. Ospanov[58a], G. Otero y Garzon[30],
H. Otono[85], M. Ouchrif[34d], F. Ould-Saada[130], A. Ouraou[142], K.P. Oussoren[118], Q. Ouyang[15a],
M. Owen[55], R.E. Owen[21], V.E. Ozcan[12c], N. Ozturk[8], K. Pachal[149], A. Pacheco Pages[14],
L. Pacheco Rodriguez[142], C. Padilla Aranda[14], S. Pagan Griso[18], M. Paganini[181], G. Palacino[63],
S. Palazzo[40b,40a], S. Palestini[35], M. Palka[81b], D. Pallin[37], I. Panagoulias[10], C.E. Pandini[52],
J.G. Panduro Vazquez[91], P. Pani[35], D. Pantea[27b], L. Paolozzi[52], T.D. Papadopoulou[10], K. Papageorgiou[9,j],
A. Paramonov[6], D. Paredes Hernandez[61b], B. Parida[58c], A.J. Parker[87], K.A. Parker[44], M.A. Parker[31],
F. Parodi[53b,53a], J.A. Parsons[38], U. Parzefall[50], V.R. Pascuzzi[165], J.M.P. Pasner[143], E. Pasqualucci[70a],
S. Passaggio[53b], F. Pastore[91], P. Pasuwan[43a,43b], S. Pataraia[97], J.R. Pater[98], A. Pathak[179,k], T. Pauly[35],
B. Pearson[113], S. Pedraza Lopez[172], R. Pedro[136a,136b], S.V. Peleganchuk[120b,120a], O. Penc[137], C. Peng[15d],
H. Peng[58a], J. Penwell[63], B.S. Peralva[78a], M.M. Perego[142], A.P. Pereira Peixoto[136a], D.V. Perepelitsa[29],
F. Peri[19], L. Perini[66a,66b], H. Pernegger[35], S. Perrella[67a,67b], V.D. Peshekhonov[77,*], K. Peters[44],
R.F.Y. Peters[98], B.A. Petersen[35], T.C. Petersen[39], E. Petit[56], A. Petridis[1], C. Petridou[160], P. Petroff[128],
E. Petrolo[70a], M. Petrov[131], F. Petrucci[72a,72b], N.E. Pettersson[100], A. Peyaud[142], R. Pezoa[144b], T. Pham[102],
F.H. Phillips[104], P.W. Phillips[141], G. Piacquadio[152], E. Pianori[176], A. Picazio[100], M.A. Pickering[131],
R. Piegaia[30], J.E. Pilcher[36], A.D. Pilkington[98], M. Pinamonti[71a,71b], J.L. Pinfold[3], M. Pitt[178],
M-A. Pleier[29], V. Pleskot[139], E. Plotnikova[77], D. Pluth[76], P. Podberezko[120b,120a], R. Poettgen[94],
R. Poggi[68a,68b], L. Poggioli[128], I. Pogrebnyak[104], D. Pohl[24], I. Pokharel[51], G. Polesello[68a], A. Poley[44],
A. Policicchio[40b,40a], R. Polifka[35], A. Polini[23b], C.S. Pollard[44], V. Polychronakos[29], D. Ponomarenko[110],
L. Pontecorvo[70a], G.A. Popeneciu[27d], D.M. Portillo Quintero[132], S. Pospisil[138], K. Potamianos[44],
I.N. Potrap[77], C.J. Potter[31], H. Potti[11], T. Poulsen[94], J. Poveda[35], M.E. Pozo Astigarraga[35],

P. Pralavorio[99], S. Prell[76], D. Price[98], M. Primavera[65a], S. Prince[101], N. Proklova[110], K. Prokofiev[61c],
F. Prokoshin[144b], S. Protopopescu[29], J. Proudfoot[6], M. Przybycien[81a], A. Puri[171], P. Puzo[128], J. Qian[103],
Y. Qin[98], A. Quadt[51], M. Queitsch-Maitland[44], A. Qureshi[1], S.K. Radhakrishnan[152], P. Rados[102],
F. Ragusa[66a,66b], G. Rahal[95], J.A. Raine[98], S. Rajagopalan[29], T. Rashid[128], S. Raspopov[5],
M.G. Ratti[66a,66b], D.M. Rauch[44], F. Rauscher[112], S. Rave[97], B. Ravina[146], I. Ravinovich[178],
J.H. Rawling[98], M. Raymond[35], A.L. Read[130], N.P. Readioff[56], M. Reale[65a,65b], D.M. Rebuzzi[68a,68b],
A. Redelbach[175], G. Redlinger[29], R. Reece[143], R.G. Reed[32c], K. Reeves[42], L. Rehnisch[19], J. Reichert[133],
A. Reiss[97], C. Rembser[35], H. Ren[15d], M. Rescigno[70a], S. Resconi[66a], E.D. Resseguie[133], S. Rettie[173],
E. Reynolds[21], O.L. Rezanova[120b,120a], P. Reznicek[139], R. Richter[113], S. Richter[92], E. Richter-Was[81b],
O. Ricken[24], M. Ridel[132], P. Rieck[113], C.J. Riegel[180], O. Rifki[44], M. Rijssenbeek[152], A. Rimoldi[68a,68b],
M. Rimoldi[20], L. Rinaldi[23b], G. Ripellino[151], B. Ristić[35], E. Ritsch[35], I. Riu[14], J.C. Rivera Vergara[144a],
F. Rizatdinova[125], E. Rizvi[90], C. Rizzi[14], R.T. Roberts[98], S.H. Robertson[101,ae],
A. Robichaud-Veronneau[101], D. Robinson[31], J.E.M. Robinson[44], A. Robson[55], E. Rocco[97],
C. Roda[69a,69b], Y. Rodina[99,aa], S. Rodriguez Bosca[172], A. Rodriguez Perez[14], D. Rodriguez Rodriguez[172],
A.M. Rodríguez Vera[166b], S. Roe[35], C.S. Rogan[57], O. Røhne[130], R. Röhrig[113], C.P.A. Roland[63],
J. Roloff[57], A. Romaniouk[110], M. Romano[23b,23a], E. Romero Adam[172], N. Rompotis[88], M. Ronzani[121],
L. Roos[132], S. Rosati[70a], K. Rosbach[50], P. Rose[143], N-A. Rosien[51], E. Rossi[67a,67b], L.P. Rossi[53b],
L. Rossini[66a,66b], J.H.N. Rosten[31], R. Rosten[145], M. Rotaru[27b], J. Rothberg[145], D. Rousseau[128],
D. Roy[32c], A. Rozanov[99], Y. Rozen[158], X. Ruan[32c], F. Rubbo[150], F. Rühr[50], A. Ruiz-Martinez[33],
Z. Rurikova[50], N.A. Rusakovich[77], H.L. Russell[101], J.P. Rutherfoord[7], N. Ruthmann[35],
E.M. Rüttinger[44,l], Y.F. Ryabov[134], M. Rybar[171], G. Rybkin[128], S. Ryu[6], A. Ryzhov[140], G.F. Rzehorz[51],
P. Sabatini[51], G. Sabato[118], S. Sacerdoti[128], H.F-W. Sadrozinski[143], R. Sadykov[77], F. Safai Tehrani[70a],
P. Saha[119], M. Sahinsoy[59a], M. Saimpert[44], M. Saito[161], T. Saito[161], H. Sakamoto[161], A. Sakharov[121,ak],
D. Salamani[52], G. Salamanna[72a,72b], J.E. Salazar Loyola[144b], D. Salek[118], P.H. Sales De Bruin[170],
D. Salihagic[113], A. Salnikov[150], J. Salt[172], D. Salvatore[40b,40a], F. Salvatore[153], A. Salvucci[61a,61b,61c],
A. Salzburger[35], D. Sammel[50], D. Sampsonidis[160], D. Sampsonidou[160], J. Sánchez[172],
A. Sanchez Pineda[64a,64c], H. Sandaker[130], C.O. Sander[44], M. Sandhoff[180], C. Sandoval[22],
D.P.C. Sankey[141], M. Sannino[53b,53a], Y. Sano[115], A. Sansoni[49], C. Santoni[37], H. Santos[136a],
I. Santoyo Castillo[153], A. Sapronov[77], J.G. Saraiva[136a,136d], O. Sasaki[79], K. Sato[167], E. Sauvan[5],
P. Savard[165,au], N. Savic[113], R. Sawada[161], C. Sawyer[141], L. Sawyer[93,aj], C. Sbarra[23b], A. Sbrizzi[23b,23a],
T. Scanlon[92], D.A. Scannicchio[169], J. Schaarschmidt[145], P. Schacht[113], B.M. Schachtner[112],
D. Schaefer[36], L. Schaefer[133], J. Schaeffer[97], S. Schaepe[35], U. Schäfer[97], A.C. Schaffer[128], D. Schaile[112],
R.D. Schamberger[152], V.A. Schegelsky[134], D. Scheirich[139], F. Schenck[19], M. Schernau[169],
C. Schiavi[53b,53a], S. Schier[143], L.K. Schildgen[24], Z.M. Schillaci[26], E.J. Schioppa[35], M. Schioppa[40b,40a],
K.E. Schleicher[50], S. Schlenker[35], K.R. Schmidt-Sommerfeld[113], K. Schmieden[35], C. Schmitt[97],
S. Schmitt[44], S. Schmitz[97], U. Schnoor[50], L. Schoeffel[142], A. Schoening[59b], E. Schopf[24], M. Schott[97],
J.F.P. Schouwenberg[117], J. Schovancova[35], S. Schramm[52], N. Schuh[97], A. Schulte[97],
H-C. Schultz-Coulon[59a], M. Schumacher[50], B.A. Schumm[143], Ph. Schune[142], A. Schwartzman[150],
T.A. Schwarz[103], H. Schweiger[98], Ph. Schwemling[142], R. Schwienhorst[104], A. Sciandra[24], G. Sciolla[26],
M. Scornajenghi[40b,40a], F. Scuri[69a], F. Scutti[102], L.M. Scyboz[113], J. Searcy[103], C.D. Sebastiani[70a,70b],
P. Seema[24], S.C. Seidel[116], A. Seiden[143], J.M. Seixas[78b], G. Sekhniaidze[67a], K. Sekhon[103], S.J. Sekula[41],
N. Semprini-Cesari[23b,23a], S. Senkin[37], C. Serfon[130], L. Serin[128], L. Serkin[64a,64b], M. Sessa[72a,72b],
H. Severini[124], F. Sforza[168], A. Sfyrla[52], E. Shabalina[51], J.D. Shahinian[143], N.W. Shaikh[43a,43b],
L.Y. Shan[15a], R. Shang[171], J.T. Shank[25], M. Shapiro[18], A.S. Sharma[1], A. Sharma[131], P.B. Shatalov[109],
K. Shaw[64a,64b], S.M. Shaw[98], A. Shcherbakova[43a,43b], C.Y. Shehu[153], Y. Shen[124], N. Sherafati[33],
A.D. Sherman[25], P. Sherwood[92], L. Shi[155,aq], S. Shimizu[80], C.O. Shimmin[181], M. Shimojima[114],
I.P.J. Shipsey[131], S. Shirabe[85], M. Shiyakova[77], J. Shlomi[178], A. Shmeleva[108], D. Shoaleh Saadi[107],

53

M.J. Shochet[36], S. Shojaii[102], D.R. Shope[124], S. Shrestha[122], E. Shulga[110], P. Sicho[137], A.M. Sickles[171], P.E. Sidebo[151], E. Sideras Haddad[32c], O. Sidiropoulou[175], A. Sidoti[23b,23a], F. Siegert[46], Dj. Sijacki[16], J. Silva[136a], M. Silva Jr.[179], S.B. Silverstein[43a], L. Simic[77], S. Simion[128], E. Simioni[97], B. Simmons[92], M. Simon[97], P. Sinervo[165], N.B. Sinev[127], M. Sioli[23b,23a], G. Siragusa[175], I. Siral[103], S.Yu. Sivoklokov[111], J. Sjölin[43a,43b], M.B. Skinner[87], P. Skubic[124], M. Slater[21], T. Slavicek[138], M. Slawinska[82], K. Sliwa[168], R. Slovak[139], V. Smakhtin[178], B.H. Smart[5], J. Smiesko[28a], N. Smirnov[110], S.Yu. Smirnov[110], Y. Smirnov[110], L.N. Smirnova[111], O. Smirnova[94], J.W. Smith[51], M.N.K. Smith[38], R.W. Smith[38], M. Smizanska[87], K. Smolek[138], A.A. Snesarev[108], I.M. Snyder[127], S. Snyder[29], R. Sobie[174,ae], F. Socher[46], A.M. Soffa[169], A. Soffer[159], A. Søgaard[48], D.A. Soh[155], G. Sokhrannyi[89], C.A. Solans Sanchez[35], M. Solar[138], E.Yu. Soldatov[110], U. Soldevila[172], A.A. Solodkov[140], A. Soloshenko[77], O.V. Solovyanov[140], V. Solovyev[134], P. Sommer[146], H. Son[168], W. Song[141], A. Sopczak[138], F. Sopkova[28b], D. Sosa[59b], C.L. Sotiropoulou[69a,69b], S. Sottocornola[68a,68b], R. Soualah[64a,64c,i], A.M. Soukharev[120b,120a], D. South[44], B.C. Sowden[91], S. Spagnolo[65a,65b], M. Spalla[113], M. Spangenberg[176], F. Spanò[91], D. Sperlich[19], F. Spettel[113], T.M. Spieker[59a], R. Spighi[23b], G. Spigo[35], L.A. Spiller[102], M. Spousta[139], A. Stabile[66a,66b], R. Stamen[59a], S. Stamm[19], E. Stanecka[82], R.W. Stanek[6], C. Stanescu[72a], M.M. Stanitzki[44], B. Stapf[118], S. Stapnes[130], E.A. Starchenko[140], G.H. Stark[36], J. Stark[56], S.H Stark[39], P. Staroba[137], P. Starovoitov[59a], S. Stärz[35], R. Staszewski[82], M. Stegler[44], P. Steinberg[29], B. Stelzer[149], H.J. Stelzer[35], O. Stelzer-Chilton[166a], H. Stenzel[54], T.J. Stevenson[90], G.A. Stewart[55], M.C. Stockton[127], G. Stoicea[27b], P. Stolte[51], S. Stonjek[113], A. Straessner[46], M.E. Stramaglia[20], J. Strandberg[151], S. Strandberg[43a,43b], M. Strauss[124], P. Strizenec[28b], R. Ströhmer[175], D.M. Strom[127], R. Stroynowski[41], A. Strubig[48], S.A. Stucci[29], B. Stugu[17], N.A. Styles[44], D. Su[150], J. Su[135], S. Suchek[59a], Y. Sugaya[129], M. Suk[138], V.V. Sulin[108], D.M.S. Sultan[52], S. Sultansoy[4c], T. Sumida[83], S. Sun[103], X. Sun[3], K. Suruliz[153], C.J.E. Suster[154], M.R. Sutton[153], S. Suzuki[79], M. Svatos[137], M. Swiatlowski[36], S.P. Swift[2], A. Sydorenko[97], I. Sykora[28a], T. Sykora[139], D. Ta[97], K. Tackmann[44,ab], J. Taenzer[159], A. Taffard[169], R. Tafirout[166a], E. Tahirovic[90], N. Taiblum[159], H. Takai[29], R. Takashima[84], E.H. Takasugi[113], K. Takeda[80], T. Takeshita[147], Y. Takubo[79], M. Talby[99], A.A. Talyshev[120b,120a], J. Tanaka[161], M. Tanaka[163], R. Tanaka[128], R. Tanioka[80], B.B. Tannenwald[122], S. Tapia Araya[144b], S. Tapprogge[97], A. Tarek Abouelfadl Mohamed[132], S. Tarem[158], G. Tarna[27b,e], G.F. Tartarelli[66a], P. Tas[139], M. Tasevsky[137], T. Tashiro[83], E. Tassi[40b,40a], A. Tavares Delgado[136a,136b], Y. Tayalati[34e], A.C. Taylor[116], A.J. Taylor[48], G.N. Taylor[102], P.T.E. Taylor[102], W. Taylor[166b], P. Teixeira-Dias[91], D. Temple[149], H. Ten Kate[35], P.K. Teng[155], J.J. Teoh[129], F. Tepel[180], S. Terada[79], K. Terashi[161], J. Terron[96], S. Terzo[14], M. Testa[49], R.J. Teuscher[165,ae], S.J. Thais[181], T. Theveneaux-Pelzer[44], F. Thiele[39], J.P. Thomas[21], A.S. Thompson[55], P.D. Thompson[21], L.A. Thomsen[181], E. Thomson[133], Y. Tian[38], R.E. Ticse Torres[51], V.O. Tikhomirov[108,am], Yu.A. Tikhonov[120b,120a], S. Timoshenko[110], P. Tipton[181], S. Tisserant[99], K. Todome[163], S. Todorova-Nova[5], S. Todt[46], J. Tojo[85], S. Tokár[28a], K. Tokushuku[79], E. Tolley[122], M. Tomoto[115], L. Tompkins[150], K. Toms[116], B. Tong[57], P. Tornambe[50], E. Torrence[127], H. Torres[46], E. Torró Pastor[145], C. Tosciri[131], J. Toth[99,ad], F. Touchard[99], D.R. Tovey[146], C.J. Treado[121], T. Trefzger[175], F. Tresoldi[153], A. Tricoli[29], I.M. Trigger[166a], S. Trincaz-Duvoid[132], M.F. Tripiana[14], W. Trischuk[165], B. Trocmé[56], A. Trofymov[44], C. Troncon[66a], M. Trovatelli[174], F. Trovato[153], L. Truong[32b], M. Trzebinski[82], A. Trzupek[82], F. Tsai[44], K.W. Tsang[61a], J.C-L. Tseng[131], P.V. Tsiareshka[105], N. Tsirintanis[9], S. Tsiskaridze[14], V. Tsiskaridze[152], E.G. Tskhadadze[157a], I.I. Tsukerman[109], V. Tsulaia[18], S. Tsuno[79], D. Tsybychev[152], Y. Tu[61b], A. Tudorache[27b], V. Tudorache[27b], T.T. Tulbure[27a], A.N. Tuna[57], S. Turchikhin[77], D. Turgeman[178], I. Turk Cakir[4b,u], R. Turra[66a], P.M. Tuts[38], G. Ucchielli[23b,23a], I. Ueda[79], M. Ughetto[43a,43b], F. Ukegawa[167], G. Unal[35], A. Undrus[29], G. Unel[169], F.C. Ungaro[102], Y. Unno[79], K. Uno[161], J. Urban[28b], P. Urquijo[102], P. Urrejola[97], G. Usai[8], J. Usui[79], L. Vacavant[99], V. Vacek[138], B. Vachon[101], K.O.H. Vadla[130], A. Vaidya[92], C. Valderanis[112], E. Valdes Santurio[43a,43b],

M. Valente[52], S. Valentinetti[23b,23a], A. Valero[172], L. Valéry[44], R.A. Vallance[21], A. Vallier[5],
J.A. Valls Ferrer[172], T.R. Van Daalen[14], W. Van Den Wollenberg[118], H. Van der Graaf[118],
P. Van Gemmeren[6], J. Van Nieuwkoop[149], I. Van Vulpen[118], M.C. van Woerden[118], M. Vanadia[71a,71b],
W. Vandelli[35], A. Vaniachine[164], P. Vankov[118], R. Vari[70a], E.W. Varnes[7], C. Varni[53b,53a], T. Varol[41],
D. Varouchas[128], A. Vartapetian[8], K.E. Varvell[154], G.A. Vasquez[144b], J.G. Vasquez[181], F. Vazeille[37],
D. Vazquez Furelos[14], T. Vazquez Schroeder[101], J. Veatch[51], L.M. Veloce[165], F. Veloso[136a,136c],
S. Veneziano[70a], A. Ventura[65a,65b], M. Venturi[174], N. Venturi[35], V. Vercesi[68a], M. Verducci[72a,72b],
W. Verkerke[118], A.T. Vermeulen[118], J.C. Vermeulen[118], M.C. Vetterli[149,au], N. Viaux Maira[144b],
O. Viazlo[94], I. Vichou[171,*], T. Vickey[146], O.E. Vickey Boeriu[146], G.H.A. Viehhauser[131], S. Viel[18],
L. Vigani[131], M. Villa[23b,23a], M. Villaplana Perez[66a,66b], E. Vilucchi[49], M.G. Vincter[33],
V.B. Vinogradov[77], A. Vishwakarma[44], C. Vittori[23b,23a], I. Vivarelli[153], S. Vlachos[10], M. Vogel[180],
P. Vokac[138], G. Volpi[14], S.E. Von Buddenbrock[32c], E. Von Toerne[24], V. Vorobel[139], K. Vorobev[110],
M. Vos[172], J.H. Vossebeld[88], N. Vranjes[16], M. Vranjes Milosavljevic[16], V. Vrba[138], M. Vreeswijk[118],
T. Šfiligoj[89], R. Vuillermet[35], I. Vukotic[36], T. Ženiš[28a], L. Živković[16], P. Wagner[24], W. Wagner[180],
J. Wagner-Kuhr[112], H. Wahlberg[86], S. Wahrmund[46], K. Wakamiya[80], J. Walder[87], R. Walker[112],
W. Walkowiak[148], V. Wallangen[43a,43b], A.M. Wang[57], C. Wang[58b,e], F. Wang[179], H. Wang[18], H. Wang[3],
J. Wang[154], J. Wang[59b], P. Wang[41], Q. Wang[124], R.-J. Wang[132], R. Wang[58a], R. Wang[6], S.M. Wang[155],
T. Wang[38], W. Wang[155,p], W.X. Wang[58a,af], Y. Wang[58a], Z. Wang[58c], C. Wanotayaroj[44], A. Warburton[101],
C.P. Ward[31], D.R. Wardrope[92], A. Washbrook[48], P.M. Watkins[21], A.T. Watson[21], M.F. Watson[21],
G. Watts[145], S. Watts[98], B.M. Waugh[92], A.F. Webb[11], S. Webb[97], C. Weber[181], M.S. Weber[20],
S.A. Weber[33], S.M. Weber[59a], J.S. Webster[6], A.R. Weidberg[131], B. Weinert[63], J. Weingarten[51],
M. Weirich[97], C. Weiser[50], P.S. Wells[35], T. Wenaus[29], T. Wengler[35], S. Wenig[35], N. Wermes[24],
M.D. Werner[76], P. Werner[35], M. Wessels[59a], T.D. Weston[20], K. Whalen[127], N.L. Whallon[145],
A.M. Wharton[87], A.S. White[103], A. White[8], M.J. White[1], R. White[144b], D. Whiteson[169],
B.W. Whitmore[87], F.J. Wickens[141], W. Wiedenmann[179], M. Wielers[141], C. Wiglesworth[39],
L.A.M. Wiik-Fuchs[50], A. Wildauer[113], F. Wilk[98], H.G. Wilkens[35], H.H. Williams[133], S. Williams[31],
C. Willis[104], S. Willocq[100], J.A. Wilson[21], I. Wingerter-Seez[5], E. Winkels[153], F. Winklmeier[127],
O.J. Winston[153], B.T. Winter[24], M. Wittgen[150], M. Wobisch[93], A. Wolf[97], T.M.H. Wolf[118], R. Wolff[99],
M.W. Wolter[82], H. Wolters[136a,136c], V.W.S. Wong[173], N.L. Woods[143], S.D. Worm[21], B.K. Wosiek[82],
K.W. Woźniak[82], K. Wraight[55], M. Wu[36], S.L. Wu[179], X. Wu[52], Y. Wu[58a], T.R. Wyatt[98], B.M. Wynne[48],
S. Xella[39], Z. Xi[103], L. Xia[15b], D. Xu[15a], H. Xu[58a], L. Xu[29], T. Xu[142], W. Xu[103], B. Yabsley[154],
S. Yacoob[32a], K. Yajima[129], D.P. Yallup[92], D. Yamaguchi[163], Y. Yamaguchi[163], A. Yamamoto[79],
T. Yamanaka[161], F. Yamane[80], M. Yamatani[161], T. Yamazaki[161], Y. Yamazaki[80], Z. Yan[25],
H.J. Yang[58c,58d], H.T. Yang[18], S. Yang[75], Y. Yang[161], Y. Yang[155], Z. Yang[17], W-M. Yao[18], Y.C. Yap[44],
Y. Yasu[79], E. Yatsenko[5], K.H. Yau Wong[24], J. Ye[41], S. Ye[29], I. Yeletskikh[77], E. Yigitbasi[25], E. Yildirim[97],
K. Yorita[177], K. Yoshihara[133], C.J.S. Young[35], C. Young[150], J. Yu[8], J. Yu[76], X. Yue[59a], S.P.Y. Yuen[24],
I. Yusuff[31,a], B. Zabinski[82], G. Zacharis[10], R. Zaidan[14], A.M. Zaitsev[140,al], N. Zakharchuk[44],
J. Zalieckas[17], S. Zambito[57], D. Zanzi[35], C. Zeitnitz[180], G. Zemaityte[131], J.C. Zeng[171], Q. Zeng[150],
O. Zenin[140], D. Zerwas[128], M. Zgubič[131], D.F. Zhang[58b], D. Zhang[103], F. Zhang[179], G. Zhang[58a,af],
H. Zhang[15c], J. Zhang[6], L. Zhang[50], L. Zhang[58a], M. Zhang[171], P. Zhang[15c], R. Zhang[58a,e], R. Zhang[24],
X. Zhang[58b], Y. Zhang[15d], Z. Zhang[128], X. Zhao[41], Y. Zhao[58b,128,ai], Z. Zhao[58a], A. Zhemchugov[77],
B. Zhou[103], C. Zhou[179], L. Zhou[41], M.S. Zhou[15d], M. Zhou[152], N. Zhou[58c], Y. Zhou[7], C.G. Zhu[58b],
H. Zhu[15a], J. Zhu[103], Y. Zhu[58a], X. Zhuang[15a], K. Zhukov[108], V. Zhulanov[120b,120a], A. Zibell[175],
D. Zieminska[63], N.I. Zimine[77], S. Zimmermann[50], Z. Zinonos[113], M. Zinser[97], M. Ziolkowski[148],
G. Zobernig[179], A. Zoccoli[23b,23a], T.G. Zorbas[146], R. Zou[36], M. Zur Nedden[19], L. Zwalinski[35].

[1]Department of Physics, University of Adelaide, Adelaide; Australia.

[2]Physics Department, SUNY Albany, Albany NY; United States of America.

[3]Department of Physics, University of Alberta, Edmonton AB; Canada.

[4][a]Department of Physics, Ankara University, Ankara;[b]Istanbul Aydin University, Istanbul;[c]Division of Physics, TOBB University of Economics and Technology, Ankara; Turkey.

[5]LAPP, Université Grenoble Alpes, Université Savoie Mont Blanc, CNRS/IN2P3, Annecy; France.

[6]High Energy Physics Division, Argonne National Laboratory, Argonne IL; United States of America.

[7]Department of Physics, University of Arizona, Tucson AZ; United States of America.

[8]Department of Physics, University of Texas at Arlington, Arlington TX; United States of America.

[9]Physics Department, National and Kapodistrian University of Athens, Athens; Greece.

[10]Physics Department, National Technical University of Athens, Zografou; Greece.

[11]Department of Physics, University of Texas at Austin, Austin TX; United States of America.

[12][a]Bahcesehir University, Faculty of Engineering and Natural Sciences, Istanbul;[b]Istanbul Bilgi University, Faculty of Engineering and Natural Sciences, Istanbul;[c]Department of Physics, Bogazici University, Istanbul;[d]Department of Physics Engineering, Gaziantep University, Gaziantep; Turkey.

[13]Institute of Physics, Azerbaijan Academy of Sciences, Baku; Azerbaijan.

[14]Institut de Física d'Altes Energies (IFAE), Barcelona Institute of Science and Technology, Barcelona; Spain.

[15][a]Institute of High Energy Physics, Chinese Academy of Sciences, Beijing;[b]Physics Department, Tsinghua University, Beijing;[c]Department of Physics, Nanjing University, Nanjing;[d]University of Chinese Academy of Science (UCAS), Beijing; China.

[16]Institute of Physics, University of Belgrade, Belgrade; Serbia.

[17]Department for Physics and Technology, University of Bergen, Bergen; Norway.

[18]Physics Division, Lawrence Berkeley National Laboratory and University of California, Berkeley CA; United States of America.

[19]Institut für Physik, Humboldt Universität zu Berlin, Berlin; Germany.

[20]Albert Einstein Center for Fundamental Physics and Laboratory for High Energy Physics, University of Bern, Bern; Switzerland.

[21]School of Physics and Astronomy, University of Birmingham, Birmingham; United Kingdom.

[22]Centro de Investigaciónes, Universidad Antonio Nariño, Bogota; Colombia.

[23][a]Dipartimento di Fisica e Astronomia, Università di Bologna, Bologna;[b]INFN Sezione di Bologna; Italy.

[24]Physikalisches Institut, Universität Bonn, Bonn; Germany.

[25]Department of Physics, Boston University, Boston MA; United States of America.

[26]Department of Physics, Brandeis University, Waltham MA; United States of America.

[27][a]Transilvania University of Brasov, Brasov;[b]Horia Hulubei National Institute of Physics and Nuclear Engineering, Bucharest;[c]Department of Physics, Alexandru Ioan Cuza University of Iasi, Iasi;[d]National Institute for Research and Development of Isotopic and Molecular Technologies, Physics Department, Cluj-Napoca;[e]University Politehnica Bucharest, Bucharest;[f]West University in Timisoara, Timisoara; Romania.

[28][a]Faculty of Mathematics, Physics and Informatics, Comenius University, Bratislava;[b]Department of Subnuclear Physics, Institute of Experimental Physics of the Slovak Academy of Sciences, Kosice; Slovak Republic.

[29]Physics Department, Brookhaven National Laboratory, Upton NY; United States of America.

[30]Departamento de Física, Universidad de Buenos Aires, Buenos Aires; Argentina.

[31]Cavendish Laboratory, University of Cambridge, Cambridge; United Kingdom.

[32][a]Department of Physics, University of Cape Town, Cape Town;[b]Department of Mechanical Engineering Science, University of Johannesburg, Johannesburg;[c]School of Physics, University of the

Witwatersrand, Johannesburg; South Africa.

[33] Department of Physics, Carleton University, Ottawa ON; Canada.

[34] [a] Faculté des Sciences Ain Chock, Réseau Universitaire de Physique des Hautes Energies - Université Hassan II, Casablanca; [b] Centre National de l'Energie des Sciences Techniques Nucleaires (CNESTEN), Rabat; [c] Faculté des Sciences Semlalia, Université Cadi Ayyad, LPHEA-Marrakech; [d] Faculté des Sciences, Université Mohamed Premier and LPTPM, Oujda; [e] Faculté des sciences, Université Mohammed V, Rabat; Morocco.

[35] CERN, Geneva; Switzerland.

[36] Enrico Fermi Institute, University of Chicago, Chicago IL; United States of America.

[37] LPC, Université Clermont Auvergne, CNRS/IN2P3, Clermont-Ferrand; France.

[38] Nevis Laboratory, Columbia University, Irvington NY; United States of America.

[39] Niels Bohr Institute, University of Copenhagen, Copenhagen; Denmark.

[40] [a] Dipartimento di Fisica, Università della Calabria, Rende; [b] INFN Gruppo Collegato di Cosenza, Laboratori Nazionali di Frascati; Italy.

[41] Physics Department, Southern Methodist University, Dallas TX; United States of America.

[42] Physics Department, University of Texas at Dallas, Richardson TX; United States of America.

[43] [a] Department of Physics, Stockholm University; [b] Oskar Klein Centre, Stockholm; Sweden.

[44] Deutsches Elektronen-Synchrotron DESY, Hamburg and Zeuthen; Germany.

[45] Lehrstuhl für Experimentelle Physik IV, Technische Universität Dortmund, Dortmund; Germany.

[46] Institut für Kern- und Teilchenphysik, Technische Universität Dresden, Dresden; Germany.

[47] Department of Physics, Duke University, Durham NC; United States of America.

[48] SUPA - School of Physics and Astronomy, University of Edinburgh, Edinburgh; United Kingdom.

[49] INFN e Laboratori Nazionali di Frascati, Frascati; Italy.

[50] Physikalisches Institut, Albert-Ludwigs-Universität Freiburg, Freiburg; Germany.

[51] II. Physikalisches Institut, Georg-August-Universität Göttingen, Göttingen; Germany.

[52] Département de Physique Nucléaire et Corpusculaire, Université de Genève, Genève; Switzerland.

[53] [a] Dipartimento di Fisica, Università di Genova, Genova; [b] INFN Sezione di Genova; Italy.

[54] II. Physikalisches Institut, Justus-Liebig-Universität Giessen, Giessen; Germany.

[55] SUPA - School of Physics and Astronomy, University of Glasgow, Glasgow; United Kingdom.

[56] LPSC, Université Grenoble Alpes, CNRS/IN2P3, Grenoble INP, Grenoble; France.

[57] Laboratory for Particle Physics and Cosmology, Harvard University, Cambridge MA; United States of America.

[58] [a] Department of Modern Physics and State Key Laboratory of Particle Detection and Electronics, University of Science and Technology of China, Hefei; [b] Institute of Frontier and Interdisciplinary Science and Key Laboratory of Particle Physics and Particle Irradiation (MOE), Shandong University, Qingdao; [c] School of Physics and Astronomy, Shanghai Jiao Tong University, KLPPAC-MoE, SKLPPC, Shanghai; [d] Tsung-Dao Lee Institute, Shanghai; China.

[59] [a] Kirchhoff-Institut für Physik, Ruprecht-Karls-Universität Heidelberg, Heidelberg; [b] Physikalisches Institut, Ruprecht-Karls-Universität Heidelberg, Heidelberg; Germany.

[60] Faculty of Applied Information Science, Hiroshima Institute of Technology, Hiroshima; Japan.

[61] [a] Department of Physics, Chinese University of Hong Kong, Shatin, N.T., Hong Kong; [b] Department of Physics, University of Hong Kong, Hong Kong; [c] Department of Physics and Institute for Advanced Study, Hong Kong University of Science and Technology, Clear Water Bay, Kowloon, Hong Kong; China.

[62] Department of Physics, National Tsing Hua University, Hsinchu; Taiwan.

[63] Department of Physics, Indiana University, Bloomington IN; United States of America.

[64] [a] INFN Gruppo Collegato di Udine, Sezione di Trieste, Udine; [b] ICTP, Trieste; [c] Dipartimento di

Chimica, Fisica e Ambiente, Università di Udine, Udine; Italy.

[65](a)INFN Sezione di Lecce;(b)Dipartimento di Matematica e Fisica, Università del Salento, Lecce; Italy.

[66](a)INFN Sezione di Milano;(b)Dipartimento di Fisica, Università di Milano, Milano; Italy.

[67](a)INFN Sezione di Napoli;(b)Dipartimento di Fisica, Università di Napoli, Napoli; Italy.

[68](a)INFN Sezione di Pavia;(b)Dipartimento di Fisica, Università di Pavia, Pavia; Italy.

[69](a)INFN Sezione di Pisa;(b)Dipartimento di Fisica E. Fermi, Università di Pisa, Pisa; Italy.

[70](a)INFN Sezione di Roma;(b)Dipartimento di Fisica, Sapienza Università di Roma, Roma; Italy.

[71](a)INFN Sezione di Roma Tor Vergata;(b)Dipartimento di Fisica, Università di Roma Tor Vergata, Roma; Italy.

[72](a)INFN Sezione di Roma Tre;(b)Dipartimento di Matematica e Fisica, Università Roma Tre, Roma; Italy.

[73](a)INFN-TIFPA;(b)Università degli Studi di Trento, Trento; Italy.

[74]Institut für Astro- und Teilchenphysik, Leopold-Franzens-Universität, Innsbruck; Austria.

[75]University of Iowa, Iowa City IA; United States of America.

[76]Department of Physics and Astronomy, Iowa State University, Ames IA; United States of America.

[77]Joint Institute for Nuclear Research, Dubna; Russia.

[78](a)Departamento de Engenharia Elétrica, Universidade Federal de Juiz de Fora (UFJF), Juiz de Fora;(b)Universidade Federal do Rio De Janeiro COPPE/EE/IF, Rio de Janeiro;(c)Universidade Federal de São João del Rei (UFSJ), São João del Rei;(d)Instituto de Física, Universidade de São Paulo, São Paulo; Brazil.

[79]KEK, High Energy Accelerator Research Organization, Tsukuba; Japan.

[80]Graduate School of Science, Kobe University, Kobe; Japan.

[81](a)AGH University of Science and Technology, Faculty of Physics and Applied Computer Science, Krakow;(b)Marian Smoluchowski Institute of Physics, Jagiellonian University, Krakow; Poland.

[82]Institute of Nuclear Physics Polish Academy of Sciences, Krakow; Poland.

[83]Faculty of Science, Kyoto University, Kyoto; Japan.

[84]Kyoto University of Education, Kyoto; Japan.

[85]Research Center for Advanced Particle Physics and Department of Physics, Kyushu University, Fukuoka ; Japan.

[86]Instituto de Física La Plata, Universidad Nacional de La Plata and CONICET, La Plata; Argentina.

[87]Physics Department, Lancaster University, Lancaster; United Kingdom.

[88]Oliver Lodge Laboratory, University of Liverpool, Liverpool; United Kingdom.

[89]Department of Experimental Particle Physics, Jožef Stefan Institute and Department of Physics, University of Ljubljana, Ljubljana; Slovenia.

[90]School of Physics and Astronomy, Queen Mary University of London, London; United Kingdom.

[91]Department of Physics, Royal Holloway University of London, Egham; United Kingdom.

[92]Department of Physics and Astronomy, University College London, London; United Kingdom.

[93]Louisiana Tech University, Ruston LA; United States of America.

[94]Fysiska institutionen, Lunds universitet, Lund; Sweden.

[95]Centre de Calcul de l'Institut National de Physique Nucléaire et de Physique des Particules (IN2P3), Villeurbanne; France.

[96]Departamento de Física Teorica C-15 and CIAFF, Universidad Autónoma de Madrid, Madrid; Spain.

[97]Institut für Physik, Universität Mainz, Mainz; Germany.

[98]School of Physics and Astronomy, University of Manchester, Manchester; United Kingdom.

[99]CPPM, Aix-Marseille Université, CNRS/IN2P3, Marseille; France.

[100]Department of Physics, University of Massachusetts, Amherst MA; United States of America.

[101]Department of Physics, McGill University, Montreal QC; Canada.

[102]School of Physics, University of Melbourne, Victoria; Australia.

[103]Department of Physics, University of Michigan, Ann Arbor MI; United States of America.

[104]Department of Physics and Astronomy, Michigan State University, East Lansing MI; United States of America.

[105]B.I. Stepanov Institute of Physics, National Academy of Sciences of Belarus, Minsk; Belarus.

[106]Research Institute for Nuclear Problems of Byelorussian State University, Minsk; Belarus.

[107]Group of Particle Physics, University of Montreal, Montreal QC; Canada.

[108]P.N. Lebedev Physical Institute of the Russian Academy of Sciences, Moscow; Russia.

[109]Institute for Theoretical and Experimental Physics (ITEP), Moscow; Russia.

[110]National Research Nuclear University MEPhI, Moscow; Russia.

[111]D.V. Skobeltsyn Institute of Nuclear Physics, M.V. Lomonosov Moscow State University, Moscow; Russia.

[112]Fakultät für Physik, Ludwig-Maximilians-Universität München, München; Germany.

[113]Max-Planck-Institut für Physik (Werner-Heisenberg-Institut), München; Germany.

[114]Nagasaki Institute of Applied Science, Nagasaki; Japan.

[115]Graduate School of Science and Kobayashi-Maskawa Institute, Nagoya University, Nagoya; Japan.

[116]Department of Physics and Astronomy, University of New Mexico, Albuquerque NM; United States of America.

[117]Institute for Mathematics, Astrophysics and Particle Physics, Radboud University Nijmegen/Nikhef, Nijmegen; Netherlands.

[118]Nikhef National Institute for Subatomic Physics and University of Amsterdam, Amsterdam; Netherlands.

[119]Department of Physics, Northern Illinois University, DeKalb IL; United States of America.

[120][a]Budker Institute of Nuclear Physics, SB RAS, Novosibirsk;[b]Novosibirsk State University Novosibirsk; Russia.

[121]Department of Physics, New York University, New York NY; United States of America.

[122]Ohio State University, Columbus OH; United States of America.

[123]Faculty of Science, Okayama University, Okayama; Japan.

[124]Homer L. Dodge Department of Physics and Astronomy, University of Oklahoma, Norman OK; United States of America.

[125]Department of Physics, Oklahoma State University, Stillwater OK; United States of America.

[126]Palacký University, RCPTM, Joint Laboratory of Optics, Olomouc; Czech Republic.

[127]Center for High Energy Physics, University of Oregon, Eugene OR; United States of America.

[128]LAL, Université Paris-Sud, CNRS/IN2P3, Université Paris-Saclay, Orsay; France.

[129]Graduate School of Science, Osaka University, Osaka; Japan.

[130]Department of Physics, University of Oslo, Oslo; Norway.

[131]Department of Physics, Oxford University, Oxford; United Kingdom.

[132]LPNHE, Sorbonne Université, Paris Diderot Sorbonne Paris Cité, CNRS/IN2P3, Paris; France.

[133]Department of Physics, University of Pennsylvania, Philadelphia PA; United States of America.

[134]Konstantinov Nuclear Physics Institute of National Research Centre "Kurchatov Institute", PNPI, St. Petersburg; Russia.

[135]Department of Physics and Astronomy, University of Pittsburgh, Pittsburgh PA; United States of America.

[136][a]Laboratório de Instrumentação e Física Experimental de Partículas - LIP;[b]Departamento de Física, Faculdade de Ciências, Universidade de Lisboa, Lisboa;[c]Departamento de Física, Universidade de Coimbra, Coimbra;[d]Centro de Física Nuclear da Universidade de Lisboa, Lisboa;[e]Departamento de Física, Universidade do Minho, Braga;[f]Departamento de Física Teorica y del Cosmos, Universidad

de Granada, Granada (Spain);[g]Dep Física and CEFITEC of Faculdade de Ciências e Tecnologia, Universidade Nova de Lisboa, Caparica; Portugal.

[137]Institute of Physics, Academy of Sciences of the Czech Republic, Prague; Czech Republic.

[138]Czech Technical University in Prague, Prague; Czech Republic.

[139]Charles University, Faculty of Mathematics and Physics, Prague; Czech Republic.

[140]State Research Center Institute for High Energy Physics, NRC KI, Protvino; Russia.

[141]Particle Physics Department, Rutherford Appleton Laboratory, Didcot; United Kingdom.

[142]IRFU, CEA, Université Paris-Saclay, Gif-sur-Yvette; France.

[143]Santa Cruz Institute for Particle Physics, University of California Santa Cruz, Santa Cruz CA; United States of America.

[144][a]Departamento de Física, Pontificia Universidad Católica de Chile, Santiago;[b]Departamento de Física, Universidad Técnica Federico Santa María, Valparaíso; Chile.

[145]Department of Physics, University of Washington, Seattle WA; United States of America.

[146]Department of Physics and Astronomy, University of Sheffield, Sheffield; United Kingdom.

[147]Department of Physics, Shinshu University, Nagano; Japan.

[148]Department Physik, Universität Siegen, Siegen; Germany.

[149]Department of Physics, Simon Fraser University, Burnaby BC; Canada.

[150]SLAC National Accelerator Laboratory, Stanford CA; United States of America.

[151]Physics Department, Royal Institute of Technology, Stockholm; Sweden.

[152]Departments of Physics and Astronomy, Stony Brook University, Stony Brook NY; United States of America.

[153]Department of Physics and Astronomy, University of Sussex, Brighton; United Kingdom.

[154]School of Physics, University of Sydney, Sydney; Australia.

[155]Institute of Physics, Academia Sinica, Taipei; Taiwan.

[156]Academia Sinica Grid Computing, Institute of Physics, Academia Sinica, Taipei; Taiwan.

[157][a]E. Andronikashvili Institute of Physics, Iv. Javakhishvili Tbilisi State University, Tbilisi;[b]High Energy Physics Institute, Tbilisi State University, Tbilisi; Georgia.

[158]Department of Physics, Technion, Israel Institute of Technology, Haifa; Israel.

[159]Raymond and Beverly Sackler School of Physics and Astronomy, Tel Aviv University, Tel Aviv; Israel.

[160]Department of Physics, Aristotle University of Thessaloniki, Thessaloniki; Greece.

[161]International Center for Elementary Particle Physics and Department of Physics, University of Tokyo, Tokyo; Japan.

[162]Graduate School of Science and Technology, Tokyo Metropolitan University, Tokyo; Japan.

[163]Department of Physics, Tokyo Institute of Technology, Tokyo; Japan.

[164]Tomsk State University, Tomsk; Russia.

[165]Department of Physics, University of Toronto, Toronto ON; Canada.

[166][a]TRIUMF, Vancouver BC;[b]Department of Physics and Astronomy, York University, Toronto ON; Canada.

[167]Division of Physics and Tomonaga Center for the History of the Universe, Faculty of Pure and Applied Sciences, University of Tsukuba, Tsukuba; Japan.

[168]Department of Physics and Astronomy, Tufts University, Medford MA; United States of America.

[169]Department of Physics and Astronomy, University of California Irvine, Irvine CA; United States of America.

[170]Department of Physics and Astronomy, University of Uppsala, Uppsala; Sweden.

[171]Department of Physics, University of Illinois, Urbana IL; United States of America.

[172]Instituto de Física Corpuscular (IFIC), Centro Mixto Universidad de Valencia - CSIC, Valencia; Spain.

[173]Department of Physics, University of British Columbia, Vancouver BC; Canada.

[174]Department of Physics and Astronomy, University of Victoria, Victoria BC; Canada.

[175]Fakultät für Physik und Astronomie, Julius-Maximilians-Universität Würzburg, Würzburg; Germany.

[176]Department of Physics, University of Warwick, Coventry; United Kingdom.

[177]Waseda University, Tokyo; Japan.

[178]Department of Particle Physics, Weizmann Institute of Science, Rehovot; Israel.

[179]Department of Physics, University of Wisconsin, Madison WI; United States of America.

[180]Fakultät für Mathematik und Naturwissenschaften, Fachgruppe Physik, Bergische Universität Wuppertal, Wuppertal; Germany.

[181]Department of Physics, Yale University, New Haven CT; United States of America.

[182]Yerevan Physics Institute, Yerevan; Armenia.

[a] Also at Department of Physics, University of Malaya, Kuala Lumpur; Malaysia.

[b] Also at Borough of Manhattan Community College, City University of New York, NY; United States of America.

[c] Also at Centre for High Performance Computing, CSIR Campus, Rosebank, Cape Town; South Africa.

[d] Also at CERN, Geneva; Switzerland.

[e] Also at CPPM, Aix-Marseille Université, CNRS/IN2P3, Marseille; France.

[f] Also at Département de Physique Nucléaire et Corpusculaire, Université de Genève, Genève; Switzerland.

[g] Also at Departament de Fisica de la Universitat Autonoma de Barcelona, Barcelona; Spain.

[h] Also at Departamento de Física Teorica y del Cosmos, Universidad de Granada, Granada (Spain); Spain.

[i] Also at Department of Applied Physics and Astronomy, University of Sharjah, Sharjah; United Arab Emirates.

[j] Also at Department of Financial and Management Engineering, University of the Aegean, Chios; Greece.

[k] Also at Department of Physics and Astronomy, University of Louisville, Louisville, KY; United States of America.

[l] Also at Department of Physics and Astronomy, University of Sheffield, Sheffield; United Kingdom.

[m] Also at Department of Physics, California State University, Fresno CA; United States of America.

[n] Also at Department of Physics, California State University, Sacramento CA; United States of America.

[o] Also at Department of Physics, King's College London, London; United Kingdom.

[p] Also at Department of Physics, Nanjing University, Nanjing; China.

[q] Also at Department of Physics, St. Petersburg State Polytechnical University, St. Petersburg; Russia.

[r] Also at Department of Physics, University of Fribourg, Fribourg; Switzerland.

[s] Also at Department of Physics, University of Michigan, Ann Arbor MI; United States of America.

[t] Also at Dipartimento di Fisica E. Fermi, Università di Pisa, Pisa; Italy.

[u] Also at Giresun University, Faculty of Engineering, Giresun; Turkey.

[v] Also at Graduate School of Science, Osaka University, Osaka; Japan.

[w] Also at Hellenic Open University, Patras; Greece.

[x] Also at Horia Hulubei National Institute of Physics and Nuclear Engineering, Bucharest; Romania.

[y] Also at II. Physikalisches Institut, Georg-August-Universität Göttingen, Göttingen; Germany.

[z] Also at Institucio Catalana de Recerca i Estudis Avancats, ICREA, Barcelona; Spain.

[aa] Also at Institut de Física d'Altes Energies (IFAE), Barcelona Institute of Science and Technology, Barcelona; Spain.

[ab] Also at Institut für Experimentalphysik, Universität Hamburg, Hamburg; Germany.

[ac] Also at Institute for Mathematics, Astrophysics and Particle Physics, Radboud University Nijmegen/Nikhef, Nijmegen; Netherlands.

^{ad} Also at Institute for Particle and Nuclear Physics, Wigner Research Centre for Physics, Budapest; Hungary.

^{ae} Also at Institute of Particle Physics (IPP); Canada.

^{af} Also at Institute of Physics, Academia Sinica, Taipei; Taiwan.

^{ag} Also at Institute of Physics, Azerbaijan Academy of Sciences, Baku; Azerbaijan.

^{ah} Also at Institute of Theoretical Physics, Ilia State University, Tbilisi; Georgia.

^{ai} Also at LAL, Université Paris-Sud, CNRS/IN2P3, Université Paris-Saclay, Orsay; France.

^{aj} Also at Louisiana Tech University, Ruston LA; United States of America.

^{ak} Also at Manhattan College, New York NY; United States of America.

^{al} Also at Moscow Institute of Physics and Technology State University, Dolgoprudny; Russia.

^{am} Also at National Research Nuclear University MEPhI, Moscow; Russia.

^{an} Also at Near East University, Nicosia, North Cyprus, Mersin; Turkey.

^{ao} Also at Ochadai Academic Production, Ochanomizu University, Tokyo; Japan.

^{ap} Also at Physikalisches Institut, Albert-Ludwigs-Universität Freiburg, Freiburg; Germany.

^{aq} Also at School of Physics, Sun Yat-sen University, Guangzhou; China.

^{ar} Also at The City College of New York, New York NY; United States of America.

^{as} Also at The Collaborative Innovation Center of Quantum Matter (CICQM), Beijing; China.

^{at} Also at Tomsk State University, Tomsk, and Moscow Institute of Physics and Technology State University, Dolgoprudny; Russia.

^{au} Also at TRIUMF, Vancouver BC; Canada.

^{av} Also at Universita di Napoli Parthenope, Napoli; Italy.

* Deceased